



Test of CP-invariance of the Higgs boson in vector-boson fusion production and its decay into four leptons

The ATLAS Collaboration

A search for CP violation in the decay kinematics and vector-boson production of the Higgs boson is performed in the $H \rightarrow ZZ^* \rightarrow 4\ell$ ($\ell = e, \mu$) decay channel. The results are based on proton–proton collision data produced at the LHC at a centre-of-mass energy of 13 TeV and recorded by the ATLAS detector from 2015 to 2018, corresponding to an integrated luminosity of 139 fb^{-1} . Matrix element-based optimal observables are used to constrain CP-odd couplings beyond the Standard Model in the framework of Standard Model effective field theory expressed in the Warsaw and Higgs bases. Differential fiducial cross-section measurements of the optimal observables are also performed, and a new fiducial cross-section measurement for vector-boson-fusion production is provided. All measurements are in agreement with the Standard Model prediction of a CP-even Higgs boson.

Contents

1	Introduction	3
2	Theoretical framework and analysis methodology	4
2.1	EFT framework	4
2.2	Optimal observables	5
2.3	Morphing method	6
3	ATLAS detector	7
4	Data set and event simulation	8
5	Event reconstruction, selection and backgrounds	9
5.1	Object reconstruction	9
5.2	Event selection	10
5.3	Backgrounds	10
6	Overview of analysis	11
6.1	Direct coupling measurement	11
6.2	Differential cross-section measurement	14
7	Systematic uncertainties	17
7.1	Experimental uncertainties	17
7.2	Theoretical uncertainties	18
7.3	Uncertainties specific to the differential cross-section extraction	19
7.4	Monte Carlo statistics	19
8	Results	19
8.1	Direct coupling measurement results	19
8.2	Differential optimal-observable cross-section results	31
8.3	VBF-enriched fiducial cross-section results	33
9	Conclusion	34
	Appendix	36
A	Additional differential cross-section results	36

1 Introduction

The observed baryon asymmetry of the universe is one of the important open questions of physics today. To explain this, the Sakharov criteria [1] require sufficient charge conjugation (C) and parity (P) violation. The only known source of CP violation in the Standard Model (SM) is a complex phase in the Cabibbo–Kobayashi–Maskawa (CKM) matrix [2, 3] for quark mixing. Other sources of CP violation may exist in the neutrino sector or the strong interaction. The CKM complex phase does not lead to a sufficient amount of CP violation to explain the baryon asymmetry. This motivates the exploration of potential new sources of CP violation, as performed in the present analysis of the production and decay of the Higgs boson [4, 5].

The spin-parity (J^P) of the Higgs boson is predicted to be 0^+ by the Standard Model.¹ Any sign of CP-violation in the production or decay of the Higgs boson would therefore be an unambiguous indication of beyond the Standard Model phenomena (BSM). With 25 fb^{-1} of proton–proton collision data collected from the LHC with a centre-of-mass energy, \sqrt{s} , of 7 and 8 TeV, the ATLAS and CMS experiments excluded the pure spin-parity states 0^- , 1^+ , 1^- , 2^+ and 2^- at more than 99% confidence level (CL) based on the observed Higgs boson decays ($\gamma\gamma$, ZZ , WW) [6–9]. These results also provided the first limits on a possible CP-odd contribution to Higgs boson to vector-boson couplings (HVV) in Higgs boson decays. With the same data set there was a first search for CP-odd HVV couplings in vector-boson fusion (VBF) production in the $H \rightarrow \tau\tau$ decay channel [10]. With an increased integrated luminosity of 139 fb^{-1} of LHC collisions at $\sqrt{s} = 13 \text{ TeV}$, an order of magnitude more Higgs boson candidates were collected. Constraints on CP-invariance were tightened for the HVV couplings and extended to Higgs Yukawa couplings to fermions in $H \rightarrow \tau\tau$ decays and associated Higgs boson top pair ($t\bar{t}H$) production in both the diphoton and $b\bar{b}$ decay channels [11–21].

For the $H \rightarrow ZZ^* \rightarrow 4\ell$ channel ($\ell = e, \mu$), constraints on CP-even and CP-odd BSM couplings have been set with 139 fb^{-1} at $\sqrt{s} = 13 \text{ TeV}$ for Higgs boson production cross-section measurements, by comparing observations with SM expectations [22]. However, potential deviations of the Higgs boson production cross-sections could be explained by either a CP-even or CP-odd BSM coupling, and would not distinguish between them. The present analysis searches for a visible CP-odd effect in VBF production and the $H \rightarrow ZZ^* \rightarrow 4\ell$ decay by employing *optimal observables* [23–25], which are CP-odd by construction, with 139 fb^{-1} of data collected at $\sqrt{s} = 13 \text{ TeV}$ by the ATLAS detector [26]. About 200 Higgs bosons decaying into four leptons are expected to be reconstructed in the detector for this sample, including about 10 events in a VBF production phase space.

The optimal observables are constructed from matrix elements of the Standard Model effective field theory (SMEFT) [27], a specific formalism of an effective field theory (EFT). An optimal-observable distribution is symmetric for the CP-even Higgs boson and becomes asymmetric when contributions from CP-odd BSM couplings are present. There are three dimension-six operators with BSM CP-odd couplings in the SMEFT Lagrangian that can contribute to VBF production or the $H \rightarrow ZZ^* \rightarrow 4\ell$ decay, each associated with a Wilson coefficient. In this analysis, these three operators are considered in the Warsaw basis, and each operator has a different sensitivity to VBF production and the $H \rightarrow ZZ^* \rightarrow 4\ell$ decay. The optimal-observable distributions are used in two ways: the observed distributions are used directly to constrain CP-odd couplings, and they are unfolded to a fiducial phase space, complementing the $H \rightarrow ZZ^* \rightarrow 4\ell$ differential cross-section measurements in Ref. [28], to allow reinterpretations in different models. Since the present search is looking for a distinct CP-odd signature, the extraction of the

¹ In the following, the J^P label is used to indicate the spin and CP quantum numbers.

CP-odd coupling constraints is based only on the shape of the optimal-observable distributions, ignoring the expected change in cross-section. Including cross-sections has only a small effect on the constraints, as shown in Section 8.1. The fiducial phase space for the unfolded optimal-observable distributions is the same as for the $H \rightarrow ZZ^* \rightarrow 4\ell$ fiducial measurement [28], and is dominated by gluon–gluon fusion ggF production that allows constraints on CP-odd operators which are sensitive to the $H \rightarrow ZZ^* \rightarrow 4\ell$ decay. Extracting the differential distributions for the VBF optimal observables in a VBF-enriched fiducial phase space would improve the sensitivity to the CP-odd operator that is more sensitive to VBF production, however this is not yet within statistical reach. Instead this paper presents an inclusive cross-section measurement in a VBF fiducial phase space. This measurement can be used to constrain BSM models affecting the Higgs boson to ZZ^* vertex through their expected impact on event rates.

2 Theoretical framework and analysis methodology

While the analysis is designed to be sensitive to signatures of CP violation independently of a particular BSM physics model, the SMEFT framework is used to guide the analysis strategy and interpret the results. This framework also provides the coupling scenarios used to define the optimal observables at the centre of the analysis strategy. Both the SMEFT framework and the optimal-observable formalism are described in more detail in the following. In addition, the known dependence of cross-sections on the BSM couplings in the framework of SMEFT is exploited to parameterize the signal prediction in the direct BSM coupling measurement as described in Section 2.3.

2.1 EFT framework

In SMEFT, a complete set of higher-order-in-mass operators invariant under the SM gauge group $SU(3)_C \times SU(2)_L \times U(1)_Y$ is built from the SM fields [27]. If the dimension-five operator is ignored because it violates lepton number [29], the leading contributions to physical observables are expected to be from dimension-six operators. In this case the SMEFT Lagrangian becomes:

$$\mathcal{L}_{\text{SMEFT}} = \mathcal{L}_{\text{SM}} + \sum_i \frac{c_i}{\Lambda^2} O_i^{(6)}, \quad (1)$$

where $O_i^{(6)}$ are the operators of mass-dimension six, which are invariant under the SM gauge group, the c_i are the corresponding dimensionless real coupling constants, the Wilson coefficients, and Λ is the energy cutoff scale of the effective field theory.

There are several complete sets of these dimension-six operators. One such set, used in many existing LHC EFT interpretations [30–33], is the *Warsaw basis*, which contains 59 independent operators assuming lepton and baryon number conservation [34, 35]. Three CP-odd operators, listed in the first three rows of Table 1, are composed of the Higgs boson doublet and the gauge-field-strength tensors of the unbroken gauge symmetry. These contribute to the HVV vertex for both VBF production and vector-boson decays ($\gamma\gamma, ZZ, WW$).

The same phenomena are described by an alternative complete set of operators, based on the mass eigenstates after the spontaneous symmetry breaking instead of the fields of the unbroken gauge symmetry. This formulation is expressed in terms of the physical states of SM gauge bosons W^+, W^-, Z , and γ . With these operators it is possible to build another basis [36, 37] that can probe the effects of the Higgs boson

couplings to other particles, and is more closely linked to experimental physical observables than the Warsaw basis. It is called the *Higgs basis* in which three independent CP-odd couplings, listed in Table 1 together with their operators, mediate the same phenomena as the Warsaw-basis couplings. Each coupling of one basis can be expressed as a linear combination of the three couplings in the other basis.

Finally, a common parameterization used in existing experimental searches for CP-violation at the HVV vertex [10, 30] assumes a single BSM CP-odd Higgs boson coupling denoted by \tilde{d} . In [10], it was considered that the different contributions from the various electroweak gauge-boson fusion processes could not be distinguished experimentally, and assumed that the BSM CP-odd Higgs boson couplings $c_{H\tilde{W}}$ and $c_{H\tilde{B}}$ in the Warsaw basis are equal, leading to the remaining coupling $c_{H\tilde{W}B}$ being zero. The CP-odd parameter \tilde{d} is related to the Warsaw-basis couplings by the parameterization $c_{H\tilde{W}} = c_{H\tilde{B}} = \frac{\Lambda^2}{v^2} \tilde{d}$, where v is the Higgs boson vacuum expectation value. In the Higgs basis, it is equivalent to the direction $\tilde{c}_{z\gamma} = 0$, $\tilde{c}_{\gamma\gamma} = \sin^2 \theta_W \cos^2 \theta_W \tilde{c}_{zz}$, where θ_W is the Weinberg angle.

The focus of this paper is on interpretations in the Warsaw-basis framework, but results are also provided for the Higgs basis and \tilde{d} to facilitate comparisons.

Table 1: SMEFT CP-odd dimension-six operators in the Warsaw and Higgs bases relevant for the measurement of CP-invariance in the $H \rightarrow ZZ^* \rightarrow 4\ell$ decay channel. The gauge field strength tensors are denoted $W_{\mu\nu}^I$ and $B_{\mu\nu}$, while Φ is the scalar doublet Higgs boson field. The photon and Z-boson field strength tensors after electroweak symmetry breaking are denoted as $A_{\mu\nu}$ and $Z_{\mu\nu}$, respectively, and h denotes the massive Higgs field after electroweak symmetry breaking. Combinations of couplings in one basis can be translated into equivalent combinations of couplings from the other basis that describe the same phenomena [36, 37].

Operator	Structure	Coupling
Warsaw Basis		
$O_{\Phi\tilde{W}}$	$\Phi^\dagger \Phi \tilde{W}_{\mu\nu}^I W^{\mu\nu I}$	$c_{H\tilde{W}}$
$O_{\Phi\tilde{W}B}$	$\Phi^\dagger \tau^I \Phi \tilde{W}_{\mu\nu}^I B^{\mu\nu}$	$c_{H\tilde{W}B}$
$O_{\Phi\tilde{B}}$	$\Phi^\dagger \Phi \tilde{B}_{\mu\nu} B^{\mu\nu}$	$c_{H\tilde{B}}$
Higgs Basis		
$O_{hZ\tilde{Z}}$	$h Z_{\mu\nu} \tilde{Z}^{\mu\nu}$	\tilde{c}_{zz}
$O_{hZ\tilde{A}}$	$h Z_{\mu\nu} \tilde{A}^{\mu\nu}$	$\tilde{c}_{z\gamma}$
$O_{hA\tilde{A}}$	$h A_{\mu\nu} \tilde{A}^{\mu\nu}$	$\tilde{c}_{\gamma\gamma}$

2.2 Optimal observables

The cross-section for the combination of a set of CP-odd couplings, c_i , within the SM is proportional to the square of the matrix element composed of the sum of the individual matrix elements:

$$\begin{aligned}
|\mathcal{M}|^2 &= \left| \mathcal{M}_{\text{SM}} + \sum_i \frac{c_i}{\Lambda^2} \mathcal{M}_{\text{BSM},i} \right|^2 \\
&= |\mathcal{M}_{\text{SM}}|^2 + 2 \sum_i \frac{c_i}{\Lambda^2} \Re(\mathcal{M}_{\text{SM}}^* \mathcal{M}_{\text{BSM},i}) + \sum_i \sum_j \frac{c_i c_j}{\Lambda^4} \Re(\mathcal{M}_{\text{BSM},i}^* \mathcal{M}_{\text{BSM},j})
\end{aligned}$$

The expanded sum has a first term that is the squared SM matrix element, and a last term that represents the quadratic BSM contributions and the interference between BSM terms. These first and last terms are CP-even. The middle term is composed of the cross terms between the SM and BSM couplings (\Re is the real part) and represents the interference between the SM and BSM processes.² This term is CP-odd and therefore suitable as a probe for CP violation.

Normalising the interference term by the SM term forms an ‘optimal observable’ for each coupling, which can be used to detect a CP asymmetry:

$$OO = \frac{2\Re(\mathcal{M}_{\text{SM}}^* \mathcal{M}_{\text{BSM}})}{|\mathcal{M}_{\text{SM}}|^2}.$$

These observables are CP-odd by construction, implying a symmetric distribution with a vanishing mean in the absence of CP violation. Any asymmetry observed in the distribution of the optimal observables would be direct evidence for CP-violation in the HVV coupling. The LO matrix elements entering the optimal observable are calculated using MADGRAPH5_AMC@NLO [38] with the NNPDF2.3LO [39] parton distribution function (PDF) set. Two types of optimal observables are considered. *Production-level* optimal observables reflect the VBF production vertex, not considering the Higgs boson decay. They are constructed using VBF production matrix elements calculated from the reconstructed four-momentum of the Higgs boson candidate and the two leading jets assumed to form the VBF topology. The VBF production matrix element calculation is a PDF-weighted sum of matrix elements for several partonic processes. In addition, *decay-level* optimal observables are constructed using the matrix element describing the Higgs boson decay from the reconstructed four-momenta of the four decay leptons. These decay-level optimal observables are agnostic to the production vertex, and only a single matrix element is needed for an optimal-observable evaluation. For each type of optimal observable, there is a choice of which BSM coupling to assume when calculating the interference term. A dedicated observable is constructed for each of the seven EFT coupling parameters, three for each basis and one for \vec{d} . While each observable is sufficiently general to be sensitive to CP-violating effects from different couplings to those assumed in its construction, the sensitivity to a CP-odd effect of a particular coupling is maximized using an observable made with the same coupling.

2.3 Morphing method

The distribution of the optimal observable for a signal process with an arbitrary combination of active EFT couplings is predicted as the weighted sum of a limited number of simulated predictions, described in Section 4. The weights entering the sum are polynomial functions of the assumed EFT couplings, calculated using the *morphing method* [40]. This relies on the fact that, as shown in Eq. (2), the cross-section in each phase space bin, σ , is a polynomial function of the EFT coupling,

$$\sigma = \sum_{k=0}^4 c^k A_k = \vec{c} \cdot \vec{A}, \quad \text{with } \vec{c} = (1, c, c^2, c^3, c^4) \quad \text{and } \vec{A} = (A_0, A_1, A_2, A_3, A_4) \quad (3)$$

where c is the EFT coupling under study and A_k denotes the component of the cross-section proportional to the k^{th} power of the BSM coupling. If up to two HVV vertices are present, one for production and one for the decay, the maximum power in the BSM coupling is 4 as assumed above. The same method applies to combinations of multiple active couplings and to different numbers of HVV vertices. In this

² $2\Re(\mathcal{M}_{\text{SM}}^* \mathcal{M}_{\text{BSM}}) = \mathcal{M}_{\text{SM}}^* \mathcal{M}_{\text{BSM}} + \mathcal{M}_{\text{SM}} \mathcal{M}_{\text{BSM}}^*$

case, \vec{c} contains all combinations of powers of the BSM couplings appearing in the amplitude, and \vec{A} the corresponding cross-section contributions. The dimensionality of \vec{A} and \vec{c} then corresponds to the number of such unique coupling power combinations, including the case without any BSM couplings (SM-only amplitude). For example, for one vertex and three BSM couplings denoted c_1 , c_2 , and c_3 , there would be ten elements $(1, c_1, c_2, c_3, c_1^2, c_2^2, c_3^2, c_1c_2, c_1c_3, c_2c_3)$, and for two vertices and three BSM couplings, the dimensionality would increase to 35.

A set of simulated samples for different combinations of coupling values $\vec{c}_{\text{Sample } i}$ can be interpreted as a vector of cross-sections, which depends on the coupling values via a matrix C ,

$$\vec{\sigma}_{\text{simulated}} = C \times \vec{A}, \text{ with } C = [\vec{c}_{\text{Sample } 1}, \vec{c}_{\text{Sample } 2}, \dots]$$

Inverting this relation, which is only possible if the number of simulated samples is equivalent to the dimensionality of \vec{A} , and inserting into Eq. (3) allows the cross-section for an arbitrary coupling set to be expressed as a linear combination of the existing, simulated cross-sections:

$$\sigma = \vec{c} \cdot \vec{A} = \vec{c} \cdot (\vec{C}^{-1} \cdot \vec{\sigma}_{\text{simulated}}) = \sum_j \underbrace{(\vec{C}_j^{-1} \cdot \vec{c})}_{w_j(\vec{c})} \sigma_j$$

where the $w_j(\vec{c})$ are the weights to be applied to each of the simulated samples to obtain the signal prediction.

3 ATLAS detector

The ATLAS detector at the LHC is a multipurpose particle detector with a forward–backward symmetric cylindrical geometry and a near 4π coverage in solid angle.³ It consists of an inner tracking detector (ID) surrounded by a thin superconducting solenoid providing a 2 T axial magnetic field, electromagnetic and hadron calorimeters, and a muon spectrometer (MS). The ID covers the pseudorapidity range $|\eta| < 2.5$. It consists of silicon pixel, silicon microstrip, and transition radiation tracking detectors. Lead/liquid-argon (LAr) sampling calorimeters provide electromagnetic (EM) energy measurements with high granularity. A steel/scintillator-tile hadron calorimeter covers the central pseudorapidity range ($|\eta| < 1.7$). The endcap and forward regions are instrumented with LAr calorimeters for both the EM and hadronic energy measurements up to $|\eta| = 4.9$. The MS surrounds the calorimeters and is based on three large superconducting air-core toroidal magnets with eight coils each. The field integral of the toroids ranges between 2.0 and 6.0 T m across most of the detector. The MS includes a system of precision tracking chambers and fast detectors for triggering. A two-level trigger system is used to select events. The first-level trigger is implemented in hardware and uses a subset of the detector information to accept events at a rate below 100 kHz. This is followed by a software-based trigger that reduces the accepted event rate to 1 kHz on average, depending on the data-taking conditions. An extensive software suite [41] is used in data simulation, in the reconstruction and analysis of real and simulated data, in detector operations, and in the trigger and data acquisition systems of the experiment.

³ ATLAS uses a right-handed coordinate system with its origin at the nominal interaction point (IP) in the centre of the detector and the z -axis along the beam pipe. The x -axis points from the IP to the centre of the LHC ring, and the y -axis points upwards. Cylindrical coordinates (r, ϕ) are used in the transverse plane, ϕ being the azimuthal angle around the z -axis. The pseudorapidity is defined in terms of the polar angle θ as $\eta = -\ln \tan(\theta/2)$. Angular distance is measured in units of $\Delta R \equiv \sqrt{(\Delta\eta)^2 + (\Delta\phi)^2}$.

4 Data set and event simulation

This measurement uses data from proton–proton collisions with a centre-of-mass energy of 13 TeV collected between 2015 and 2018 using single-lepton, dilepton, and trilepton triggers [42, 43] as detailed in Ref. [22]. The combined efficiency of these triggers is approximately 98%, 99%, 97%, and 99% for the 4μ , $2e2\mu$, $2\mu2e$, and $4e$ final states, respectively, for the simulated $H \rightarrow ZZ^* \rightarrow 4\ell$ events passing the event selection described in Section 5 (assuming $m_H = 125$ GeV). After data-quality requirements are imposed, the integrated luminosity of the data sample is 139 fb^{-1} [44].

Details of the SM Higgs boson Monte Carlo (MC) samples used in this analysis can be found in Refs. [22, 28]. Higgs boson production via the ggF process was modelled at next-to-leading-order (NLO) accuracy in the strong coupling constant α_s using the POWHEG NNLOPS generator [45–53] with the PDF4LHC15_{NNLO} set of PDFs [54]. Higgs bosons produced via VBF or in association with a vector boson (VH) or in association with a top-quark pair ($t\bar{t}H$), were simulated at NLO accuracy with the POWHEG Box generator [47–49], using the PDF4LHC15_{NLO} PDF set. Higgs boson production in association with a top quark (tH) was simulated at NLO accuracy using the MADGRAPH5_AMC@NLO generator [38, 55] with the NNPDF3.0 PDF set [56]. For all signal processes, the EVTGEN 1.6.0 generator [57] was used for the simulation of the bottom- and charm-hadron decays. Correspondingly, the PYTHIA 8 generator [58] was used for the $H \rightarrow ZZ^* \rightarrow 4\ell$ decay and for parton showering, hadronization, and simulation of the underlying event. These samples were normalized to cross-sections obtained from the most recent predictions provided by the LHC Higgs Working Group [36].

BSM Higgs boson samples with active CP-odd EFT couplings were generated for different coupling values at leading order in α_s with MADGRAPH5_AMC@NLO and the NNPDF2.3 PDF set. The generation was performed using the effective Lagrangian of the SMEFT framework implemented via the SMEFTsim_A_U35_MwScheme_UFO_v2.1 [27, 59] model. The CKKW-L method [60] was used for the jet merging in the ggF process. The SMEFT v2 model with a $U(3)^5$ flavour symmetry and the m_W input scheme was used. The EFT cutoff scale was set to $\Lambda = 1$ TeV. Separate samples were generated for the ggF production mode and for the combination of the VBF and VH production modes. Each sample was generated at a three-dimensional coupling point for values of the Warsaw basis of Table 1, which also corresponds to a single point in the three Higgs-basis couplings. The choice of simulated coupling values was optimized to maintain high statistical power throughout the three-dimensional coupling space using the morphing method described in Section 2.

The non-resonant ZZ^* background, separated into quark-initiated $q\bar{q} \rightarrow ZZ^*$, gluon-initiated $gg \rightarrow ZZ^*$, and vector-boson scattering (EW ZZ) production, was modelled using the SHERPA 2.2.2 generator [61–64] with the NNPDF3.0_{NNLO} [56] PDF set. NLO EW corrections were applied as a function of the invariant mass of the ZZ^* system, m_{ZZ^*} [65, 66]. These samples were normalized to cross-sections obtained directly from the SHERPA simulation. Alternative $q\bar{q} \rightarrow ZZ^*$ samples, produced with the POWHEG Box v2 and MADGRAPH5_AMC@NLO generators, are used to study the theoretical modelling of the systematic uncertainties. For the alternative samples, the PYTHIA 8 generator was used for parton showering, hadronization, and simulation of the underlying event.

Background events from WZ and $t\bar{t}$ processes were generated with POWHEG Box v2, while contributions from Z bosons produced in association with jets were simulated using the SHERPA 2.2.1 generator. Minor contributions from processes with three electroweak bosons, denoted by VVV , were modelled using SHERPA 2.2.2. Small backgrounds originating from top-quark production in association with one or more electroweak bosons or additional top quarks, such as $t\bar{t}Z$, tWZ , $t\bar{t}WW$, $t\bar{t}WZ$, $t\bar{t}Z\gamma$, $t\bar{t}ZZ$, $t\bar{t}t$, $t\bar{t}t\bar{t}$, and tZ

(denoted by tXX), were simulated using the MADGRAPH5_AMC@NLO generator. The PYTHIA 8 generator was used for parton showering, hadronization, and simulation of the underlying event.

Generated events were processed through the ATLAS detector simulation [67] within the GEANT4 framework [68] and reconstructed in the same way as collision data. Additional proton–proton interactions in the same or neighbouring bunch crossings, referred to as pile-up, were included in the simulation. The pile-up events were generated using the PYTHIA 8 generator with the A3 set of tuned parameters [69] and the NNPDF2.3_{LO} PDF set.

5 Event reconstruction, selection and backgrounds

5.1 Object reconstruction

Muon candidates are reconstructed using a combination of different algorithms [70]. The reconstruction of muon candidates within $|\eta| < 2.5$ is primarily performed by a global fit to reconstructed tracks in the ID and the MS. In the central detector region ($|\eta| < 0.1$), where the MS has reduced geometrical coverage, muons are also identified by matching a reconstructed ID track to either an MS track segment (‘segment-tagged muons’) or a calorimetric energy deposit consistent with a minimum-ionising particle (‘calorimeter-tagged muons’). Calorimeter-tagged muons are required to have transverse momentum $p_T > 15$ GeV to avoid misidentifying leptons at low p_T . For both the segment-tagged and calorimeter-tagged muons, the muon momentum is measured from the ID track alone. In the forward MS region ($2.5 < |\eta| < 2.7$) outside the ID coverage, MS tracks with hits in three MS layers are accepted as ‘stand-alone muons’ and combined with track segments formed from hits in the silicon tracker, if they exist. Additionally, ‘loose’ muon-identification criteria [70] are applied to reject low-quality tracks that have missing hits in the MS or have poor agreement between the reconstructed MS and ID tracks. Muons are required to be isolated by using both calorimeter-based and track-based isolation variables and applying the ‘PflowLoose’ criteria [70]. They are matched to the hard-scatter vertex candidate by imposing a requirement $|z_0 \sin \theta| < 0.5$ mm on their longitudinal impact parameter z_0 . Cosmic rays are removed using a criterion $|d_0| < 1$ mm on the transverse impact parameter d_0 .

A reconstructed electron consists of a cluster of energy deposits in the calorimeter and a matched ID track [71]. Variable-size clusters are created dynamically from calorimeter-energy deposits, improving the invariant-mass resolution of the four-lepton system, especially when bremsstrahlung photons are present. Electron ID tracks are fitted using an optimized Gaussian-sum filter [72] that accounts for non-linear effects arising from energy loss through bremsstrahlung. Quality criteria are used to improve the purity of selected electron candidates. The quality of an electron candidate is evaluated by using a likelihood method that employs measurements from the tracking system and the calorimeter system, and quantities that combine both tracking and calorimeter information [72]. The ‘loose’ likelihood criteria, together with track hit requirements, are applied to electron candidates. Electrons are required to be isolated using both the calorimeter-based and track-based isolation variables as discussed in Ref. [22]. They are matched to the hard-scatter vertex using the same requirement as for the muons, $|z_0 \sin \theta| < 0.5$ mm.

Jets are reconstructed using a particle flow algorithm [73] from noise-suppressed positive-energy topological clusters [74] in the calorimeter using the anti- k_t algorithm [75, 76] with a radius parameter $R = 0.4$. Energy deposited in the calorimeter by charged particles is subtracted and replaced by the momenta of tracks that are matched to those topological clusters. The jet four-momentum is corrected for the non-compensating calorimeter response, signal losses due to noise threshold effects, energy lost in non-instrumented regions,

and contributions from pile-up [73, 77, 78]. Jets are required to have $p_T > 30$ GeV and $|\eta| < 4.5$. Jets with p_T ranging between 20–60 GeV for $|\eta| < 2.4$ and between 20–120 GeV for $2.5 < |\eta| < 4.5$ are suppressed if tagged as pile-up using two jet-vertex-tagger multivariate discriminants [79–82].

To avoid the double-counting of particles, a range of overlap removal criteria are applied to the electrons, muons, and jets. If any two leptons share an ID track or, in case of two electrons, have overlapping associated calorimeter energy clusters, only one is retained. Preference is given to higher- p_T leptons and to muons over electrons, unless the muon is identified using only the calorimeter, in which case the electron is maintained. Jets found within $\Delta R < 0.2$ of leptons are removed.

5.2 Event selection

Events are required to contain at least four isolated leptons emerging from a common vertex and forming two pairs of oppositely charged same-flavour leptons. Electrons are required to be within the geometrical acceptance of the ID ($|\eta| < 2.47$) and to have transverse energy $E_T > 7$ GeV, while muons must be within the geometrical acceptance of the MS ($|\eta| < 2.7$) and have $p_T > 5$ GeV (except for calorimeter-tagged muons, as explained in Section 5.1). At most one calorimeter-tagged or stand-alone muon is allowed per Higgs boson candidate. The three higher- $(p_T$ or $E_T)$ leptons in each quadruplet are required to satisfy thresholds of 20, 15, and 10 GeV, respectively. All lepton pairs within the quadruplet must have an angular separation, $\Delta R(\ell, \ell')$, larger than 0.1, and opposite-sign same-flavour pairs must have a mass above 5 GeV to avoid, for example, J/ψ pairs. Contributions from misidentified leptons are reduced by requiring the lepton tracks to have low significances of their transverse impact parameters (less than 3 (5) for e (μ)) and to be compatible with originating from a common vertex. A detailed description of the event selection can be found in Ref. [22].

The lepton pair with an invariant mass closest to the Z boson mass in each quadruplet is referred to as the leading dilepton, while the remaining pair is referred to as the subleading dilepton. The selected quadruplets are separated into four subchannels, according to the flavour of the leading and subleading pairs. In order of decreasing expected selection efficiency, they are 4μ , $2e2\mu$, $2\mu2e$, and $4e$. Only one quadruplet is selected from each event, based on the mass of the leading dilepton, the final state, and, for events with additional leptons, the largest leading-order matrix element for the Higgs boson decay, as described in Ref. [22]. Finally, final-state radiation photons are searched for in all events following the procedure described in Ref. [22]. These photons are found in 4% of the events and their energy is included in the mass computation.

5.3 Backgrounds

The dominant background contribution is non-resonant ZZ^* production, accounting for approximately 30% of events in the four-lepton invariant mass, $m_{4\ell}$, signal region, 115–130 GeV. The evaluation of the non-resonant ZZ^* is based on MC simulation, with a data-driven normalization obtained using the side-bands of the $m_{4\ell}$ distribution. The backgrounds from Z +jets, $t\bar{t}$ and WZ , denoted by ‘reducible’ in the following, are evaluated from data following the procedures described in [22, 28]. The tri-boson (WWZ , WZZ and ZZZ) and $t\bar{t}X$ backgrounds are evaluated from simulation and together with the reducible backgrounds amount to about 5% of the events in the signal region.

6 Overview of analysis

6.1 Direct coupling measurement

A binned maximum-likelihood fit to the observed distributions of optimal observables allows the EFT coupling parameters under consideration to be directly measured. The measurement targets CP-violating effects on the optimal-observable shapes and is optimized to be insensitive to any potential CP-even signature of BSM physics, which would only affect event rates. To achieve this, the impact of the EFT couplings on the event rates is neglected in the signal model, and only the shapes of the optimal-observable distributions change as a function of the BSM couplings. The rates of the SM signal prediction and background are instead left as free parameters in the statistical model and allowed to float when fitting the model to the data.

The optimal-observable distribution for the signal is predicted using the morphing method described in Section 2. In the case of production-level optimal-observable distributions, only the VBF and VH Higgs boson production modes are sensitive to BSM effects and considered as signal. The observable shape for any combination of the three EFT couplings considered here is predicted using 35 simulated samples with different injected EFT coupling values covering both processes. The number of samples is determined by the number of unique coupling combinations for three BSM couplings and two (production and decay) HVV vertices as discussed for Eq. (3) in Section 2.3.

All Higgs boson production modes represent a signal when considering decay-level optimal-observable distributions. For ggF, the shape of the observable distributions is predicted using a set of 10 simulated samples. Due to the negligible magnitude of the ttH and tH contributions in the study of decay-level observable distributions, no dedicated morphing is performed for them, and their shape is taken from the ggF prediction, with the combined yield accounted for by the free signal rate in the fit. The shape of the decay observable distributions for VBF and VH events is predicted with the same 35 samples described above.

For most of the background processes, the optimal-observable shapes are derived directly from the SM MC samples described in Section 4. This is the case for the dominant ZZ^* continuum background as well as the minor $t\bar{t}Z/t\bar{t}WW$ and triboson background contributions. The background from events with non-prompt leptons has its optimal-observable shape derived from its data-driven analysis, but plays a negligible role in the measurement. When the ggF, ttH and tH production modes are taken as background processes in the production-level optimal-observable measurement, the corresponding shape predictions are taken from the SM Higgs bosons samples described in Section 4, rather than from the BSM Higgs boson samples, to benefit from the higher theoretical precision of the prediction.

Three different types of fits are performed: *decay-only*, *production-only*, and *combined*. In each case, events are categorized to maximize analysis sensitivity, and all categories are fitted simultaneously. These categories are described in the following and illustrated in Figure 1.

A *decay-only* fit exclusively targets CP-violating effects in the Higgs boson decay. Two event categories are used. The signal region, also referred to as ‘inclusive SR’ in the following, comprises all events with $115 \text{ GeV} < m_{4\ell} < 130 \text{ GeV}$. Events with invariant masses in the side-band of the resonance, $105 \text{ GeV} < m_{4\ell} < 115 \text{ GeV}$ or $130 \text{ GeV} < m_{4\ell} < 160 \text{ GeV}$, form the background-dominated control region. This side-band, dominated by non-resonant ZZ^* decays, is denoted by ‘ ZZ^* CR’. The yield of the Higgs boson decay signal, independent of production mode, is parameterized with a normalization factor relative to the SM prediction. A second normalization factor scales the yield of the non-resonant

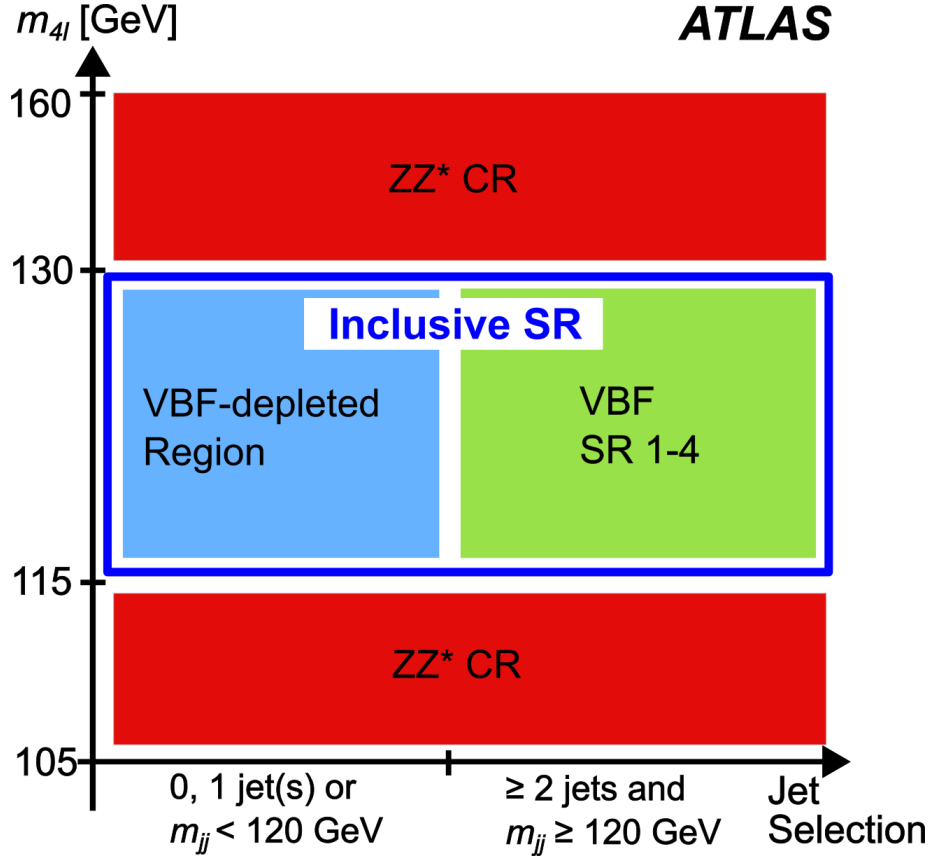


Figure 1: Illustration of the regions used in the direct BSM coupling measurement. The horizontal axis represents the jet selection requirements (≥ 2 jets and $m_{jj} \geq 120\text{GeV}$) defining the VBF-enriched signal regions (SR), while the vertical axis depicts the separation of the $m_{4\ell}$ range into resonant and non-resonant regions. The ‘inclusive SR’ comprizes events populating either the ‘VBF-depleted region’ or any of the VBF signal regions. The side-band control region (CR), dominated by non-resonant ZZ^* decays, is denoted by ‘ ZZ^* CR’. The multiple signal regions are used differently in the production-only, decay-only and combined fits.

ZZ^* background relative to the SM prediction. In both cases, the relative distribution of the yield between the signal and control region is assumed to follow the SM prediction within uncertainties as described in Section 7. Both normalization factors are free parameters in the fit. In this way, the background rate in the signal region is determined by the control region data yield. Decay-level optimal observables are considered in the signal region to test for signs of CP violation in the Higgs boson decay and to measure the BSM couplings under consideration.

A *production-only* fit searches for signs of CP-violation at the VBF production vertex. This fit uses events in the resonant $m_{4\ell}$ region ($115\text{ GeV} < m_{4\ell} < 130\text{ GeV}$) with at least two jets and $m_{jj} > 120\text{ GeV}$ for the signal extraction. To further enhance the VBF signal over other Higgs boson production modes, four VBF signal regions are defined as ascending intervals of the VBF score of a three-output neural network discriminant [22] trained to distinguish between VBF, VH and ggF events. The discriminant is trained on two-jet events using the di-jet mass, m_{jj} , the transverse momentum of the full system, $p_T^{4\ell jj}$, and the transverse momentum and η position of the individual leptons and jets, p_T^ℓ , η_ℓ , p_T^j and η_j . The discriminant interval boundaries are chosen to yield two regions with a large ggF admixture and two regions with a high VBF purity, while maintaining a steady variation in the event yield across categories. These are denoted by

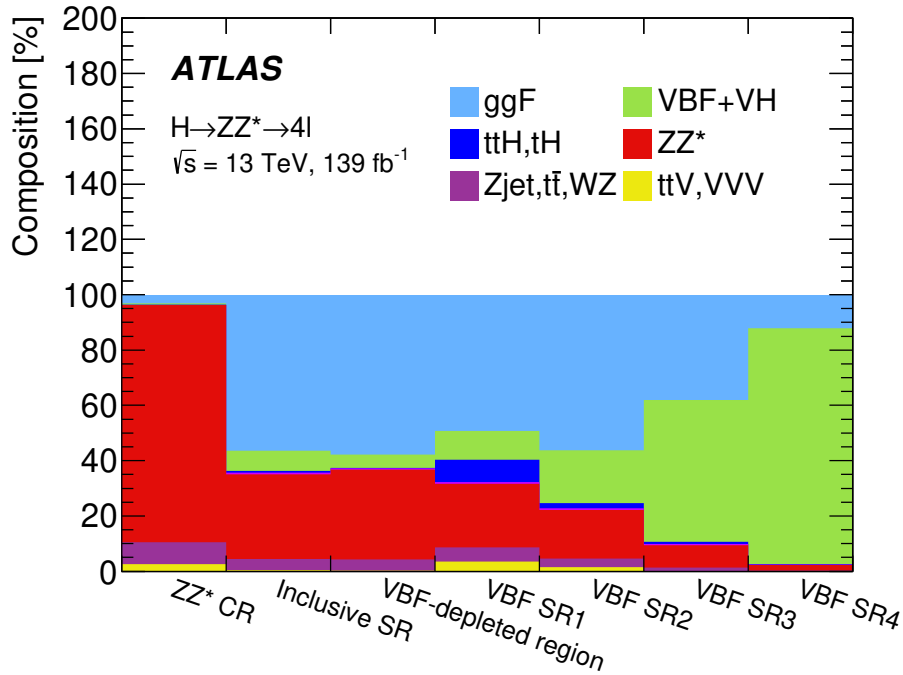


Figure 2: The composition of the predicted event yield in the event categories used for the direct EFT coupling measurements. The contribution from bbH is negligible and not visible in the plot. The MC statistical uncertainty in the fraction of each component is not shown but is below the 1% level.

‘VBF SR1’ through ‘VBF SR4’.

In addition to the four signal regions, two control regions are used. The first is the same ZZ^* CR as used in the decay-only fit, which allows the non-resonant background to be constrained. Events within the resonant $m_{4\ell}$ region that do not enter the VBF SR regions form a second control region, denoted by the ‘VBF-depleted region’. This is enriched in ggF events that represent the largest source of resonant background for this measurement. Three separate normalization factors relative to the SM prediction are assigned to the VBF/VH signal process, the ggF/ ttH/tH resonant background and the non-resonant ZZ^* background. The factors are common across all categories, and the fraction of the total yield entering each of the analysis categories is taken from the SM prediction. All three factors are free in the fit. In addition, for the VBF/VH signal process, the distribution of events among the four signal regions is allowed to vary in the fit, as BSM effects are expected to modify it. The fraction of VBF/VH events in the first two VBF regions is allowed to float in the fit while the last two regions are scaled accordingly to conserve the total yield across the four regions. The floating fraction is forced to be positive to ensure numerical stability of the fit. Production-level optimal-observable distributions are used in the signal regions (VBF SR 1–4).

Finally, a *combined* fit closely follows the production-only strategy. The VBF-depleted region takes the role of an additional signal region, in which decay-level optimal-observable distributions are fitted. Production-level observable distributions are fitted to events populating the four VBF signal regions. The same normalization strategy as for the production-only fit is used. This fit targets BSM signatures that have sensitivity in both the production and decay vertices.

In all fits, the reducible background is obtained directly from collision data and its normalization constrained to the measured value within its uncertainty.

Figure 2 shows the composition of the predicted SM yield in each of the analysis categories. The ZZ^* control region is highly pure in the non-resonant background. The VBF-depleted region and inclusive signal region are both dominated by the resonant signal, with a non-resonant admixture of the order of 30%. The VBF signal regions are increasingly pure in the resonant process, with a 30%-level non-resonant admixture in the first region. The purity of the VBF process relative to the ggF process increases across the four regions, up to a value of 90% in the final VBF SR 4 category.

In the signal regions of all three fits, the optimal-observable distributions are binned in 48 bins for the decay-level observables and in 12 bins for the production-level ones. The binning is optimized for each coupling assumption in the observable definition. The binning is constructed to yield an approximately flat distribution of expected events across the bins for a sample composed of 50% SM events and 25% events each simulated with a positive and a negative BSM coupling value close to the expected 68% CL limit.

To measure a given BSM coupling, the optimal observable evaluated with a BSM matrix element for the same coupling is used, separately for production (jj) and decay (4ℓ). This provides optimal sensitivity, as discussed in Section 2.2. When simultaneously measuring pairs of BSM couplings using decay-level optimal observables, a two-dimensional binning of the observables targeting the $c_{H\overline{W}}$ and $c_{H\overline{B}}$ couplings yields the largest sensitivity. In this case, six times six bins are used, optimized in the same way as for the one-dimensional binnings. Finally, when simultaneously measuring the \tilde{c}_{zz} and $\tilde{c}_{\gamma\gamma}$ couplings using the combined fit set-up, production-level observables targeting the \tilde{c}_{zz} coupling in the VBF signal regions are combined with decay-level observables targeting the $\tilde{c}_{\gamma\gamma}$ coupling in the VBF-depleted region. All control regions are treated as single-bin counting experiments.

Figure 3 shows expected optimal-observable distributions for production-level $OO_{jj}^{\tilde{c}_{zz}}$ and decay-level $OO_{4\ell}^{c_{H\overline{B}}}$ for the SM and two BSM samples. The optimal-observable distributions are symmetric in the SM case and asymmetric for CP-odd couplings. The two distributions have different binning: (a) has equal size binning, and (b) has an equally populated one, for a distribution composed of 50% SM and 25% for both $c_{H\overline{B}} = \pm 0.75$. Equally populated binning is used in the present analysis. The distributions of both plots, and the ratios of BSM to SM, clearly demonstrate the importance of the tails for a CP-asymmetry measurement.

6.2 Differential cross-section measurement

The main motivation for performing differential cross-section measurements is to have a model-independent result sensitive to possible deviations from the SM. The differential cross-section measurement of the optimal observables allows any CP-odd effects affecting the Higgs boson coupling to be probed. Unlike the direct coupling measurement, a differential cross-section measurement is sensitive to possible BSM effects on both the yields and the shape of the observable. The measurement is performed by unfolding the corresponding observable distribution within a fiducial phase space.

The fiducial phase space is defined using simulation at particle level and applying selection requirements to minimize model-dependent acceptance extrapolations. These are chosen to closely match the selection requirements of the detector-level analysis after the event reconstruction. The fiducial phase space definition is the same as described in Ref. [22] and summarized in Table 2.

Furthermore, as mentioned in Section 6.1, it is also interesting to investigate CP-odd effects using the VBF Higgs boson production vertex. For this reason, a fiducial cross-section is measured in a VBF-enriched phase space. In addition to the selections in Table 2, the VBF-enriched fiducial region requires the presence

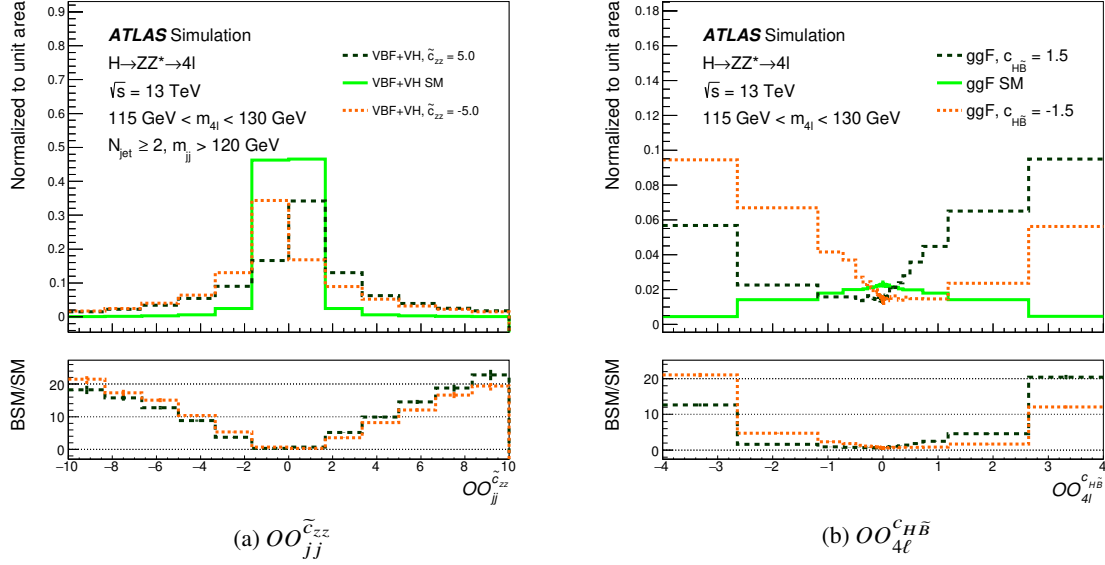


Figure 3: Expected distributions of (a) the $OO_{jj}^{c_{zz}}$ observable for VBF-produced Higgs boson candidates combining VBF SR1 through SR4 for the SM and for BSM coupling parameter values of $\tilde{c}_{zz} = \pm 5$, and (b) the $OO_{4\ell}^{c_{H\tilde{B}}}$ observable for the decay of ggF produced Higgs boson candidates in the inclusive SR for the SM and for BSM coupling parameter values of $c_{H\tilde{B}} = \pm 1.5$. (a) has 12 equal-size bins, and (b) has 48 equal population bins. In (b) the first and last bins extend up to ± 40 , but the bin range is truncated to ± 4 in the plot for clarity. The lower panels show the ratio of the BSM to the SM optimal-observable distributions.

of at least two jets with an invariant mass $m_{jj} \geq 400$ GeV, and a difference between the η of the leading and of the subleading jet of $|\Delta\eta_{jj}| \geq 3.0$. These selections replace the neural network used to define the VBF SR regions of the direct coupling measurement. Two separate fiducial cross-sections are extracted from the VBF-enriched fiducial region, resulting in different levels of VBF purity. For the first, a ‘combined production mode’ Higgs boson signal is extracted with ggF, VBF, VH and ttH considered as signal. For the second the Higgs boson signal is extracted while additionally removing the ggF production mode signal using the MC expectation. This VBF-enriched fiducial region has a signal composition of 59.3% VBF, 37.5% ggF, 1.7% VH and 1.5% ttH . The VBF purity increases to 95% if the ggF is removed as a background. Although the first fiducial cross-section is less pure in VBF signal, it is less model dependent because it has no assumption on the signal composition. The second fiducial cross-section relies on the assumption of SM ggF production.

To extract the number of signal events in each bin of a differential distribution, invariant mass templates for the Higgs boson signal and the background processes are fitted to the $m_{4\ell}$ distribution in data, following the same strategy as used in Ref. [22]. The non-resonant ZZ^* background is fitted simultaneously with the signal and constrained by extending the $m_{4\ell}$ fit range from 115–130 GeV to 105–160 GeV, similar to the control region used in the direct coupling measurement. Furthermore, the SM $ZZ^* \rightarrow 4\ell$ decay fractions are assumed. To reduce the effects of bin-to-bin statistical fluctuations of the non-resonant ZZ^* background, neighbouring bins are combined for this background estimate. The overall normalization and shape of the reducible background from a data-driven evaluation (Section 5.3) are allowed to vary within their associated systematic uncertainties (Section 7).

Table 2: List of event selection requirements that define the fiducial phase space for the cross-section measurement. SFOC lepton pairs are same-flavour opposite-charge lepton pairs. For the mass requirement of the subleading lepton pair, $m_{\text{threshold}}$ is 12 GeV for $m_{4\ell} < 140$ GeV and rises linearly until reaching 50 GeV for $m_{4\ell} = 190$ GeV.

Leptons and jets	
Leptons	$p_T > 5$ GeV, $ \eta < 2.7$
Jets	$p_T > 30$ GeV, $ y < 4.4$
Lepton selection and pairing	
Lepton kinematics	$p_T > 20, 15, 10$ GeV
Leading pair (m_{12})	SFOC lepton pair with smallest $ m_Z - m_{\ell\ell} $
Subleading pair (m_{34})	Remaining SFOC lepton pair with smallest $ m_Z - m_{\ell\ell} $
Event selection (at most one quadruplet per event)	
Mass requirements	$50 \text{ GeV} < m_{12} < 106 \text{ GeV}$ and $m_{\text{threshold}} < m_{34} < 115 \text{ GeV}$
Lepton separation	$\Delta R(\ell_i, \ell_j) > 0.1$
Lepton/Jet separation	$\Delta R(\ell_i, \text{jet}) > 0.1$
J/ψ veto	$m(\ell_i, \ell_j) > 5$ GeV for all SFOC lepton pairs
Mass window	$105 \text{ GeV} < m_{4\ell} < 160 \text{ GeV}$
If an extra lepton with $p_T > 12$ GeV is found, the quadruplet with the largest matrix element value is kept	

The expected number of events N_i in each detector-level observable bin i , expressed as a function of $m_{4\ell}$, is given by

$$N_i(m_{4\ell}) = \sum_j r_{ij} \cdot (1 + f_i^{\text{nonfid}}) \cdot \sigma_j^{\text{fid}} \cdot \mathcal{P}_i(m_{4\ell}) \cdot \mathcal{L} + N_i^{\text{bkg}}(m_{4\ell}) \quad (4)$$

with the fiducial cross-section in each fiducial bin j given by

$$\sigma_j^{\text{fid}} = \sigma_j \cdot A_j \cdot \mathcal{B}$$

where A_j is the acceptance in the fiducial phase space for a total cross-section σ_j in fiducial bin j , \mathcal{L} is the integrated luminosity, \mathcal{B} is the decay branching ratio and $N_i^{\text{bkg}}(m_{4\ell})$ is the background contribution. The index j runs over all observable bins in the fiducial phase space. The term $\mathcal{P}_i(m_{4\ell})$ is the $m_{4\ell}$ signal shape containing the fraction of events as a function of $m_{4\ell}$ expected in each reconstruction bin, taken from MC simulation. The term r_{ij} represents the detector response matrix, created with simulated signal samples and averaged across the different production modes using the expected SM cross-sections [36]. These factors correspond to the probability that an event generated within the fiducial volume in the observable bin j is reconstructed in bin i . The normalization, f_i^{nonfid} , represents the fraction of events that are outside of the fiducial region but are reconstructed within the SR. This ranges from 1.1% to 1.7% depending on the bin of the unfolded observable or the final state. The detector response matrix accounts for bin-to-bin migrations in the unfolding of the signal. The binning choice made for all observables ensures a statistical significance of more than two standard deviations for the SM signal process. The binning is also chosen to minimize migrations between bins. In most cases, the bin width is more than twice the experimental resolution.

For the VBF-enriched fiducial cross-section measurements, the signal is extracted by unfolding the two-dimensional distribution m_{jj} versus $|\Delta\eta_{jj}|$ that is divided into three bins (see Figure 14), following the strategies explained previously. The difference for the second measurement is that the ggF is considered to be a background and the expected ggF signal is moved from $\mathcal{P}_i(m_{4\ell})$ to $N_i^{\text{bkg}}(m_{4\ell})$ of Eq. (4).

7 Systematic uncertainties

The statistical uncertainty in the data is generally dominant in all aspects of the analysis, and systematic uncertainties play a minor role. Systematic uncertainties arise from experimental sources, such as lepton and jet momentum scales, resolutions and reconstruction efficiencies, and theoretical uncertainties related to the modelling of the signal and background processes. In addition, a set of uncertainties specific to the cross-section extraction method affect the differential cross-section measurement.

As the rates of all key contributing processes are determined using the collision data, normalization uncertainties affecting their total calculated cross-sections have no impact. Uncertainties in the determination of the kinematic observables characterising the final state, in particular jet and lepton momentum scale and resolutions, affect the analysis in the most direct way through the reconstructed value of the optimal observables. Uncertainties in the relative rates between the various categories, arising for example from theoretical sources, affect the results indirectly via changes in the process composition in the signal regions and migration effects in the cross-section measurement. While still small compared to statistical uncertainties, these composition uncertainties are the leading source of systematic uncertainty in the direct coupling measurement. The measured differential cross-sections are also sensitive to luminosity and lepton reconstruction and isolation efficiency uncertainties, which play a negligible role for the direct coupling measurement.

When predicting BSM effects in the direct coupling measurement, theoretical uncertainties due to the PDF, parton shower, and QCD scale variations are assigned to the signal predictions based on SM signal samples, which are simulated with higher-order precision. The same uncertainties are assigned to all corresponding BSM signal predictions, since it is observed using the MC signal samples simulated at leading-order accuracy that the uncertainties change negligibly as a function of the Wilson coefficients.

An overview of the main sources and their impact on the analysis is provided below.

7.1 Experimental uncertainties

The uncertainty in the measured differential cross-sections due to pile-up modelling is of the order of 1%. The uncertainty in the combined 2015–2018 integrated luminosity is 1.7% [83], obtained using the LUCID-2 detector [84] for the primary luminosity measurements. The luminosity uncertainty directly propagates to the measured cross-sections. Neither source affects the direct coupling measurement.

The electron (muon) reconstruction and identification efficiency uncertainties in the extracted cross-sections are of the order of 1–2% ($\leq 1\%$). Isolation efficiency uncertainties affect the results at a similar magnitude. Lepton efficiencies have a negligible impact on the direct coupling measurement since they do not induce asymmetries in the CP-sensitive observables.

Lepton energy, momentum scale and resolution uncertainties affect both the direct coupling measurement and the extracted cross-sections at the order of 1–2% level due to their relation to the reconstructed rest-frame kinematics determining the optimal observables.

The impact of uncertainties in the jet energy scale and resolution is only relevant for production-level optimal observables. There, they affect the differential cross-sections at the 1–5% level and the directly extracted coupling values at the 1–3% level.

The impact of the precision of the Higgs boson mass measurement on the signal acceptance due to the signal region mass-window requirement is considered for the cross-section extraction but found to have a negligible impact ($< 1\%$).

For the data-driven measurement of the reducible background, three sources of uncertainty are considered: statistical uncertainty, overall systematic uncertainty for muon and electron background fake estimates [22], and a shape systematic uncertainty that varies with the differential variable [28]. All of these have a negligible impact on the analysis.

7.2 Theoretical uncertainties

The theoretical modelling of the signal and background processes is affected by uncertainties due to missing higher-order corrections, modelling of parton showers and the underlying event, and PDF plus α_s uncertainties.

One of the dominant sources of theoretical uncertainty is the prediction of the ggF process, in particular its contribution to the dijet signal regions targeting production observables. To estimate the variations due to the impact of higher-order contributions not included in the calculations, the approach described in Refs. [36, 85] is used, which exploits the latest predictions for the inclusive jet cross-sections. In particular, the uncertainty from the choice of factorization and renormalization scales, the choice of resummation scales, and the migrations between the 0-jet and 1-jet phase space bins or between the 1-jet and ≥ 2 -jet bins are considered. The detailed procedure is described in Ref. [22]. The impact of these uncertainties can reach 5% of the directly measured coupling value and 1–2% of the measured differential cross-sections.

The uncertainties in the acceptance and distribution of yields among the analysis regions due to the modelling of parton showers and the underlying event are estimated with AZNLO tune [86] eigenvector variations and by comparing the results using the parton showering algorithm from PYTHIA 8 with that from HERWIG 7 [87] for all signal processes. The eigenvector variations are correlated between the Higgs boson production modes, while the algorithm uncertainty is treated as uncorrelated. This is the largest individual systematic uncertainty source when considering production-level optimal observables, with a magnitude in the range of 2–10% of the measured cross-sections in the differential measurement and 1–5% of the directly measured BSM coupling values.

For the VBF, VH and ttH production modes, the uncertainty due to missing higher orders in QCD is parameterized using the scheme outlined in Ref. [88]. Compared to the uncertainties in the ggF contribution, both the scale and the shower uncertainties in these predictions are negligible.

The impact of the PDF uncertainty is estimated with the 30 eigenvector variations of the PDF4LHC_{NLO}30 Hessian PDF set following the PDF4LHC recommendations [54]. The modification of the predictions originating from each eigenvector variation is added as a separate source of uncertainty in the model. The same procedure is applied for the ggF, VBF, VH and ttH processes. PDF uncertainties have a negligible impact.

Beside the resonant process, uncertainties in the prediction of the main non-resonant $q\bar{q} \rightarrow ZZ^*$ background process affect the analysis. As the normalization of this background is obtained from collision data, the main impact is from migration effects between various regions. The uncertainties due to missing higher-order effects in QCD are estimated by varying the factorization and renormalization QCD scales by a factor of two; the impact of the PDF uncertainty is estimated by using the MC replicas of the NNPDF3.0 PDF set. Uncertainties due to parton shower modelling for the ZZ^* process are considered as well. For the

differential cross-section measurement, a comparison of the ZZ^* predictions of the $m_{4\ell}$ spectrum used to normalize this background to the ones obtained using the alternative generators described in Section 4 is used to define an additional systematic uncertainty. The impact of these uncertainties is very small, less than 2% on the directly measured couplings and negligible for the differential cross-sections.

7.3 Uncertainties specific to the differential cross-section extraction

Unfolding-related uncertainties arise from the production mode composition that determines the average response matrices, and from residual biases introduced by the unfolding method [28]. For the former, an uncertainty is assessed by varying the production cross-sections within their measured uncertainties taken from Ref. [89], with an impact of less than 1%. The uncertainty arising from unfolding biases is obtained independently for each bin by comparing the unfolded cross-section from simulation with that expected when varying the underlying particle-level cross-sections of the simulated data sample within the expected statistical error. In the same way, the uncertainty is extended to also account for differences that arise from using an SM response matrix to measure observable distributions possibly affected by BSM behaviour by means of signal injection (up to 95% CL of a possible CP-odd coupling). The impact of this uncertainty is typically around 1–2% in the decay optimal observable, where the response matrix is largely diagonal, and increases up to 7% in the production optimal-observable distributions, which have larger bin migrations.

7.4 Monte Carlo statistics

The effect of MC statistical uncertainties is included in the statistical model used for the measurement, as the direct coupling measurement relies on precise shape predictions for the optimal observables and other systematic uncertainties are very small. The signal modelling technique results in a negligible impact of statistical uncertainties on the prediction of BSM effects. The largest contribution to the MC statistical uncertainty is linked to the non-resonant $q\bar{q} \rightarrow ZZ^*$ background prediction, affecting the measured coupling values at the level of few percent. This is negligible compared to statistical uncertainties in the data, but comparable (1–2% impact) to the leading systematic uncertainty sources for coupling measurements using decay-level observables, due to the small size of the systematic uncertainties in these measurements.

8 Results

8.1 Direct coupling measurement results

The number of events observed and the expected (pre-fit) contributions in each of the categories used in the coupling measurements, described in Section 6.1 and Figure 1, are shown in Figure 4 and Table 3. Combined statistical and systematic uncertainties are included for the predictions (see Section 7). As discussed in Section 6.1, the ZZ^* CR and Inclusive SR contribute to the decay observable fits, and the rest contribute to the production-only and combined observable fits. In all categories, the number of events observed and the expectation agree within one to two standard deviations. The largest difference occurs in the most sensitive VBF category, VBF SR4, where the small number of observed events exceeds the expectation by about a factor of two.

Table 3: The numbers of expected and observed events in the event categories for the direct CP measurement, in the mass range $115 \text{ GeV} < m_{4\ell} < 130 \text{ GeV}$. The sum of the number of expected SM Higgs boson events and the estimated background yields is compared with the data. Combined statistical and systematic uncertainties are included for the predictions. The Inclusive SR, used in the decay-only fit, is composed of the VBF-depleted Region and VBF SR1 to SR4.

	ZZ^* CR	Inclusive SR	VBF-depleted Region	VBF			
				SR1	SR2	SR3	SR4
ggF	8.2 ± 1.3	181 ± 12	165 ± 12	$7.5^{+3.0}_{-2.4}$	$5.6^{+1.8}_{-1.5}$	2.2 ± 0.6	0.49 ± 0.17
bbH	$0.087^{+0.016}_{-0.015}$	1.85 ± 0.05	1.65 ± 0.05	0.11 ± 0.01	$0.072^{+0.010}_{-0.009}$	$0.020^{+0.005}_{-0.003}$	< 0.01
VBF/VH	1.39 ± 0.16	23.8 ± 0.7	13.8 ± 0.6	$1.60^{+0.09}_{-0.08}$	1.89 ± 0.11	3.01 ± 0.18	3.5 ± 0.4
ttH, tH	$0.22^{+0.03}_{-0.04}$	$1.89^{+0.21}_{-0.22}$	0.44 ± 0.05	1.22 ± 0.14	0.179 ± 0.023	$0.046^{+0.009}_{-0.010}$	< 0.01
ttV, VVV	6.79 ± 0.13	1.31 ± 0.06	0.62 ± 0.04	0.53 ± 0.04	0.150 ± 0.020	< 0.01	< 0.01
ZZ^*	229^{+20}_{-25}	98^{+6}_{-9}	92^{+6}_{-8}	$3.5^{+1.3}_{-1.7}$	1.7 ± 0.6	$0.48^{+0.16}_{-0.15}$	$0.086^{+0.025}_{-0.028}$
Zjet, $t\bar{t}, WZ$	21 ± 5	13 ± 4	12 ± 3	0.8 ± 0.9	0.3 ± 0.6	0.07 ± 0.26	0.01 ± 0.09
Total SM	267^{+21}_{-26}	321^{+14}_{-15}	286^{+14}_{-15}	15 ± 3	$9.9^{+2.0}_{-1.7}$	5.9 ± 0.7	4.1 ± 0.5
Data	294	311	276	14	9	4	8

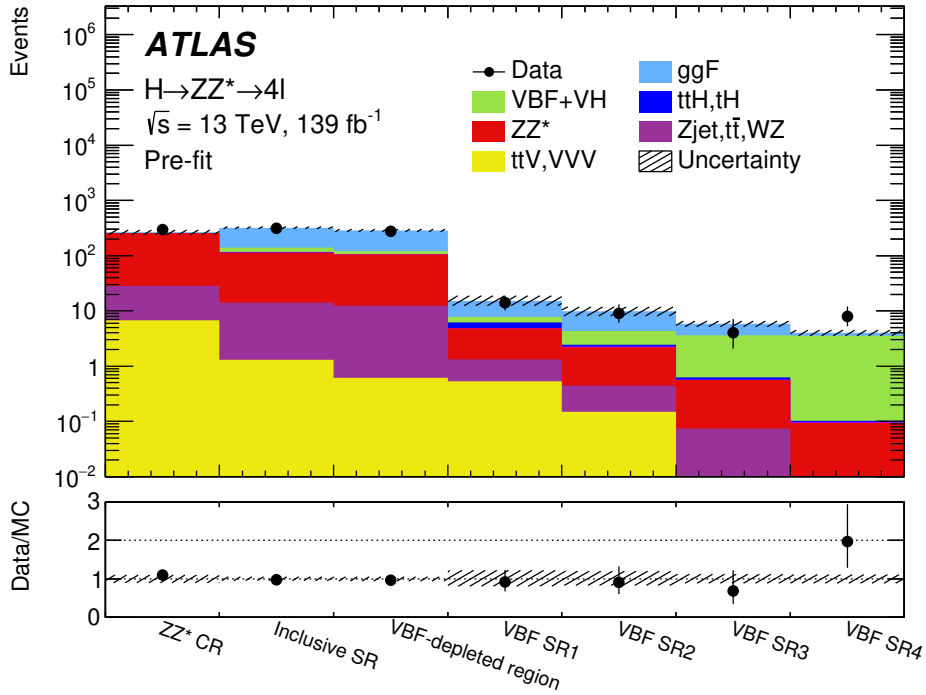


Figure 4: The number of observed events and the expected contributions in each of the categories used in the decay-only, production-only, and combined observable fits for the coupling measurements. The contribution from bbH is negligible and not visible in the plot. The lower panel shows the ratio of data to expectation. The shaded bands in both the upper and lower panels correspond to the combined statistical and systematic uncertainties in the predictions.

The observed and expected distributions for the production-level observable $OO_{jj}^{\widetilde{c}_{zz}}$ in each of the four VBF signal regions are shown in Figure 5. The corresponding observed and expected distributions for the decay level observables $OO_{4\ell}^{c_{H\widetilde{B}}}$, $OO_{4\ell}^{c_{H\widetilde{W}B}}$, $OO_{4\ell}^{c_{H\widetilde{W}}}$, and $OO_{4\ell}^{\widetilde{d}}$ are shown in Figure 6. The expected distributions for the SM are shown as stacked histograms, and the two lines show the expectation for an additional positive or negative CP-odd BSM coupling that has a clear excess in the tail. The combined statistical and systematic uncertainties are shown in the ratio plot below each distribution. Overall there is good agreement between data and the SM expectation. The mean value for the data is given for each distribution, calculated from the observable value for each event. All mean values are compatible with zero, indicating that the data exhibit no measurable asymmetry.

In absence of positive evidence for BSM physics, 68% and 95% confidence intervals on the CP-odd couplings (\mathbf{c}_{BSM}) are extracted with the profile likelihood ratio [90] statistical test, using the negative-log likelihood (NLL) test statistic:

$$-2 \ln \lambda(x|\mathbf{c}_{\text{BSM}}) = -2 \ln \frac{\mathcal{L}(x|\mathbf{c}_{\text{BSM}}, \hat{\theta})}{\mathcal{L}(x|\hat{\mathbf{c}}_{\text{BSM}}, \hat{\theta})} \quad (5)$$

where θ corresponds to the set of systematic uncertainties, or nuisance parameters. The numerator denotes the conditional likelihood estimator of θ , (*i.e.*, $\hat{\theta}$ is the value of θ that maximizes the likelihood function for a given \mathbf{c}_{BSM}), and the denominator denotes the maximized likelihood estimator (*i.e.*, $\hat{\mathbf{c}}_{\text{BSM}}$ and $\hat{\theta}$ are the values of \mathbf{c}_{BSM} and θ that maximize the unconditional likelihood function). The effect of the nuisance parameters is to broaden the profile likelihood ratio reflecting the loss of information originating from the inclusion of systematic uncertainties. For each BSM coupling, a scan across the values of \mathbf{c}_{BSM} of the NLL is performed by fitting all other parameters (normalization parameters, other BSM couplings, and nuisance parameters) to obtain the values that minimize the NLL for the current value of the coupling being scanned, or couplings for two-dimensional scans. This result relies on the assumption that for any value of the coupling being scanned, the NLL behaves as a χ^2 distribution with one degree of freedom (*asymptotic approximation* [91]). Based on this, the confidence intervals are constructed from the scan parameter values for which the NLL crosses the 68% and 95% quantile locations of a χ^2 distribution with one degree of freedom. The validity of the asymptotic approximation for this measurement was confirmed by sampling the distribution of the test statistic observed on toy datasets obtained by random sampling from the predicted likelihood model.

The expected sensitivity of the seven couplings explored in this analysis (Section 2.3) are given in Table 4. The expected 95% confidence intervals estimated separately for either VBF production or Higgs boson to four-lepton decay and as well for their combination are shown for each coupling. There are about ten VBF events expected in the signal region and over 200 expected Higgs boson decays from all production modes in the inclusive signal region, giving a significant statistical advantage to the decay observable fits. For the Higgs basis that has couplings in the mass Lagrangian, production is predominantly sensitive to the \widetilde{c}_{zz} coupling with a limited sensitivity to $\widetilde{c}_{z\gamma}$, and decay is sensitive to both $\widetilde{c}_{z\gamma}$ and $\widetilde{c}_{\gamma\gamma}$. This can be understood from the fact that the VBF production includes also W -boson diagrams and occurs at larger energy scales compared to the decay vertex, which happens at the scale of the Higgs mass and exclusively via neutral gauge bosons, enhancing the role of virtual photon diagrams. For the Warsaw basis that has couplings in the interaction Lagrangian before SU(2) symmetry breaking, the physical interpretation is less intuitive: $c_{H\widetilde{W}}$ has sensitivity to both production and decay with the latter having improved sensitivity due to the larger number of events, $c_{H\widetilde{B}}$ and $c_{H\widetilde{W}B}$ are both only sensitive to the decay. Finally \widetilde{d} , which is proportional to $c_{H\widetilde{B}}$ with the constraints $c_{H\widetilde{B}} = c_{H\widetilde{W}}$ and $c_{H\widetilde{W}B} = 0$, is mostly sensitive to the decay. The combined observable fits use the VBF SR1 to VBF SR4 for the production

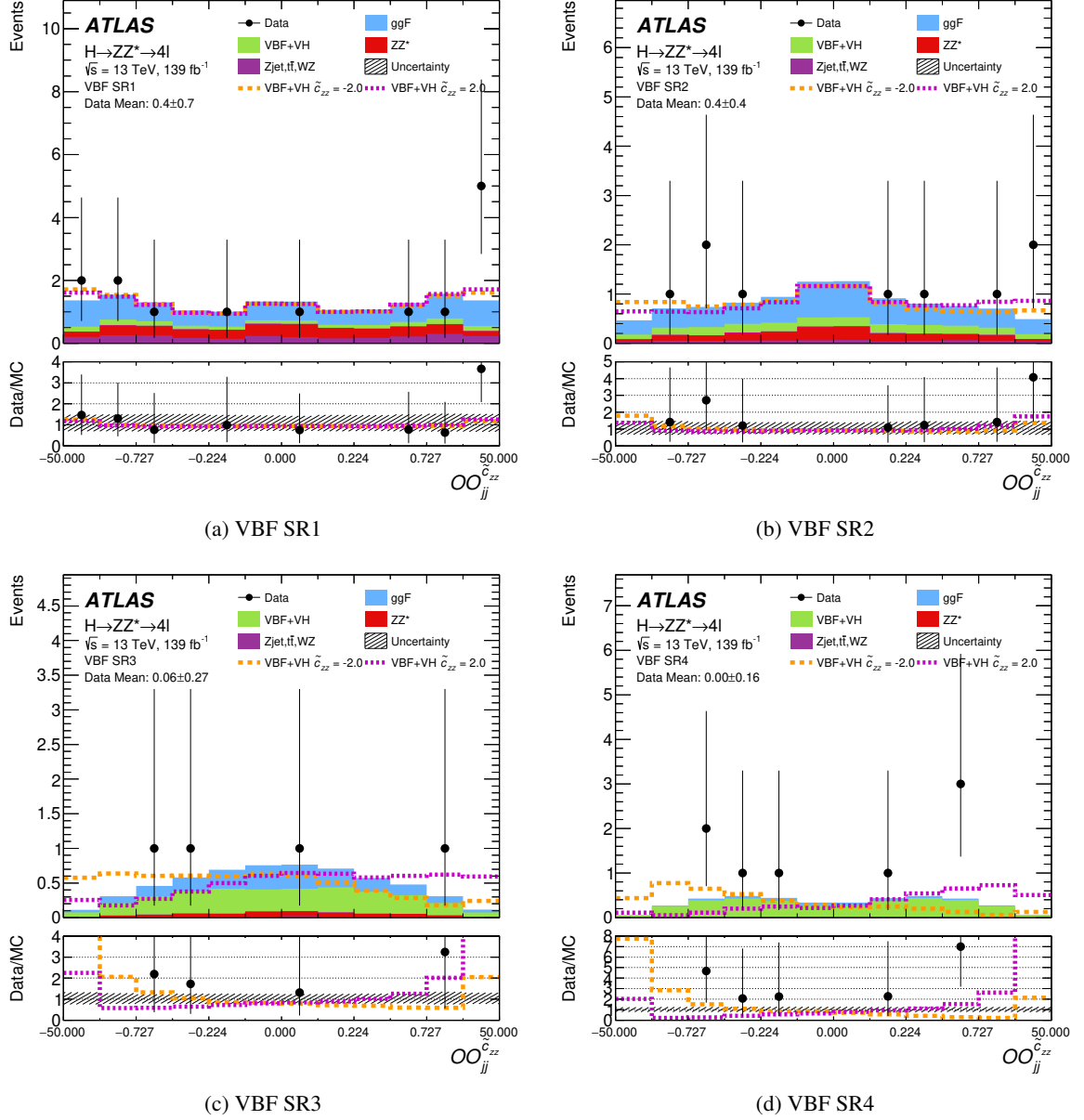


Figure 5: The observed and expected distributions for the production-level observable $OO_{jj}^{\tilde{c}_{ZZ}}$ in each of the four VBF signal regions: (a) SR1, (b) SR2, (c) SR3, and (d) SR4. The expected distribution for the VBF signal and the backgrounds from ggF, ZZ^* , and reducible backgrounds are shown as a stacked histogram. Also shown are the expected distributions in presence of CP-odd contributions for $\tilde{c}_{ZZ} = \pm 2.0$, assuming the VBF/VH event rate remains that of the SM. The bin size is variable, optimized for an approximately flat distribution for the SM combined with a positive and negative BSM scenario. The mean value of the optimal observable across the data events is given with its standard deviation. The lower panels show the ratio of data to expectation and the shaded band corresponds to the combined statistical and systematic uncertainties in the predictions.

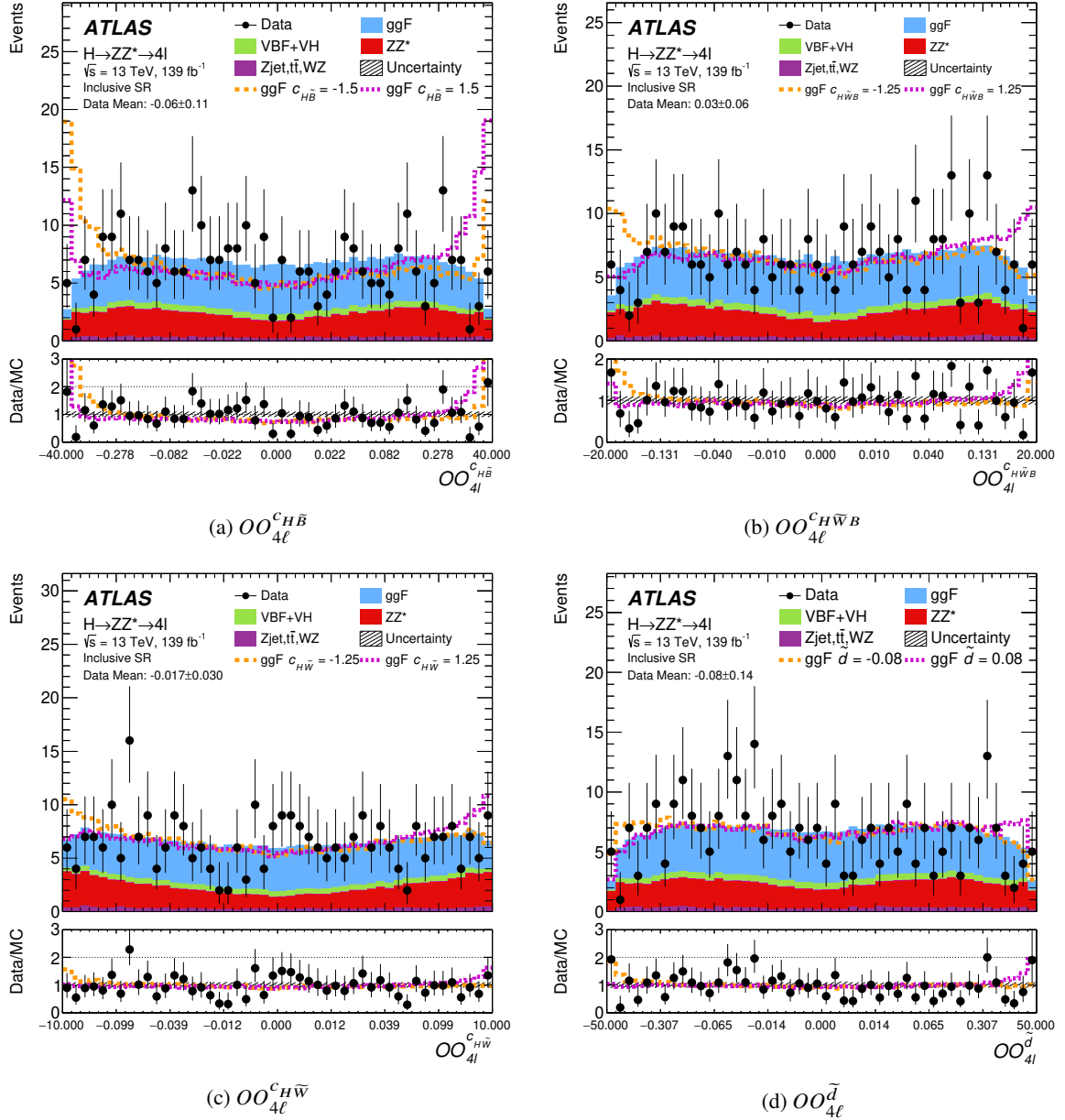


Figure 6: The observed and expected distributions for the decay level observables: (a) $OO_{4l}^{c_{H\bar{B}}}$, (b) $OO_{4l}^{c_{H\bar{W}B}}$, (c) $OO_{4l}^{c_{H\bar{W}}}$ and (d) $OO_{4l}^{\bar{d}}$. The expected distribution for the ggF and VBF signals and the backgrounds from ZZ^* and reducible backgrounds are shown as a stacked histogram. Also shown are the expected distributions in presence of CP-odd contributions for (a) $c_{H\bar{B}} = \pm 1.5$, (b) $c_{H\bar{W}B} = \pm 1.25$, (c) $c_{H\bar{W}} = \pm 1.5$ and (d) $\bar{d} = \pm 1.25$, assuming the signal event rate remains that of the SM. The bin size is variable, optimized for an approximately flat distribution for the SM combined with a positive and negative BSM scenario. There are no observed events that fall outside the optimal-observable distribution range, with rate expectations below 0.1%. The mean value of the optimal observable across the data events is given with its standard deviation. The lower panels show the ratio of data to expectation and the shaded band corresponds to the combined statistical and systematic uncertainties in the predictions.

observable and the VBF-depleted signal region for the decay observable. This reduces by about 10% the number of events entering the decay observable fit, i.e., those in VBF SR1 to VBF SR4, and can lead to a degraded sensitivity of the combined fit compared to the decay fit in the inclusive signal region. This is the case for $\tilde{c}_{z\gamma}$ and \tilde{d} , since their production sensitivity is poor. Whereas for $c_{H\widetilde{W}}$, which has a more balanced sensitivity for production and decay, the combination limits improve over either production or decay only.

Table 4: The expected 95% confidence intervals of production-only, decay-only and combined production and decay likelihood scans for the CP-odd Wilson coefficients in the Warsaw and Higgs bases for an integrated luminosity of 139 fb^{-1} at $\sqrt{s} = 13 \text{ TeV}$. Only one Wilson coefficient is fitted at a time while all others are set to zero. Limits denoted by ‘-’ indicates no sensitivity. All couplings scale as $1/\Lambda^2$ with the assumed value of $\Lambda = 1 \text{ TeV}$.

EFT coupling	Expected 95% CL		
	production-only	decay-only	combined
$c_{H\widetilde{B}}$	–	± 0.37	–
$c_{H\widetilde{W}B}$	–	± 0.72	–
$c_{H\widetilde{W}}$	± 4.8	± 1.34	± 1.27
\tilde{d}	± 0.63	± 0.018	± 0.019
\tilde{c}_{zz}	± 2.4	–	–
$\tilde{c}_{z\gamma}$	± 6.6	± 0.76	± 0.80
$\tilde{c}_{\gamma\gamma}$	–	± 0.76	–

The expected and observed distributions for the \tilde{c}_{zz} coupling NLL production scans are shown in Figure 7(a). The observed central value for \tilde{c}_{zz} at 0.78 and the non-parabolic shape of the NLL is due to the small excess of VBF candidates at positive \tilde{c}_{zz} in SR1 (Figure 5(a)). The effect of systematic uncertainties, primarily jet-related, is about 15% for the expected 95% CL. In the observed NLL scan, a local enhancement of the impact of systematic uncertainties for small absolute values of the BSM coupling is driven by the ggF parton-shower uncertainty, which primarily affects the migration of ggF events between the control region and the VBF-enriched signal regions, as discussed in Section 7.2. For small couplings, where the VBF optimal-observable distribution is like the SM, this uncertainty allows the fit model to adapt to the observed local downward fluctuation in the central bins of the VBF SR1, leading to a comparably large impact of this uncertainty. In Figure 7(b), the observed NLL distributions are shown for $c_{H\widetilde{W}}$ for production, decay and their combination, as well as the expected distribution for the combination. The observed central value at 1.5 of the production-only $c_{H\widetilde{W}}$ scan arises from the same excess of VBF candidates as for \tilde{c}_{zz} . Combining with the decay-only scan (central value about 0.1), reduces the combined central value to 0.6. There is a small effect of systematic uncertainties on the production-only limits, with a local increase of their impact around zero originating from the same effect described above for the \tilde{c}_{zz} coupling. The $c_{H\widetilde{W}}$ decay-only scan has a better statistical precision than the production-only scan and relies only on the well-measured lepton kinematics, so the effect of systematic uncertainties is negligible.

The observed and expected NLL observable scans for the decay level couplings for the Warsaw basis $c_{H\widetilde{B}}$, $c_{H\widetilde{W}B}$, $c_{H\widetilde{W}}$ and \tilde{d} are shown in Figure 8, and for the Higgs basis $\tilde{c}_{z\gamma}$ and $\tilde{c}_{\gamma\gamma}$ are shown in Figure 9. Similarly to the combined scan of $c_{H\widetilde{W}}$ in Figure 7(b), the decay-only optimal-observable fits have a negligible contribution from systematic uncertainties. Due to the small upward fluctuation of the data in

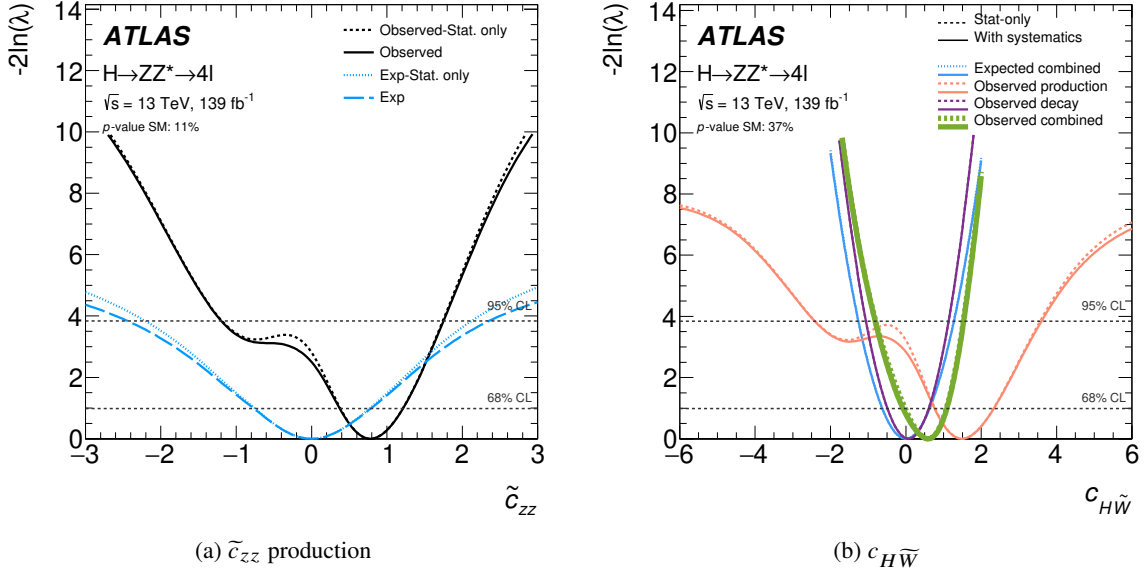


Figure 7: The NLL observable scans as a function of (a) \tilde{c}_{zz} for the production-only $OO_{jj}^{\tilde{c}_{zz}}$ fit, and (b) $c_{H\tilde{W}}$ for production-only $OO_{jj}^{c_{H\tilde{W}}}$, decay-only $OO_{4\ell}^{c_{H\tilde{W}}}$, and combined fits. The \tilde{c}_{zz} coupling NLL scan shows the expected and observed distributions with (solid line) and without (dashed line) systematic uncertainties. For the $c_{H\tilde{W}}$ coupling, sensitive to both production and decay, the expected NLL scan is shown only for the combined fit (blue). The observed NLL scans for $c_{H\tilde{W}}$ are shown for production-only, decay-only, and their combined (thicker line) fit. The p -value for agreement with the SM is 0.11 (0.37) for the \tilde{c}_{zz} ($c_{H\tilde{W}}$) coupling NLL scan. All couplings scale as $1/\Lambda^2$ with the assumed value of $\Lambda = 1$ TeV.

the first and last observable bins in Figure 6 the observed NLL scans for $OO_{4\ell}^{c_{H\tilde{B}}}$, $OO_{4\ell}^{c_{H\tilde{W}B}}$ and $OO_{4\ell}^{\tilde{d}}$ are less constraining than expected. The small upward fluctuation around zero for $OO_{4\ell}^{c_{H\tilde{W}}}$ leads to tighter limits than expected. In the Higgs basis, the observed decay-only scans for $OO_{4\ell}^{\tilde{c}_{z\gamma}}$ and $OO_{4\ell}^{\tilde{c}_{\gamma\gamma}}$ are also less constrained.

The observed and expected 68% and 95% CL two-dimensional contours for all three pairings of the Warsaw-basis couplings, $c_{H\tilde{B}}$, $c_{H\tilde{W}B}$ and $c_{H\tilde{W}}$, are shown in Figures 10(a)–10(c). The two-dimensional observable $OO_{4\ell}^{c_{H\tilde{B}}}$ vs $OO_{4\ell}^{c_{H\tilde{W}}}$ is used for these decay-only contours. This observable pair is found empirically to have the best expected sensitivity compared with any of the individual observables or other observable pairings. The observed minima in Figures 10(a)–10(c) all lie along the diagonals of the confidence interval ellipses, well within the 68% CL. These diagonals are relatively flat in terms of the likelihood minima. Figure 10(d) shows the two-dimensional contours for scans along \tilde{c}_{zz} versus $\tilde{c}_{\gamma\gamma}$, where \tilde{c}_{zz} is sensitive only to the production and $\tilde{c}_{\gamma\gamma}$ is sensitive only to the decay. For \tilde{c}_{zz} , the events in VBF SR1 to SR4 are used with the observable $OO_{jj}^{\tilde{c}_{zz}}$ in 12 bins, as shown in Figure 7(a), and for $\tilde{c}_{z\gamma}$ the events in the VBF-depleted region are used with $OO_{4\ell}^{\tilde{c}_{z\gamma}}$ in 48 bins as shown in Figure 9(b). As shown in Eq. (1), all couplings of Figures 7–10 scale as $1/\Lambda^2$ with the assumed value of $\Lambda = 1$ TeV.

Figure 11 and Table 5 summarize the expected and observed confidence intervals at 68% and 95% CL for the CP-odd Wilson coefficients. The limits for the Higgs-basis Wilson coupling \tilde{c}_{zz} are from a production-only observable fit. Those for the coupling $c_{H\tilde{W}}$ are from a combined-observable fit as this coupling has

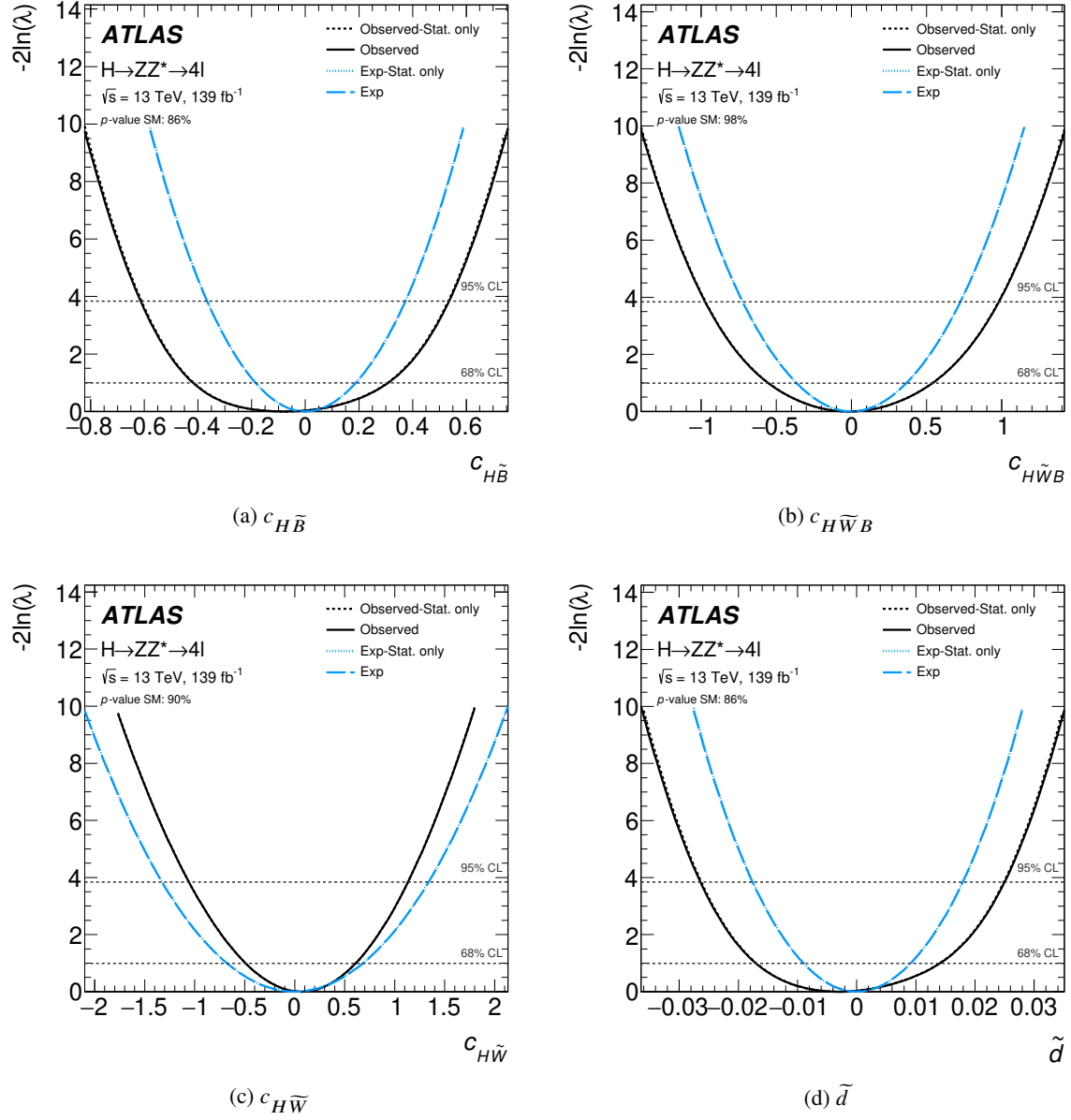


Figure 8: The NLL observable scans for the Warsaw-basis couplings for decay-only fits: (a) $c_{H\tilde{B}}$ ($OO_{4\ell}^{c_{H\tilde{B}}}$), (b) $c_{H\tilde{W}B}$ ($OO_{4\ell}^{c_{H\tilde{W}B}}$), (c) $c_{H\tilde{W}}$ ($OO_{4\ell}^{c_{H\tilde{W}}}$), and (d) \tilde{d} ($OO_{4\ell}^{\tilde{d}}$). The expected and observed distributions are shown with (solid line) and without (dashed line) systematic uncertainties. The p -values for agreement with the SM are 0.86, 0.98, 0.90 and 0.86 for the $c_{H\tilde{B}}$, $c_{H\tilde{W}B}$, $c_{H\tilde{W}}$, and \tilde{d} coupling NLL scans, respectively. All couplings scale as $1/\Lambda^2$ with the assumed value of $\Lambda = 1$ TeV.

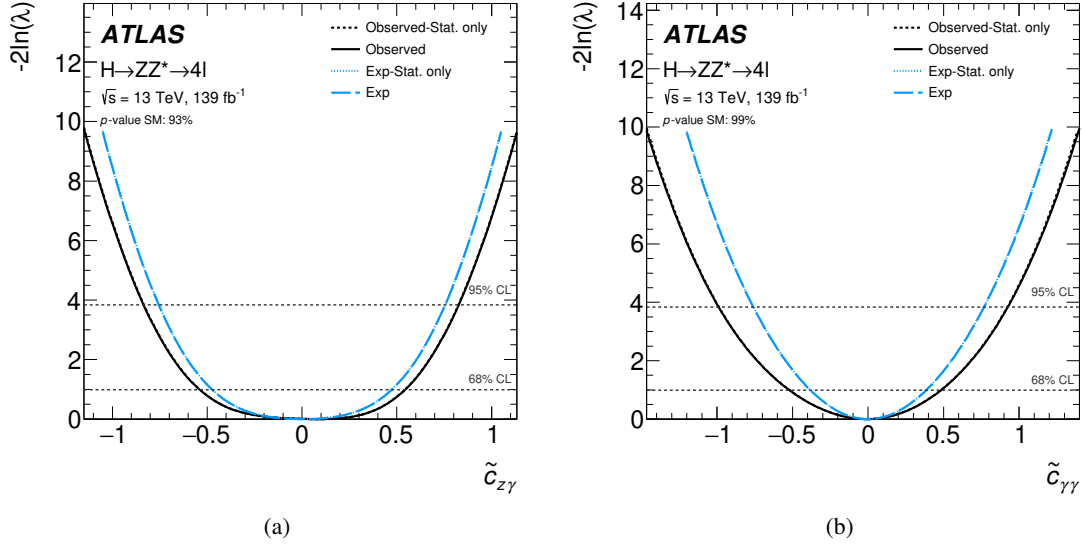


Figure 9: The NLL observable fits for the Higgs-basis couplings for decay-only fits: (a) $\tilde{c}_{z\gamma}$ ($OO_{4\ell}^{\tilde{c}_{z\gamma}}$) and (b) $\tilde{c}_{\gamma\gamma}$ ($OO_{4\ell}^{\tilde{c}_{\gamma\gamma}}$). The expected and observed distributions are shown with (solid line) and without (dashed line) systematic uncertainties. The p -value for agreement with the SM is 0.93 (0.99) for the $\tilde{c}_{z\gamma}$ ($\tilde{c}_{\gamma\gamma}$) coupling NLL scan. All couplings scale as $1/\Lambda^2$ with the assumed value of $\Lambda = 1$ TeV.

sensitivity in both production and decay. The rest of the couplings are from a decay-only observable fit, having little sensitivity to the VBF production, as previously shown in Table 4.

Table 5: The expected and observed confidence intervals at 68% and 95% CL for the CP-odd Wilson coefficients for an integrated luminosity of 139 fb^{-1} at $\sqrt{s} = 13$ TeV. Only one Wilson coefficient is fitted at a time while all others are set to zero. The observed best fit value and p -value for agreement with the SM is provided. The last column indicates whether the limits come from production (prod), decay or a combination of production and decay (comb). All couplings scale as $1/\Lambda^2$ with the assumed value of $\Lambda = 1$ TeV.

EFT coupling parameter	Expected		Observed		Best-fit value	SM p -value	Fit type
	68% CL	95% CL	68% CL	95% CL			
$c_{H\tilde{B}}$	[-0.18, 0.19]	[-0.37, 0.37]	[-0.42, 0.31]	[-0.61, 0.54]	-0.078	0.86	decay
$c_{H\tilde{W}B}$	[-0.36, 0.36]	[-0.72, 0.72]	[-0.56, 0.53]	[-0.97, 0.98]	-0.017	0.99	decay
$c_{H\tilde{W}}$	[-0.63, 0.63]	[-1.26, 1.28]	[-0.07, 1.09]	[-0.81, 1.54]	0.60	0.37	comb
\tilde{d}	[-0.009, 0.009]	[-0.018, 0.018]	[-0.017, 0.014]	[-0.026, 0.025]	-0.003	0.86	decay
\tilde{c}_{zz}	[-0.77, 0.79]	[-2.4, 2.4]	[0.37, 1.21]	[-1.20, 1.75]	0.78	0.11	prod
$\tilde{c}_{z\gamma}$	[-0.47, 0.47]	[-0.76, 0.76]	[-0.54, 0.54]	[-0.84, 0.83]	0.083	0.93	decay
$\tilde{c}_{\gamma\gamma}$	[-0.38, 0.38]	[-0.76, 0.77]	[-0.52, 0.48]	[-0.99, 0.93]	-0.01	0.99	decay

The prediction of the optimal-observable distribution using the morphing method described in Section 2.3 includes both a linear and quadratic dependence on the BSM matrix element (see Eq. (2)). Only the linear term generates an asymmetry of the optimal-observable distribution, while the quadratic term leads to a

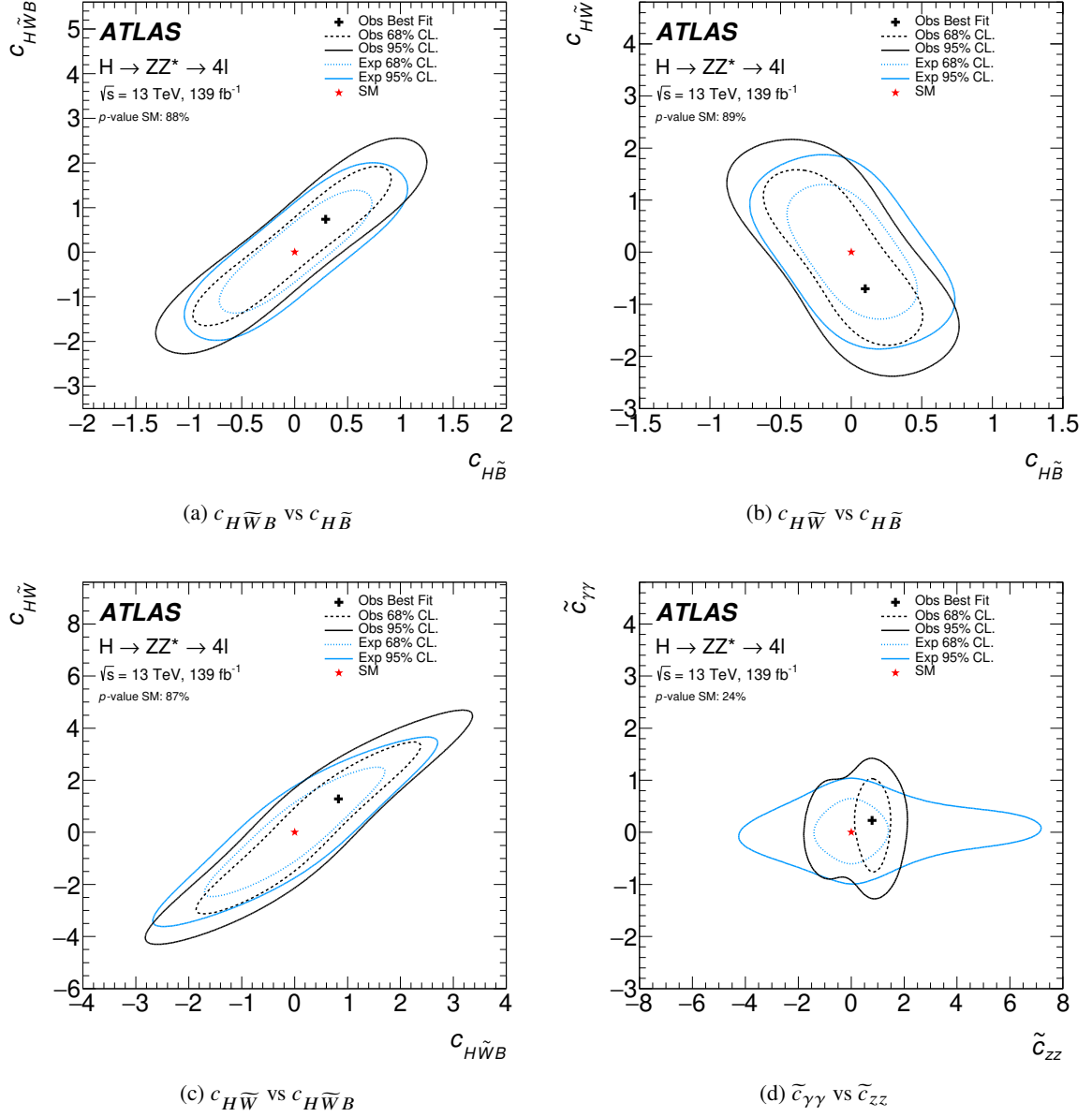


Figure 10: The observed and expected 68% and 95% CL two-dimensional contours for all three pairings of the Warsaw-basis couplings: (a) $c_{H\tilde{W}B}$ versus $c_{H\tilde{B}}$, (b) $c_{H\tilde{W}}$ versus $c_{H\tilde{B}}$ and (c) $c_{H\tilde{W}}$ versus $c_{H\tilde{W}B}$. These use the two-dimensional observable $OO_{4\ell}^{c_{H\tilde{B}}}$ versus $OO_{4\ell}^{c_{H\tilde{W}}}$. In (d), the two-dimensional contours for scans along $\tilde{c}_{\gamma\gamma}$, sensitive only to the decay, and \tilde{c}_{zz} , sensitive only to the production are shown, where the observable $OO_{4\ell}^{\tilde{c}_{\gamma\gamma}}$ is used for the decay and $OO_{jj}^{\tilde{c}_{zz}}$ for the production. All couplings scale as $1/\Lambda^2$ with the assumed value of $\Lambda = 1 \text{ TeV}$.

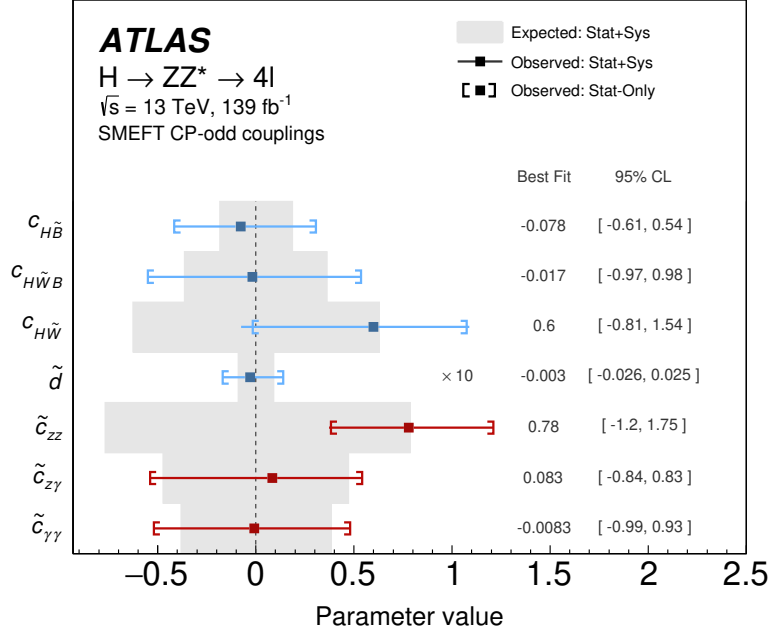


Figure 11: The expected and observed measurements of the CP-odd Wilson coefficients for an integrated luminosity of 139 fb^{-1} at $\sqrt{s} = 13 \text{ TeV}$. The data points and 68% CL uncertainty bars show the observed values with statistical and systematic uncertainties, and the statistical-only uncertainties are shown as square brackets. The Warsaw-basis couplings and \tilde{d} are in blue and the Higgs-basis couplings are in red. The $c_{H\tilde{W}}$ measurement is from the combined production and decay fit, and the \tilde{c}_{zz} measurement is from the production-only fit. The other measurements are from decay-only fits, having little sensitivity to the VBF production. The \tilde{d} best fit point and uncertainty bars are scaled by a factor of ten. The best fit values and 95% CL limits are shown separately. Only one Wilson coefficient is fitted at a time while all others are set to zero. All couplings scale as $1/\Lambda^2$ with the assumed value of $\Lambda = 1 \text{ TeV}$.

symmetric shape modification. The result of the morphing is normalized to the SM to allow a shape-only analysis, but since the quadratic terms contribute to the shapes in a symmetric way, they can still influence the measurements. This is tested using the morphing method with only linear terms for $c_{H\tilde{B}}$ decay-only and $c_{H\tilde{W}}$ production and decay. For both, the 68% CL (95% CL) limits with linear-only terms change by $\sim 1\%$ ($\sim 3\%$), indicating a negligible contribution from the quadratic terms. The effect of extending the shape-only analysis to include the change in total cross-section for each coupling value is also investigated. This can affect the production cross-section (for VBF), the branching fraction and the detector event acceptance. The SM normalization is scaled by the relative total cross-section for each coupling value to that of the SM estimated in the leading-order SMEFT simulation, which for example decreases the cross-section by less than 10% for $c_{H\tilde{W}}$ at its 95% CL limit value of Table 5. The coupling cross-section change has a small effect on the decay-only limits as the predicted 68% (95%) CL exclusion limits tighten by less than 5% (10%). There is an important effect for production-only measurements with the expected limits tightening by 10% (50%). The cross-sections are CP-even quantities and are only affected by the quadratic term, as the linear term integrates to zero over the optimal-observable distribution. Therefore the larger coupling values allowed by the production scans result in a more pronounced effect on the limits from the quadratic term driving the rate change. Finally, the present analysis assumes that the CP-even couplings c_{HB} , c_{HWB} and c_{HW} are all zero. The effects of a non-zero CP-even coupling are evaluated. For couplings on the order of the current experimental limits [92] the effect on the production-only limits

is negligible. For the decay analysis, a CP-even coupling would weaken the limits and increase an observed non-zero CP-odd value by a few percent.

Figure 12 provides a comparison of the present measurements with those from [11, 19, 22, 30]. The 68% confidence levels are compared for the Warsaw-basis couplings ($c_{H\tilde{B}}$, $c_{H\tilde{W}B}$ and $c_{H\tilde{W}}$) and the \tilde{d} coupling. The $H \rightarrow ZZ^* \rightarrow 4\ell$ simplified-template-cross-section (STXS) measurements [22] provide two degenerate positive/negative values as the measured cross-sections are only sensitive to the BSM quadratic terms ($|\mathcal{M}_{BSM}|^2$ of Eq. (2)). The STXS measurements are based on event rates in CP-insensitive categories and so cannot distinguish between a CP-even and CP-odd effect. This also explains the higher expected sensitivity of the present measurement that includes the four-lepton decays. The expected values for the present measurement are the most sensitive, except for $c_{H\tilde{W}}$ of the VBF $H \rightarrow \gamma\gamma$ decay channel measurement [30] that has a larger number of VBF produced events. For \tilde{d} , the improved sensitivity of the present measurement arises from the contribution of the $H \rightarrow ZZ^* \rightarrow 4\ell$ decays. The CMS result [19] uses rate information in addition to shapes, but less granularity in the decay-level observable binning, and the differences in the expected sensitivity are consistent with this difference in strategy.

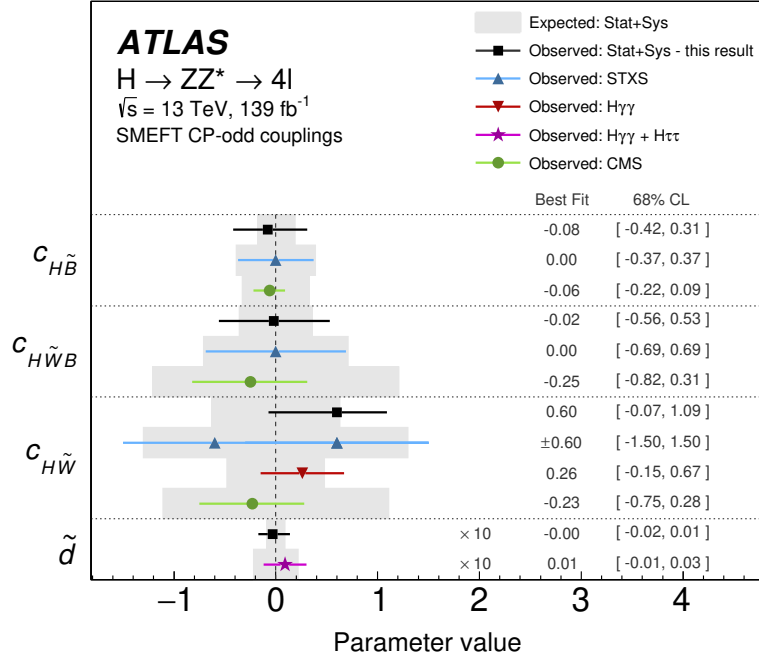


Figure 12: Comparison of results for the present measurement, the $H \rightarrow ZZ^* \rightarrow 4\ell$ STXS cross-section measurement of Ref. [22], the ATLAS $H \rightarrow \gamma\gamma$ VBF measurement [30] of $c_{H\tilde{W}}$, combined VBF measurement of \tilde{d} in $H \rightarrow \gamma\gamma$ and $H \rightarrow \tau\tau$ decay channels [11, 30], and the CMS anomalous Higgs boson couplings measurement [19]. The data points and 68% CL uncertainty bars show the observed values with statistical and systematic uncertainties. The \tilde{d} best fit points and uncertainty bars are scaled by a factor of ten.

In conclusion, the results of the coupling measurement are all in agreement with the SM. A fluctuation in the optimal observables leads to a slight preference for a non-zero BSM coupling in the production-level analysis, which is compatible with the SM at better than two standard deviations and not confirmed by the decay-level analysis.

8.2 Differential optimal-observable cross-section results

The differential cross-sections for the optimal observables are measured using a binned profile likelihood ratio fit, fitting simultaneously the $m_{4\ell}$ distribution in each bin across all bins of a given distribution, as described in Section 6.2.

The measured differential cross-section for the production optimal observable $OO_{jj}^{c_{H\bar{W}}}$ and those for the decay optimal observables $OO_{4\ell}^{c_{H\bar{W}}}$, $OO_{4\ell}^{c_{H\bar{B}}}$ and $OO_{4\ell}^{c_{H\bar{W}B}}$ are shown in Figure 13. The couplings used for these optimal observables correspond to those with good expected sensitivity for VBF production or four-lepton decay of the direct coupling measurement, as previously described. The first bin of Figure 13(a) is not part of the $OO_{jj}^{c_{H\bar{W}}}$ differential distribution but rather contains events with fewer than two selected jets with $p_T > 30$ GeV. These events are included as part of the fiducial distribution unfolding as they have a correlation of up to 15% with the cross-section measurements of the $OO_{jj}^{c_{H\bar{W}}}$ differential bins as can be seen in Figure 15(a) of Appendix A. This correlation arises from the jet energy resolution. The larger number of decay events and the relatively better resolution for leptons allows a finer binning for the decay observable differential distributions. The correlation between neighbouring bins is up to 30% for $OO_{4\ell}^{c_{H\bar{W}}}$ with 12 bins, and up to 20% for the six bin distributions of $OO_{4\ell}^{c_{H\bar{B}}}$ and $OO_{4\ell}^{c_{H\bar{W}B}}$, as shown in Appendix A.

These figures show the measured differential cross-section compared with SM predictions for ggF production provided by NNLOPS and MADGRAPH5_AMC@NLO-FxFx (MG5 FxFx), which are both normalized to the N³LO calculation [93, 94]. The other Higgs boson production modes, denoted by XH , are normalized to the most accurate predictions available, as given in [28]. All of the figures include the p -values that quantify the probability of compatibility of the measurements and the corresponding SM prediction for ggF + XH , including the theoretical uncertainties in the ggF predictions. For the p -value estimations, QCD scale and PDF uncertainties for NNLOPS are evaluated individually for each bin; however for MG5 FxFx only total QCD scale and PDF uncertainties are available for all bins. In both cases the theoretical uncertainties are treated as correlated across the bins. All p -values reveal a good compatibility of the data with the SM predictions. For $OO_{4\ell}^{c_{H\bar{W}}}$ in Figure 13(b), the lower p -value is from a large fluctuation in one differential bin.

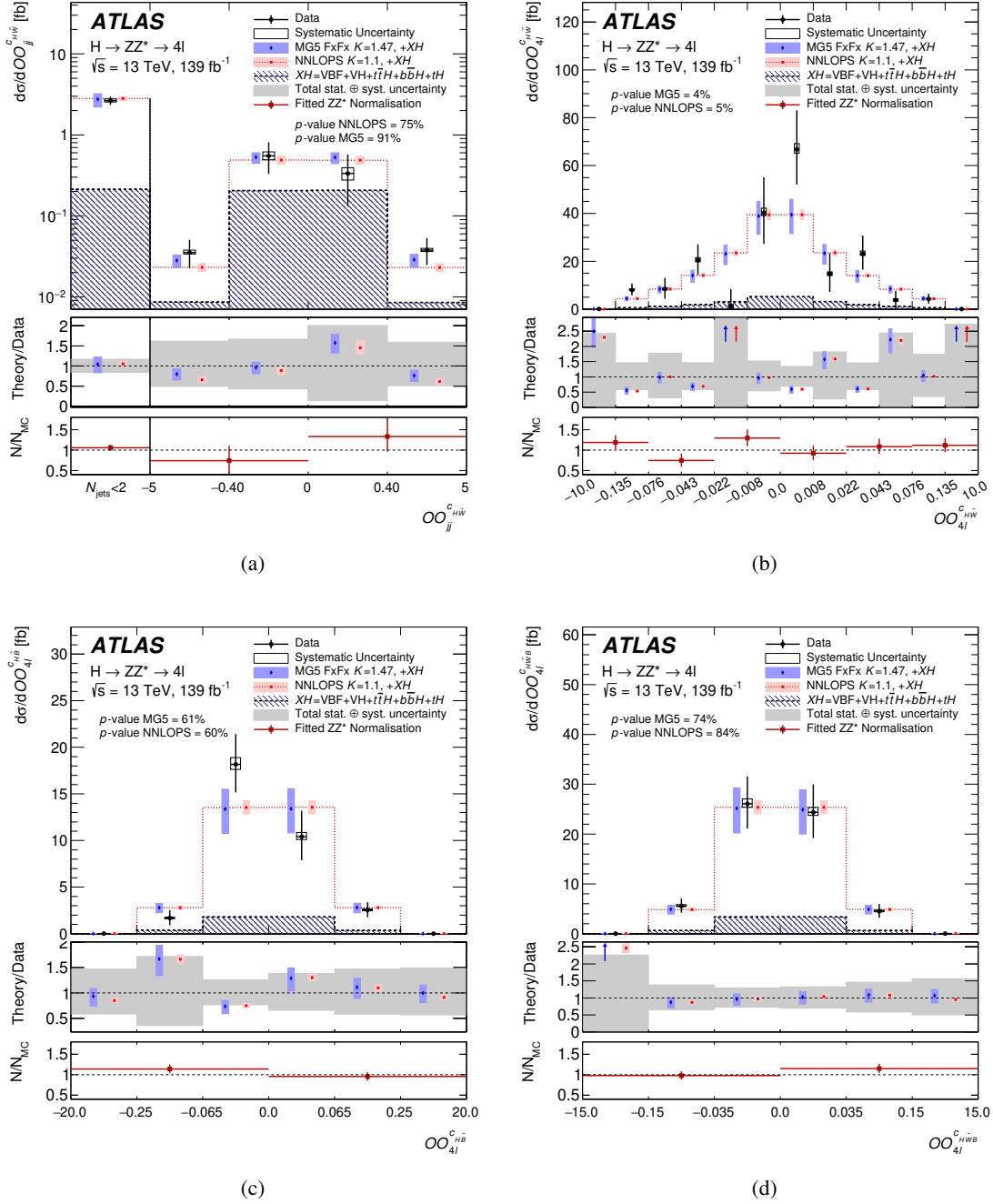


Figure 13: Results for differential fiducial cross-section for the optimal observables (a) $OO_{jj}^{C_{H\bar{W}}}$, (b) $OO_{4\ell}^{C_{H\bar{W}}}$, (c) $OO_{4\ell}^{C_{H\bar{B}}}$ and (d) $OO_{4\ell}^{C_{H\bar{W}B}}$. The first bin of $OO_{jj}^{C_{H\bar{W}}}$ distribution contains events with fewer than two jets that satisfy the jet selection requirements. The error bars on the data points show the total uncertainties, while the systematic uncertainties are indicated by the boxes. The shaded bands on the expected differential cross-sections indicate the PDF and scale systematic uncertainties. The central panel shows the ratio of different predictions to the data, and the grey area represents the total uncertainty in the measurement. The bottom panel shows the ratios of the fitted values of the ZZ^* normalization factors to the predictions from MC simulation. As indicated by the horizontal error bars, the same ZZ^* normalizations are estimated for different cross-section bins of the distributions.

8.3 VBF-enriched fiducial cross-section results

As described in Section 6.2, the VBF-enriched fiducial cross-section measurement is performed by dividing the two-dimensional plane m_{jj} versus $|\Delta\eta_{jj}|$ into three bins with a signal region defined by $m_{jj} \geq 400$ GeV and $|\Delta\eta_{jj}| \geq 3.0$, and two control regions outside this selection. The expected and observed events in this two-dimensional plane can be seen in Figure 14. Events are unfolded to the corresponding fiducial phase space and two VBF-enriched fiducial cross-sections are extracted: with and without the ggF contribution included as part of the signal region. The results for these two measurements are presented in Table 6.

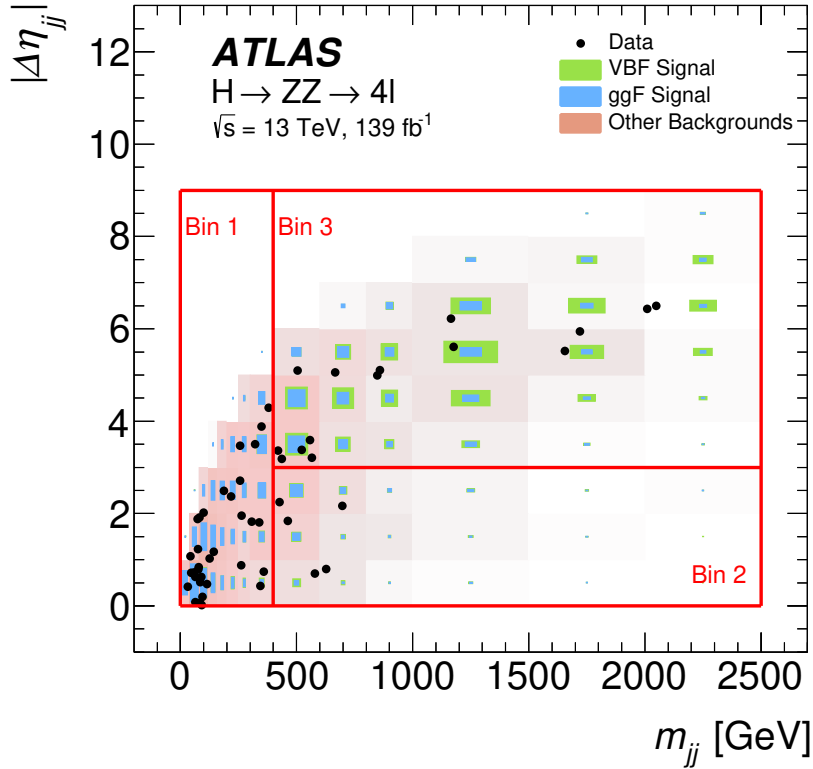


Figure 14: The expected and observed events in the m_{jj} vs $|\Delta\eta_{jj}|$ two-dimensional plane for the VBF-enriched fiducial cross-section. The dots depict data and the shaded areas represent the simulated signal for VBF, ggF, and other backgrounds, respectively. The lines depict the bin boundaries for unfolding into the corresponding fiducial phase space.

Table 6: Expected and observed VBF fiducial cross-sections measured in a VBF-enriched fiducial region with and without including the ggF contribution as part of the signal region.

VBF-enriched region	Signal for cross-section estimates	Purity of VBF signal	Expected cross-section [fb]	Observed cross-section [fb]
$N_{\text{jets}} \geq 2, m_{jj} \geq 400$ GeV $ \Delta\eta_{jj} \geq 3.0$	All production modes	59 %	$0.134^{+0.065}_{-0.053} \quad ^{+0.014}_{-0.012}$	$0.215^{+0.075}_{-0.063} \quad ^{+0.016}_{-0.013}$
	VBF + VH + ttH	95 %	$0.088^{+0.063}_{-0.053} \quad ^{+0.017}_{-0.020}$	$0.172^{+0.072}_{-0.062} \quad ^{+0.016}_{-0.018}$

For both cases, the measured fiducial cross-section is larger than the expected, with a signal strength of about 1.6 and 2, but remain compatible with the SM as evaluated from p -values. In the first scenario the p -value compatibility with NNLOPS and MG5 FxFx is 82% and 80%, respectively. In the second scenario, where the ggF is subtracted, the p -value compatibility with the SM predictions for the remaining three production modes is 19%.

These measured fiducial cross-sections can be compared with the VBF production cross-section of $H \rightarrow ZZ^* \rightarrow 4\ell$ decay channel measured in the context of the STXS framework [22]. The STXS measurement has a relative observed cross-section times branching ratio $(\sigma \cdot \mathcal{B})/(\sigma \cdot \mathcal{B})_{\text{SM}}$ of 1.21 ± 0.45 for the VBF production mode. The STXS measurement extracts the VBF signal using neural networks, similar to the direct measurement above, and combines VBF signals from several kinematic bins separated according to the number of jets and $p_{\text{T}}^{4\ell}$. The present fiducial analysis instead applies explicit selections on m_{jj} and $|\Delta\eta_{jj}|$ for events with two jets, which selects events in a different phase space. All three measurements yield cross-sections that are compatible with the SM expectations.

9 Conclusion

A measurement searching for CP violation in VBF Higgs boson production and its decay into four leptons is presented based on proton–proton collision data produced at the LHC at a centre-of-mass energy of 13 TeV and recorded by the ATLAS detector from 2015 to 2018, corresponding to an integrated luminosity of 139 fb^{-1} . The measurement is performed using optimal observables defined as the ratio of the matrix elements squared for the interference of the SM and CP-odd BSM couplings to the SM matrix element squared. Limits are obtained in both the Higgs and Warsaw bases using the SMEFT. They are dominated by the interference term between the SM and BSM contributions linear in the Wilson coefficients, $\mathcal{O}(\Lambda^{-2})$ in the cross-section, with only a small sensitivity to the pure BSM contributions quadratic in the Wilson coefficients, $\mathcal{O}(\Lambda^{-4})$. This qualitatively implies a low expected sensitivity to missing dimension-eight contributions that also enter at $\mathcal{O}(\Lambda^{-4})$ in the cross-section, and it is therefore an improvement on analyses relying on rates rather than shapes. Measurements of fiducial differential cross-sections of the optimal-observable distributions are also presented, completing the set of fiducial differential cross-section measurements in the Higgs boson to four-lepton channel. In addition, fiducial cross-sections for VBF production are measured for a VBF-enriched fiducial region for two scenarios: with and without the explicit subtraction of the ggF background. All measurements are consistent with the SM expectation of a CP-even Higgs boson. No significant CP-odd component is observed.

The data for all tables and the figures with differential distributions can be viewed at [HEPData](#).

Acknowledgements

We thank CERN for the very successful operation of the LHC, as well as the support staff from our institutions without whom ATLAS could not be operated efficiently.

We acknowledge the support of ANPCyT, Argentina; YerPhI, Armenia; ARC, Australia; BMWFW and FWF, Austria; ANAS, Azerbaijan; CNPq and FAPESP, Brazil; NSERC, NRC and CFI, Canada; CERN; ANID, Chile; CAS, MOST and NSFC, China; Minciencias, Colombia; MEYS CR, Czech Republic; DNRF and DNSRC, Denmark; IN2P3-CNRS and CEA-DRF/IRFU, France; SRNSFG, Georgia; BMBF, HGF and

MPG, Germany; GSRI, Greece; RGC and Hong Kong SAR, China; ISF and Benozziyo Center, Israel; INFN, Italy; MEXT and JSPS, Japan; CNRST, Morocco; NWO, Netherlands; RCN, Norway; MEiN, Poland; FCT, Portugal; MNE/IFA, Romania; MESTD, Serbia; MSSR, Slovakia; ARRS and MIZŠ, Slovenia; DSI/NRF, South Africa; MICINN, Spain; SRC and Wallenberg Foundation, Sweden; SERI, SNSF and Cantons of Bern and Geneva, Switzerland; MOST, Taiwan; TENMAK, Türkiye; STFC, United Kingdom; DOE and NSF, United States of America. In addition, individual groups and members have received support from BCKDF, CANARIE, Compute Canada and CRC, Canada; PRIMUS 21/SCI/017 and UNCE SCI/013, Czech Republic; COST, ERC, ERDF, Horizon 2020 and Marie Skłodowska-Curie Actions, European Union; Investissements d’Avenir Labex, Investissements d’Avenir IDEX and ANR, France; DFG and AvH Foundation, Germany; Herakleitos, Thales and Aristeia programmes co-financed by EU-ESF and the Greek NSRF, Greece; BSF-NSF and MINERVA, Israel; Norwegian Financial Mechanism 2014-2021, Norway; NCN and NAWA, Poland; La Caixa Banking Foundation, CERCA Programme Generalitat de Catalunya and PROMETEO and GenT Programmes Generalitat Valenciana, Spain; Göran Gustafssons Stiftelse, Sweden; The Royal Society and Leverhulme Trust, United Kingdom.

The crucial computing support from all WLCG partners is acknowledged gratefully, in particular from CERN, the ATLAS Tier-1 facilities at TRIUMF (Canada), NDGF (Denmark, Norway, Sweden), CC-IN2P3 (France), KIT/GridKA (Germany), INFN-CNAF (Italy), NL-T1 (Netherlands), PIC (Spain), ASGC (Taiwan), RAL (UK) and BNL (USA), the Tier-2 facilities worldwide and large non-WLCG resource providers. Major contributors of computing resources are listed in Ref. [95].

Appendix

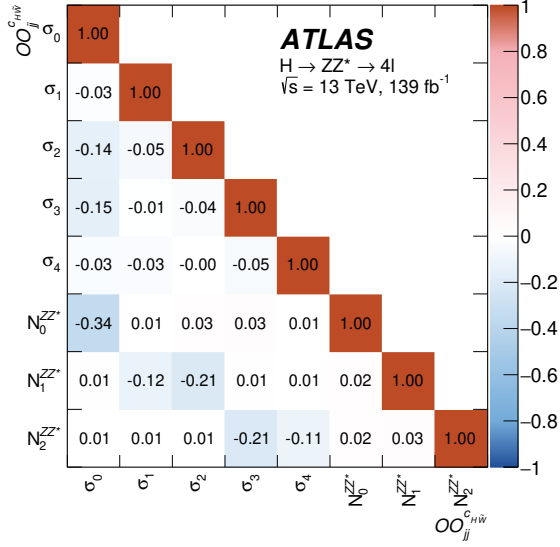
A Additional differential cross-section results

This appendix shows additional results of the differential fiducial cross-section measurements presented in Figure 8.2.

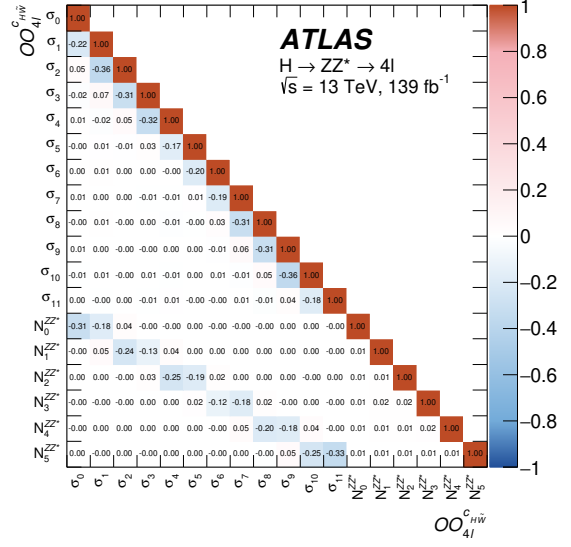
Figure 15 shows the correlation matrices for the differential fiducial cross-sections presented in Figure 13. Non-negligible anti-correlations exist between the cross-sections in neighbouring bins due to detector resolution effects. In addition, there are anti-correlations between the cross-section for $N_{\text{jets}} < 2$ and the four optimal observable bins in the $OO_{jj}^{cH\bar{W}}$ measurement shown in Figure 15(a), driven by jet energy resolution. Finally, the normalization of the $q\bar{q} \rightarrow ZZ^*$ background is anti-correlated with the signal cross-sections measured in the respective bins.

Figure 16 shows the differential fiducial cross-section for the $OO_{jj}^{\tilde{c}zz}$ observable and the associated correlation matrix. This observable is strongly correlated with $OO_{jj}^{cH\bar{W}}$ and the two measurements thus share many features.

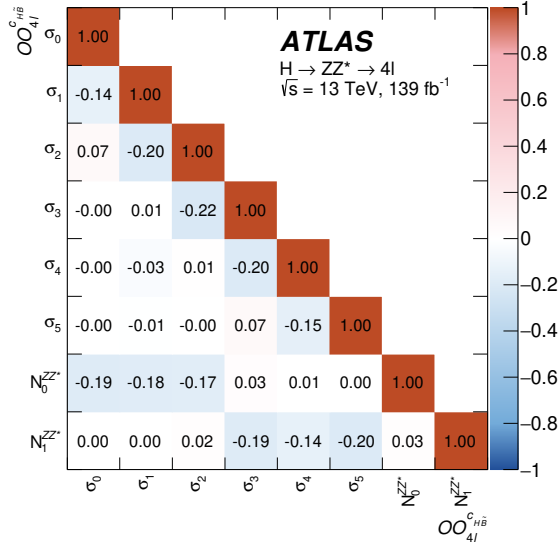
Figure 17(a) shows the per-bin fiducial cross-section values and the correlation matrix for the extraction of the VBF-enriched fiducial cross-section described in Figure 8.3.



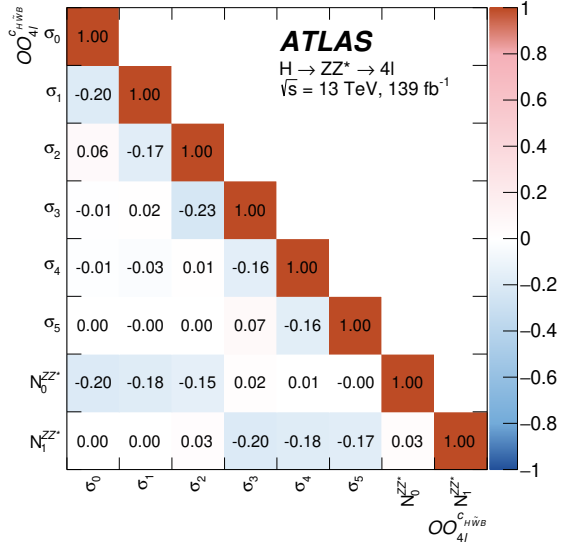
(a)



(b)



(c)



(d)

Figure 15: Correlation matrices between the measured differential fiducial cross-section and ZZ* normalization bins for the (a) $OO_{jj}^{C_{H\bar{W}}}$, (b) $OO_{4l}^{C_{H\bar{W}}}$, (c) $OO_{4l}^{C_{H\bar{B}}}$ and (d) $OO_{4l}^{C_{H\bar{W}B}}$ optimal observables. The bin labeled σ_0 of (a) is not part of the $OO_{jj}^{C_{H\bar{W}}}$ differential distribution, but contains events with fewer than two selected jets with $p_T > 30$ GeV.

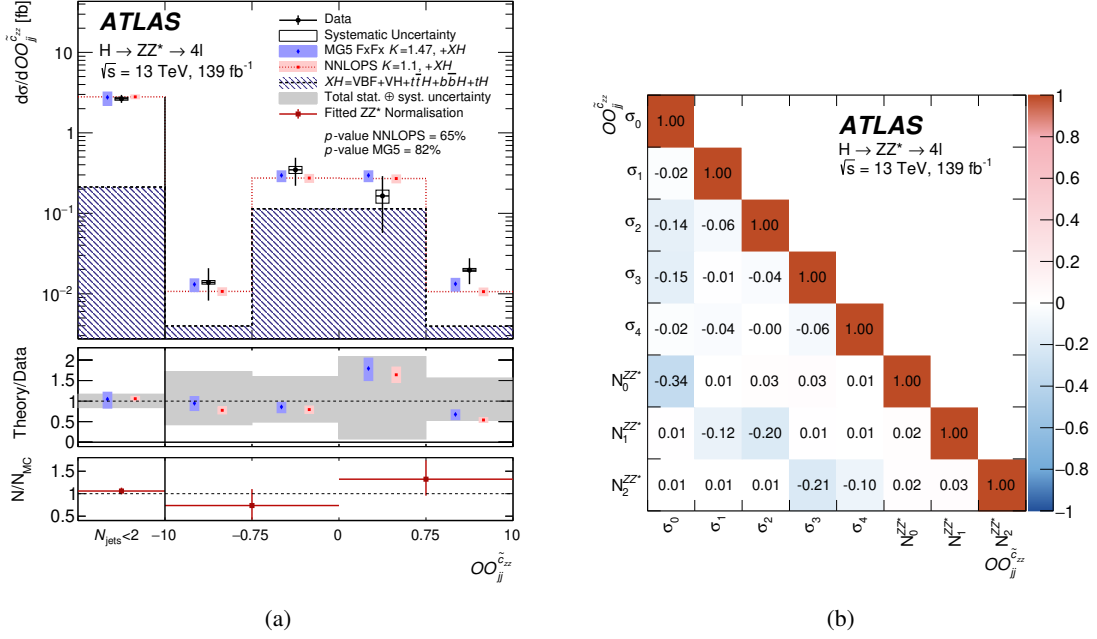


Figure 16: (a) Results for the differential fiducial cross-section for the $OO_{jj}^{C_{zz}}$ optimal observable, along with (b) the corresponding correlation matrix between the measured cross-sections and the ZZ^* background normalization factors. The first bin of (a) is not part of the $OO_{jj}^{C_{zz}}$ differential distribution, but contains events with fewer than two selected jets with $p_T > 30$ GeV. This bin corresponds to σ_0 of (b).

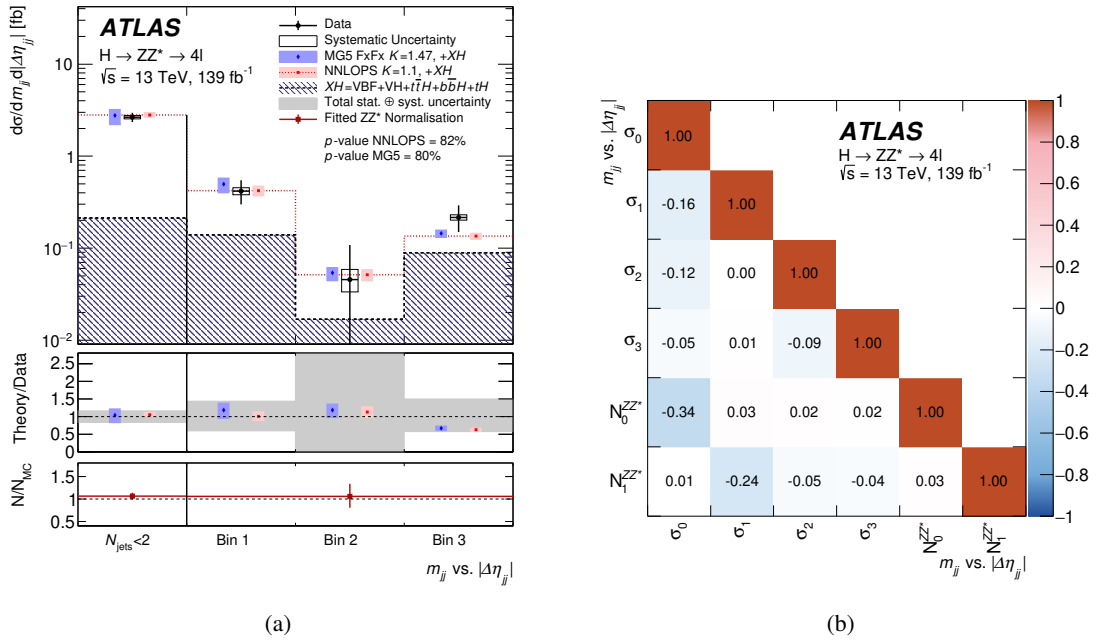


Figure 17: (a) Results for the VBF-enriched fiducial cross-section measurement extracted from the double-differential fiducial cross-section for m_{jj} versus $|\Delta\eta_{jj}|$, along with (b) the corresponding correlation matrix between the measured cross-sections and the ZZ^* background normalization factors.

References

- [1] A. D. Sakharov, *Violation of CP Invariance, C asymmetry, and baryon asymmetry of the universe*, *Pisma Zh. Eksp. Teor. Fiz.* **5** (1967) 32.
- [2] N. Cabibbo, *Unitary Symmetry and Leptonic Decays*, *Phys. Rev. Lett.* **10** (1963) 531.
- [3] M. Kobayashi and T. Maskawa, *CP Violation in the Renormalizable Theory of Weak Interaction*, *Prog. Theor. Phys.* **49** (1973) 652.
- [4] ATLAS Collaboration, *Observation of a new particle in the search for the Standard Model Higgs boson with the ATLAS detector at the LHC*, *Phys. Lett. B* **716** (2012) 1, arXiv: 1207.7214 [hep-ex].
- [5] CMS Collaboration, *Observation of a new boson at a mass of 125 GeV with the CMS experiment at the LHC*, *Phys. Lett. B* **716** (2012) 30, arXiv: 1207.7235 [hep-ex].
- [6] ATLAS Collaboration, *Evidence for the spin-0 nature of the Higgs boson using ATLAS data*, *Phys. Lett. B* **726** (2013) 120, arXiv: 1307.1432 [hep-ex].
- [7] ATLAS Collaboration, *Study of the spin and parity of the Higgs boson in diboson decays with the ATLAS detector*, *Eur. Phys. J. C* **75** (2015) 476, arXiv: 1506.05669 [hep-ex], Erratum: *Eur. Phys. J. C* **76** (2016) 152.
- [8] CMS Collaboration, *Study of the Mass and Spin-Parity of the Higgs Boson Candidate Via Its Decays to Z Boson Pairs*, *Phys. Rev. Lett.* **110** (2013) 081803, arXiv: 1212.6639 [hep-ex].
- [9] CMS Collaboration, *Constraints on the spin-parity and anomalous HVV couplings of the Higgs boson in proton collisions at 7 and 8 TeV*, *Phys. Rev. D* **92** (2015) 012004, arXiv: 1411.3441 [hep-ex].
- [10] ATLAS Collaboration, *Test of CP Invariance in vector-boson fusion production of the Higgs boson using the Optimal Observable method in the ditau decay channel with the ATLAS detector*, *Eur. Phys. J. C* **76** (2016) 658, arXiv: 1602.04516 [hep-ex].
- [11] ATLAS Collaboration, *Test of CP invariance in vector-boson fusion production of the Higgs boson in the $H \rightarrow \tau\tau$ channel in proton-proton collisions at $\sqrt{s} = 13$ TeV with the ATLAS detector*, *Phys. Lett. B* **805** (2020) 135426, arXiv: 2002.05315 [hep-ex].
- [12] ATLAS Collaboration, *Constraints on Higgs boson properties using $WW^*(\rightarrow e\nu\mu\nu)jj$ production in 36.1 fb^{-1} of $\sqrt{s} = 13$ TeV pp collisions with the ATLAS detector*, *Eur. Phys. J. C* **82** (2021) 622, arXiv: 2109.13808 [hep-ex].
- [13] ATLAS Collaboration, *CP Properties of Higgs Boson Interactions with Top Quarks in the $t\bar{t}H$ and tH Processes Using $H \rightarrow \gamma\gamma$ with the ATLAS Detector*, *Phys. Rev. Lett.* **125** (2020) 061802, arXiv: 2004.04545 [hep-ex].
- [14] ATLAS Collaboration, *Measurement of the CP properties of Higgs boson interactions with τ -leptons with the ATLAS detector*, (2022), arXiv: 2212.05833 [hep-ex].
- [15] ATLAS Collaboration, *Probing the CP nature of the top-Higgs Yukawa coupling in $t\bar{t}H$ and tH events with $H \rightarrow b\bar{b}$ decays using the ATLAS detector at the LHC*, (2023), arXiv: 2303.05974 [hep-ex].

- [16] CMS Collaboration, *Constraints on anomalous Higgs boson couplings using production and decay information in the four-lepton final state*, *Phys. Lett. B* **775** (2017) 1, arXiv: [1707.00541 \[hep-ex\]](#).
- [17] CMS Collaboration, *Constraints on anomalous HVV couplings from the production of Higgs bosons decaying to τ lepton pairs*, *Phys. Rev. D* **100** (2019) 112002, arXiv: [1903.06973 \[hep-ex\]](#).
- [18] CMS Collaboration, *Measurements of the Higgs boson width and anomalous HVV couplings from on-shell and off-shell production in the four-lepton final state*, *Phys. Rev. D* **99** (2019) 112003, arXiv: [1901.00174 \[hep-ex\]](#).
- [19] CMS Collaboration, *Constraints on anomalous Higgs boson couplings to vector bosons and fermions in its production and decay using the four-lepton final state*, *Phys. Rev. D* **104** (2021) 052004, arXiv: [2104.12152 \[hep-ex\]](#).
- [20] CMS Collaboration, *Measurements of $t\bar{t}H$ Production and the CP Structure of the Yukawa Interaction between the Higgs Boson and Top Quark in the Diphoton Decay Channel*, *Phys. Rev. Lett.* **125** (2020) 061801, arXiv: [2003.10866 \[hep-ex\]](#).
- [21] CMS Collaboration, *Analysis of the CP structure of the Yukawa coupling between the Higgs boson and τ leptons in proton–proton collisions at $\sqrt{s} = 13$ TeV*, *JHEP* **06** (2022) 012, arXiv: [2110.04836 \[hep-ex\]](#).
- [22] ATLAS Collaboration, *Higgs boson production cross-section measurements and their EFT interpretation in the 4ℓ decay channel at $\sqrt{s} = 13$ TeV with the ATLAS detector*, *Eur. Phys. J. C* **80** (2020) 957, arXiv: [2004.03447 \[hep-ex\]](#), Erratum: *Eur. Phys. J. C* **81** (2021) 29.
- [23] D. Atwood and A. Soni, *Analysis for magnetic moment and electric dipole moment form-factors of the top quark via $e^+e^- \rightarrow t\bar{t}$* , *Phys. Rev. D* **45** (1992) 2405.
- [24] M. Davier, L. Duflot, F. Le Diberder and A. Rouge, *The Optimal method for the measurement of tau polarization*, *Phys. Lett. B* **306** (1993) 411.
- [25] M. Diehl and O. Nachtmann, ‘Optimal observables for measuring three gauge boson couplings in $e^+e^- \rightarrow W^+W^-$ ’, *Physics with e^+e^- Linear Colliders (The European Working Groups 4 Feb - 1 Sep 1995: Session 2)*, 1996 301, arXiv: [hep-ph/9603207](#).
- [26] ATLAS Collaboration, *The ATLAS Experiment at the CERN Large Hadron Collider*, *JINST* **3** (2008) S08003.
- [27] I. Brivio and M. Trott, *The Standard Model as an Effective Field Theory*, *Phys. Rept.* **793** (2019) 1, arXiv: [1706.08945 \[hep-ph\]](#).
- [28] ATLAS Collaboration, *Measurements of the Higgs boson inclusive and differential fiducial cross sections in the 4ℓ decay channel at $\sqrt{s} = 13$ TeV*, *Eur. Phys. J. C* **80** (2020) 942, arXiv: [2004.03969 \[hep-ex\]](#).
- [29] S. Weinberg, *Baryon- and Lepton-Nonconserving Processes*, *Phys. Rev. Lett.* **43** (1979) 1566.
- [30] ATLAS Collaboration, *Study of the CP property of the Higgs boson to electroweak boson coupling in the VBF $H \rightarrow \gamma\gamma$ channel with the ATLAS detector*, (2022), arXiv: [2208.02338 \[hep-ex\]](#).
- [31] ATLAS Collaboration, *Measurement of the properties of Higgs boson production at $\sqrt{s} = 13$ TeV in the $H \rightarrow \gamma\gamma$ channel using 139fb^{-1} of pp collision data with the ATLAS experiment*, (2022), arXiv: [2207.00348 \[hep-ex\]](#).

- [32] ATLAS Collaboration, *Combined effective field theory interpretation of Higgs boson and weak boson production and decay with ATLAS data and electroweak precision observables*, ATL-PHYS-PUB-2022-037, 2022, URL: <https://cds.cern.ch/record/2816369>.
- [33] CMS Collaboration, *Measurement of the inclusive and differential $t\bar{t}\gamma$ cross sections in the dilepton channel and effective field theory interpretation in proton–proton collisions at $\sqrt{s} = 13$ TeV*, *JHEP* **05** (2022) 091, arXiv: [2201.07301](https://arxiv.org/abs/2201.07301) [[hep-ex](#)].
- [34] W. Buchmüller and D. Wyler, *Effective lagrangian analysis of new interactions and flavour conservation*, *Nuclear Physics B* **268** (1986) 621, ISSN: 0550-3213.
- [35] B. Grzadkowski, M. Iskrzynski, M. Misiak and J. Rosiek, *Dimension-Six Terms in the Standard Model Lagrangian*, *JHEP* **10** (2010) 085, arXiv: [1008.4884](https://arxiv.org/abs/1008.4884) [[hep-ph](#)].
- [36] D. de Florian et al., *Handbook of LHC Higgs Cross Sections: 4. Deciphering the Nature of the Higgs Sector*, (2016), arXiv: [1610.07922](https://arxiv.org/abs/1610.07922) [[hep-ph](#)].
- [37] A. Azatov et al., *Off-shell Higgs Interpretations Task Force: Models and Effective Field Theories Subgroup Report*, (2022), arXiv: [2203.02418](https://arxiv.org/abs/2203.02418) [[hep-ph](#)].
- [38] J. Alwall et al., *The automated computation of tree-level and next-to-leading order differential cross sections, and their matching to parton shower simulations*, *JHEP* **07** (2014) 079, arXiv: [1405.0301](https://arxiv.org/abs/1405.0301) [[hep-ph](#)].
- [39] R. D. Ball et al., *Parton distributions with LHC data*, *Nucl. Phys. B* **867** (2013) 244, arXiv: [1207.1303](https://arxiv.org/abs/1207.1303) [[hep-ph](#)].
- [40] ATLAS Collaboration, *A morphing technique for signal modelling in a multidimensional space of coupling parameters*, ATL-PHYS-PUB-2015-047, 2015, URL: <https://cds.cern.ch/record/2066980>.
- [41] ATLAS Collaboration, *The ATLAS Collaboration Software and Firmware*, ATL-SOFT-PUB-2021-001, 2021, URL: <https://cds.cern.ch/record/2767187>.
- [42] ATLAS Collaboration, *Performance of the ATLAS muon triggers in Run 2*, *JINST* **15** (2020) P09015, arXiv: [2004.13447](https://arxiv.org/abs/2004.13447) [[hep-ex](#)].
- [43] ATLAS Collaboration, *Performance of electron and photon triggers in ATLAS during LHC Run 2*, *Eur. Phys. J. C* **80** (2020) 47, arXiv: [1909.00761](https://arxiv.org/abs/1909.00761) [[hep-ex](#)].
- [44] ATLAS Collaboration, *ATLAS data quality operations and performance for 2015–2018 data-taking*, *JINST* **15** (2020) P04003, arXiv: [1911.04632](https://arxiv.org/abs/1911.04632) [[physics.ins-det](#)].
- [45] K. Hamilton, P. Nason, E. Re and G. Zanderighi, *NNLOPS simulation of Higgs boson production*, *JHEP* **10** (2013) 222, arXiv: [1309.0017](https://arxiv.org/abs/1309.0017) [[hep-ph](#)].
- [46] K. Hamilton, P. Nason and G. Zanderighi, *Finite quark-mass effects in the NNLOPS POWHEG+MiNLO Higgs generator*, *JHEP* **05** (2015) 140, arXiv: [1501.04637](https://arxiv.org/abs/1501.04637) [[hep-ph](#)].
- [47] S. Alioli, P. Nason, C. Oleari and E. Re, *A general framework for implementing NLO calculations in shower Monte Carlo programs: the POWHEG BOX*, *JHEP* **06** (2010) 043, arXiv: [1002.2581](https://arxiv.org/abs/1002.2581) [[hep-ph](#)].

- [48] P. Nason, *A new method for combining NLO QCD with shower Monte Carlo algorithms*, [JHEP **11** \(2004\) 040](#), arXiv: [hep-ph/0409146](#).
- [49] S. Frixione, P. Nason and C. Oleari, *Matching NLO QCD computations with parton shower simulations: the POWHEG method*, [JHEP **11** \(2007\) 070](#), arXiv: [0709.2092 \[hep-ph\]](#).
- [50] K. Hamilton, P. Nason and G. Zanderighi, *MINLO: multi-scale improved NLO*, [JHEP **10** \(2012\) 155](#), arXiv: [1206.3572 \[hep-ph\]](#).
- [51] J. M. Campbell et al., *NLO Higgs boson production plus one and two jets using the POWHEG BOX, MadGraph4 and MCFM*, [JHEP **07** \(2012\) 092](#), arXiv: [1202.5475 \[hep-ph\]](#).
- [52] K. Hamilton, P. Nason, C. Oleari and G. Zanderighi, *Merging H/W/Z + 0 and 1 jet at NLO with no merging scale: a path to parton shower + NNLO matching*, [JHEP **05** \(2013\) 082](#), arXiv: [1212.4504 \[hep-ph\]](#).
- [53] S. Catani and M. Grazzini, *Next-to-Next-to-Leading-Order Subtraction Formalism in Hadron Collisions and its Application to Higgs-boson Production at the Large Hadron Collider*, [Phys. Rev. Lett. **98** \(2007\) 222002](#), arXiv: [hep-ph/0703012 \[hep-ph\]](#).
- [54] J. Butterworth et al., *PDF4LHC recommendations for LHC Run II*, [J. Phys. G **43** \(2016\) 023001](#), arXiv: [1510.03865 \[hep-ph\]](#).
- [55] M. Wiesemann et al., *Higgs production in association with bottom quarks*, [JHEP **02** \(2015\) 132](#), arXiv: [1409.5301 \[hep-ph\]](#).
- [56] R. D. Ball et al., *Parton distributions for the LHC run II*, [JHEP **04** \(2015\) 040](#), arXiv: [1410.8849 \[hep-ph\]](#).
- [57] D. J. Lange, *The EvtGen particle decay simulation package*, [Nucl. Instrum. Meth. A **462** \(2001\) 152](#).
- [58] T. Sjöstrand, S. Mrenna and P. Skands, *A brief introduction to PYTHIA 8.1*, [Comput. Phys. Commun. **178** \(2008\) 852](#), arXiv: [0710.3820 \[hep-ph\]](#).
- [59] I. Brivio, Y. Jiang and M. Trott, *The SMEFTsim package, theory and tools*, [JHEP **12** \(2017\) 070](#), arXiv: [1709.06492 \[hep-ph\]](#).
- [60] L. Lönnblad, *Correcting the Colour-Dipole Cascade Model with Fixed Order Matrix Elements*, [JHEP **05** \(2002\) 046](#), arXiv: [hep-ph/0112284](#).
- [61] T. Gleisberg et al., *Event generation with SHERPA 1.1*, [JHEP **02** \(2009\) 007](#), arXiv: [0811.4622 \[hep-ph\]](#).
- [62] T. Gleisberg and S. Höche, *Comix, a new matrix element generator*, [JHEP **12** \(2008\) 039](#), arXiv: [0808.3674 \[hep-ph\]](#).
- [63] F. Cascioli, P. Maierhöfer and S. Pozzorini, *Scattering Amplitudes with Open Loops*, [Phys. Rev. Lett. **108** \(2012\) 111601](#), arXiv: [1111.5206 \[hep-ph\]](#).
- [64] E. Bothmann et al., *Event generation with Sherpa 2.2*, [SciPost Phys. **7** \(2019\) 034](#), arXiv: [1905.09127 \[hep-ph\]](#).
- [65] B. Biedermann, A. Denner, S. Dittmaier, L. Hofer and B. Jäger, *Electroweak corrections to $pp \rightarrow \mu^+ \mu^- e^+ e^- + X$ at the LHC: a Higgs background study*, [Phys. Rev. Lett. **116** \(2016\) 161803](#), arXiv: [1601.07787 \[hep-ph\]](#).

- [66] B. Biedermann, A. Denner, S. Dittmaier, L. Hofer and B. Jäger, *Next-to-leading-order electroweak corrections to the production of four charged leptons at the LHC*, *JHEP* **01** (2017) 033, arXiv: [1611.05338 \[hep-ph\]](#).
- [67] ATLAS Collaboration, *The ATLAS Simulation Infrastructure*, *Eur. Phys. J. C* **70** (2010) 823, arXiv: [1005.4568 \[physics.ins-det\]](#).
- [68] GEANT4 Collaboration, S. Agostinelli et al., *GEANT4 – a simulation toolkit*, *Nucl. Instrum. Meth. A* **506** (2003) 250.
- [69] ATLAS Collaboration, *The Pythia 8 A3 tune description of ATLAS minimum bias and inelastic measurements incorporating the Donnachie–Landshoff diffractive model*, ATL-PHYS-PUB-2016-017, 2016, URL: <https://cds.cern.ch/record/2206965>.
- [70] ATLAS Collaboration, *Muon reconstruction and identification efficiency in ATLAS using the full Run 2 pp collision data set at $\sqrt{s} = 13$ TeV*, *Eur. Phys. J. C* **81** (2021) 578, arXiv: [2012.00578 \[hep-ex\]](#).
- [71] ATLAS Collaboration, *Electron and photon performance measurements with the ATLAS detector using the 2015–2017 LHC proton–proton collision data*, *JINST* **14** (2019) P12006, arXiv: [1908.00005 \[hep-ex\]](#).
- [72] ATLAS Collaboration, *Electron reconstruction and identification in the ATLAS experiment using the 2015 and 2016 LHC proton–proton collision data at $\sqrt{s} = 13$ TeV*, *Eur. Phys. J. C* **79** (2019) 639, arXiv: [1902.04655 \[hep-ex\]](#).
- [73] ATLAS Collaboration, *Jet reconstruction and performance using particle flow with the ATLAS Detector*, *Eur. Phys. J. C* **77** (2017) 466, arXiv: [1703.10485 \[hep-ex\]](#).
- [74] ATLAS Collaboration, *Topological cell clustering in the ATLAS calorimeters and its performance in LHC Run 1*, *Eur. Phys. J. C* **77** (2017) 490, arXiv: [1603.02934 \[hep-ex\]](#).
- [75] M. Cacciari, G. P. Salam and G. Soyez, *The anti- k_t jet clustering algorithm*, *JHEP* **04** (2008) 063, arXiv: [0802.1189 \[hep-ph\]](#).
- [76] M. Cacciari, G. P. Salam and G. Soyez, *FastJet user manual*, *Eur. Phys. J. C* **72** (2012) 1896, arXiv: [1111.6097 \[hep-ph\]](#).
- [77] ATLAS Collaboration, *Jet energy scale measurements and their systematic uncertainties in proton–proton collisions at $\sqrt{s} = 13$ TeV with the ATLAS detector*, *Phys. Rev. D* **96** (2017) 072002, arXiv: [1703.09665 \[hep-ex\]](#).
- [78] ATLAS Collaboration, *Jet mass reconstruction with the ATLAS Detector in early Run 2 data*, ATL-CONF-2016-035, 2016, URL: <https://cds.cern.ch/record/2200211>.
- [79] ATLAS Collaboration, *Tagging and suppression of pileup jets with the ATLAS detector*, ATL-CONF-2014-018, 2014, URL: <https://cds.cern.ch/record/1700870>.
- [80] ATLAS Collaboration, *Performance of pile-up mitigation techniques for jets in pp collisions at $\sqrt{s} = 8$ TeV using the ATLAS detector*, *Eur. Phys. J. C* **76** (2016) 581, arXiv: [1510.03823 \[hep-ex\]](#).
- [81] ATLAS Collaboration, *Forward Jet Vertex Tagging: A new technique for the identification and rejection of forward pileup jets*, ATL-PHYS-PUB-2015-034, 2015, URL: <https://cds.cern.ch/record/2042098>.

- [82] ATLAS Collaboration, *Forward jet vertex tagging using the particle flow algorithm*, ATL-PHYS-PUB-2019-026, 2019, URL: <https://cds.cern.ch/record/2683100>.
- [83] ATLAS Collaboration, *Luminosity determination in pp collisions at $\sqrt{s} = 13$ TeV using the ATLAS detector at the LHC*, ATLAS-CONF-2019-021, 2019, URL: <https://cds.cern.ch/record/2677054>.
- [84] G. Avoni et al., *The new LUCID-2 detector for luminosity measurement and monitoring in ATLAS*, *JINST* **13** (2018) P07017.
- [85] I. W. Stewart and F. J. Tackmann, *Theory uncertainties for Higgs mass and other searches using jet bins*, *Phys. Rev. D* **85** (2012) 034011, arXiv: [1107.2117](https://arxiv.org/abs/1107.2117) [hep-ph].
- [86] ATLAS Collaboration, *Measurement of the Z/γ^* boson transverse momentum distribution in pp collisions at $\sqrt{s} = 7$ TeV with the ATLAS detector*, *JHEP* **09** (2014) 145, arXiv: [1406.3660](https://arxiv.org/abs/1406.3660) [hep-ex].
- [87] J. Bellm et al., *Herwig 7.0/Herwig++ 3.0 release note*, *Eur. Phys. J. C* **76** (2016) 196, arXiv: [1512.01178](https://arxiv.org/abs/1512.01178) [hep-ph].
- [88] J. Bendauid et al., *Les Houches 2017: Physics at TeV Colliders Standard Model Working Group Report*, 2018, arXiv: [1803.07977](https://arxiv.org/abs/1803.07977) [hep-ph].
- [89] ATLAS Collaboration, *Measurement of the Higgs boson coupling properties in the $H \rightarrow ZZ^* \rightarrow 4\ell$ decay channel at $\sqrt{s} = 13$ TeV with the ATLAS detector*, *JHEP* **03** (2018) 095, arXiv: [1712.02304](https://arxiv.org/abs/1712.02304) [hep-ex].
- [90] G. Cowan, K. Cranmer, E. Gross and O. Vitells, *Asymptotic formulae for likelihood-based tests of new physics*, *Eur. Phys. J. C* **71** (2011) 1554, arXiv: [1007.1727](https://arxiv.org/abs/1007.1727) [physics.data-an], Erratum: *Eur. Phys. J. C* **73** (2013) 2501.
- [91] G. Bohm and G. Zech, *Introduction to statistics and data analysis for physicists*, Hamburg: DESY, 2014, ISBN: 978-3-935702-88-1.
- [92] ATLAS Collaboration, *Measurements of the Higgs boson inclusive and differential fiducial cross-sections in the diphoton decay channel with pp collisions at $\sqrt{s} = 13$ TeV with the ATLAS detector*, *JHEP* **08** (2022) 027, arXiv: [2202.00487](https://arxiv.org/abs/2202.00487) [hep-ex].
- [93] C. Anastasiou, C. Duhr, F. Dulat, F. Herzog and B. Mistlberger, *Higgs Boson Gluon-Fusion Production in QCD at Three Loops*, *Phys. Rev. Lett.* **114** (2015) 212001, arXiv: [1503.06056](https://arxiv.org/abs/1503.06056) [hep-ph].
- [94] C. Anastasiou et al., *High precision determination of the gluon fusion Higgs boson cross-section at the LHC*, *JHEP* **05** (2016) 058, arXiv: [1602.00695](https://arxiv.org/abs/1602.00695) [hep-ph].
- [95] ATLAS Collaboration, *ATLAS Computing Acknowledgements*, ATL-SOFT-PUB-2021-003, 2021, URL: <https://cds.cern.ch/record/2776662>.

The ATLAS Collaboration

G. Aad ¹⁰², B. Abbott ¹²⁰, K. Abeling ⁵⁵, N.J. Abicht ⁴⁹, S.H. Abidi ²⁹, A. Aboulhorma ^{35e}, H. Abramowicz ¹⁵¹, H. Abreu ¹⁵⁰, Y. Abulaiti ¹¹⁷, A.C. Abusleme Hoffman ^{137a}, B.S. Acharya ^{69a,69b,n}, C. Adam Bourdarios ⁴, L. Adamczyk ^{85a}, L. Adamek ¹⁵⁵, S.V. Addepalli ²⁶, M.J. Addison ¹⁰¹, J. Adelman ¹¹⁵, A. Adiguzel ^{21c}, T. Adye ¹³⁴, A.A. Affolder ¹³⁶, Y. Afik ³⁶, M.N. Agaras ¹³, J. Agarwala ^{73a,73b}, A. Aggarwal ¹⁰⁰, C. Agheorghiesei ^{27c}, A. Ahmad ³⁶, F. Ahmadov ^{38,y}, W.S. Ahmed ¹⁰⁴, S. Ahuja ⁹⁵, X. Ai ^{62a}, G. Aielli ^{76a,76b}, M. Ait Tamlihat ^{35e}, B. Aitbenkikh ^{35a}, I. Aizenberg ¹⁶⁸, M. Akbiyik ¹⁰⁰, T.P.A. Åkesson ⁹⁸, A.V. Akimov ³⁷, D. Akiyama ¹⁶⁷, N.N. Akolkar ²⁴, K. Al Houry ⁴¹, G.L. Alberghi ^{23b}, J. Albert ¹⁶⁴, P. Albicocco ⁵³, G.L. Albouy ⁶⁰, S. Alderweireldt ⁵², M. Aleksa ³⁶, I.N. Aleksandrov ³⁸, C. Alexa ^{27b}, T. Alexopoulos ¹⁰, A. Alfonsi ¹¹⁴, F. Alfonsi ^{23b}, M. Algren ⁵⁶, M. Alhroob ¹²⁰, B. Ali ¹³², H.M.J. Ali ⁹¹, S. Ali ¹⁴⁸, S.W. Alibocus ⁹², M. Aliev ³⁷, G. Alimonti ^{71a}, W. Alkahi ⁵⁵, C. Allaire ⁶⁶, B.M.M. Allbrooke ¹⁴⁶, J.F. Allen ⁵², C.A. Allendes Flores ^{137f}, P.P. Allport ²⁰, A. Aloisio ^{72a,72b}, F. Alonso ⁹⁰, C. Alpigiani ¹³⁸, M. Alvarez Estevez ⁹⁹, A. Alvarez Fernandez ¹⁰⁰, M.G. Alvigi ^{72a,72b}, M. Aly ¹⁰¹, Y. Amaral Coutinho ^{82b}, A. Ambler ¹⁰⁴, C. Amelung ³⁶, M. Amerl ¹⁰¹, C.G. Ames ¹⁰⁹, D. Amidei ¹⁰⁶, S.P. Amor Dos Santos ^{130a}, K.R. Amos ¹⁶², V. Ananiev ¹²⁵, C. Anastopoulos ¹³⁹, T. Andeen ¹¹, J.K. Anders ³⁶, S.Y. Andrean ^{47a,47b}, A. Andreazza ^{71a,71b}, S. Angelidakis ⁹, A. Angerami ^{41,aa}, A.V. Anisenkov ³⁷, A. Annovi ^{74a}, C. Antel ⁵⁶, M.T. Anthony ¹³⁹, E. Antipov ¹⁴⁵, M. Antonelli ⁵³, D.J.A. Antrim ^{17a}, F. Anulli ^{75a}, M. Aoki ⁸³, T. Aoki ¹⁵³, J.A. Aparisi Pozo ¹⁶², M.A. Aparo ¹⁴⁶, L. Aperio Bella ⁴⁸, C. Appelt ¹⁸, N. Aranzabal ³⁶, C. Arcangeletti ⁵³, A.T.H. Arce ⁵¹, E. Arena ⁹², J-F. Arguin ¹⁰⁸, S. Argyropoulos ⁵⁴, J.-H. Arling ⁴⁸, A.J. Armbruster ³⁶, O. Arnaez ⁴, H. Arnold ¹¹⁴, Z.P. Arrubarrena Tame ¹⁰⁹, G. Artoni ^{75a,75b}, H. Asada ¹¹¹, K. Asai ¹¹⁸, S. Asai ¹⁵³, N.A. Asbah ⁶¹, J. Assahsah ^{35d}, K. Assamagan ²⁹, R. Astalos ^{28a}, S. Atashi ¹⁵⁹, R.J. Atkin ^{33a}, M. Atkinson ¹⁶¹, N.B. Atlay ¹⁸, H. Atmani ^{62b}, P.A. Atmasiddha ¹⁰⁶, K. Augsten ¹³², S. Auricchio ^{72a,72b}, A.D. Auriol ²⁰, V.A. Austrup ¹⁰¹, G. Avolio ³⁶, K. Axiotis ⁵⁶, G. Azuelos ^{108,ac}, D. Babal ^{28b}, H. Bachacou ¹³⁵, K. Bachas ^{152,q}, A. Bachiu ³⁴, F. Backman ^{47a,47b}, A. Badea ⁶¹, P. Bagnaia ^{75a,75b}, M. Bahmani ¹⁸, A.J. Bailey ¹⁶², V.R. Bailey ¹⁶¹, J.T. Baines ¹³⁴, C. Bakalis ¹⁰, O.K. Baker ¹⁷¹, E. Bakos ¹⁵, D. Bakshi Gupta ⁸, R. Balasubramanian ¹¹⁴, E.M. Baldin ³⁷, P. Balek ^{85a}, E. Ballabene ^{23b,23a}, F. Balli ¹³⁵, L.M. Baltes ^{63a}, W.K. Balunas ³², J. Balz ¹⁰⁰, E. Banas ⁸⁶, M. Bandieramonte ¹²⁹, A. Bandyopadhyay ²⁴, S. Bansal ²⁴, L. Barak ¹⁵¹, M. Barakat ⁴⁸, E.L. Barberio ¹⁰⁵, D. Barberis ^{57b,57a}, M. Barbero ¹⁰², G. Barbour ⁹⁶, K.N. Barends ^{33a}, T. Barillari ¹¹⁰, M-S. Barisits ³⁶, T. Barklow ¹⁴³, P. Baron ¹²², D.A. Baron Moreno ¹⁰¹, A. Baroncelli ^{62a}, G. Barone ²⁹, A.J. Barr ¹²⁶, J.D. Barr ⁹⁶, L. Barranco Navarro ^{47a,47b}, F. Barreiro ⁹⁹, J. Barreiro Guimarães da Costa ^{14a}, U. Barron ¹⁵¹, M.G. Barros Teixeira ^{130a}, S. Barsov ³⁷, F. Bartels ^{63a}, R. Bartoldus ¹⁴³, A.E. Barton ⁹¹, P. Bartos ^{28a}, A. Basan ¹⁰⁰, M. Baselga ⁴⁹, A. Bassalat ⁶⁶, M.J. Basso ^{156a}, C.R. Basson ¹⁰¹, R.L. Bates ⁵⁹, S. Batlamous ^{35e}, J.R. Batley ³², B. Batool ¹⁴¹, M. Battaglia ¹³⁶, D. Battulga ¹⁸, M. Bauce ^{75a,75b}, M. Bauer ³⁶, P. Bauer ²⁴, L.T. Bazzano Hurrell ³⁰, J.B. Beacham ⁵¹, T. Beau ¹²⁷, P.H. Beauchemin ¹⁵⁸, F. Becherer ⁵⁴, P. Bechtel ²⁴, H.P. Beck ^{19,p}, K. Becker ¹⁶⁶, A.J. Beddall ^{21d}, V.A. Bednyakov ³⁸, C.P. Bee ¹⁴⁵, L.J. Beemster ¹⁵, T.A. Beermann ³⁶, M. Begalli ^{82d,82d}, M. Begel ²⁹, A. Behera ¹⁴⁵, J.K. Behr ⁴⁸, J.F. Beirer ⁵⁵, F. Beisiegel ²⁴, M. Belfkir ^{116b}, G. Bella ¹⁵¹, L. Bellagamba ^{23b}, A. Bellerive ³⁴, P. Bellos ²⁰, K. Beloborodov ³⁷, N.L. Belyaev ³⁷, D. Bencheikroun ^{35a}, F. Bendebba ^{35a},

Y. Benhammou [ID151](#), M. Benoit [ID29](#), J.R. Bensingler [ID26](#), S. Bentvelsen [ID114](#), L. Beresford [ID48](#),
 M. Beretta [ID53](#), E. Bergeaas Kuutmann [ID160](#), N. Berger [ID4](#), B. Bergmann [ID132](#), J. Beringer [ID17a](#),
 G. Bernardi [ID5](#), C. Bernius [ID143](#), F.U. Bernlochner [ID24](#), F. Bernon [ID36,102](#), T. Berry [ID95](#), P. Berta [ID133](#),
 A. Berthold [ID50](#), I.A. Bertram [ID91](#), S. Bethke [ID110](#), A. Betti [ID75a,75b](#), A.J. Bevan [ID94](#), M. Bhamjee [ID33c](#),
 S. Bhatta [ID145](#), D.S. Bhattacharya [ID165](#), P. Bhattarai [ID26](#), V.S. Bhopatkar [ID121](#), R. Bi [ID29,ae](#),
 R.M. Bianchi [ID129](#), G. Bianco [ID23b,23a](#), O. Biebel [ID109](#), R. Bielski [ID123](#), M. Biglietti [ID77a](#),
 T.R.V. Billoud [ID132](#), M. Bindi [ID55](#), A. Bingul [ID21b](#), C. Bini [ID75a,75b](#), A. Biondini [ID92](#),
 C.J. Birch-sykes [ID101](#), G.A. Bird [ID20,134](#), M. Birman [ID168](#), M. Biros [ID133](#), T. Bisanz [ID49](#),
 E. Bisceglie [ID43b,43a](#), D. Biswas [ID141](#), A. Bitadze [ID101](#), K. Bjørke [ID125](#), I. Bloch [ID48](#), C. Blocker [ID26](#),
 A. Blue [ID59](#), U. Blumenschein [ID94](#), J. Blumenthal [ID100](#), G.J. Bobbink [ID114](#), V.S. Bobrovnikov [ID37](#),
 M. Boehler [ID54](#), B. Boehm [ID165](#), D. Bogavac [ID36](#), A.G. Bogdanchikov [ID37](#), C. Bohm [ID47a](#),
 V. Boisvert [ID95](#), P. Bokan [ID48](#), T. Bold [ID85a](#), M. Bomben [ID5](#), M. Bona [ID94](#), M. Boonekamp [ID135](#),
 C.D. Booth [ID95](#), A.G. Borbély [ID59](#), I.S. Bordulev [ID37](#), H.M. Borecka-Bielska [ID108](#), L.S. Borgna [ID96](#),
 G. Borissov [ID91](#), D. Bortoletto [ID126](#), D. Boscherini [ID23b](#), M. Bosman [ID13](#), J.D. Bossio Sola [ID36](#),
 K. Bouaouda [ID35a](#), N. Bouchhar [ID162](#), J. Boudreau [ID129](#), E.V. Bouhova-Thacker [ID91](#), D. Boumediene [ID40](#),
 R. Bouquet [ID5](#), A. Boveia [ID119](#), J. Boyd [ID36](#), D. Boye [ID29](#), I.R. Boyko [ID38](#), J. Bracinik [ID20](#),
 N. Brahim [ID62d](#), G. Brandt [ID170](#), O. Brandt [ID32](#), F. Braren [ID48](#), B. Brau [ID103](#), J.E. Brau [ID123](#),
 R. Brenner [ID168](#), L. Brenner [ID114](#), R. Brenner [ID160](#), S. Bressler [ID168](#), D. Britton [ID59](#), D. Britzger [ID110](#),
 I. Brock [ID24](#), G. Brooijmans [ID41](#), W.K. Brooks [ID137f](#), E. Brost [ID29](#), L.M. Brown [ID164,1](#), L.E. Bruce [ID61](#),
 T.L. Bruckler [ID126](#), P.A. Bruckman de Renstrom [ID86](#), B. Brüers [ID48](#), D. Bruncko [ID28b,*](#), A. Bruni [ID23b](#),
 G. Bruni [ID23b](#), M. Bruschi [ID23b](#), N. Brusino [ID75a,75b](#), T. Buanes [ID16](#), Q. Buat [ID138](#), D. Buchin [ID110](#),
 A.G. Buckley [ID59](#), M.K. Bugge [ID125](#), O. Bulekov [ID37](#), B.A. Bullard [ID143](#), S. Burdin [ID92](#),
 C.D. Burgard [ID49](#), A.M. Burger [ID40](#), B. Burghgrave [ID8](#), O. Burlayenko [ID54](#), J.T.P. Burr [ID32](#),
 C.D. Burton [ID11](#), J.C. Burzynski [ID142](#), E.L. Busch [ID41](#), V. Büscher [ID100](#), P.J. Bussey [ID59](#),
 J.M. Butler [ID25](#), C.M. Buttar [ID59](#), J.M. Butterworth [ID96](#), W. Buttinger [ID134](#), C.J. Buxo Vazquez [ID107](#),
 A.R. Buzykaev [ID37](#), G. Cabras [ID23b](#), S. Cabrera Urbán [ID162](#), D. Caforio [ID58](#), H. Cai [ID129](#), Y. Cai [ID14a,14e](#),
 V.M.M. Cairo [ID36](#), O. Cakir [ID3a](#), N. Calace [ID36](#), P. Calafiura [ID17a](#), G. Calderini [ID127](#), P. Calfayan [ID68](#),
 G. Callea [ID59](#), L.P. Caloba [ID82b](#), D. Calvet [ID40](#), S. Calvet [ID40](#), T.P. Calvet [ID102](#), M. Calvetti [ID74a,74b](#),
 R. Camacho Toro [ID127](#), S. Camarda [ID36](#), D. Camarero Munoz [ID26](#), P. Camarri [ID76a,76b](#),
 M.T. Camerlingo [ID72a,72b](#), D. Cameron [ID125](#), C. Camincher [ID164](#), M. Campanelli [ID96](#), A. Camplani [ID42](#),
 V. Canale [ID72a,72b](#), A. Canesse [ID104](#), M. Cano Bret [ID80](#), J. Cantero [ID162](#), Y. Cao [ID161](#), F. Capocasa [ID26](#),
 M. Capua [ID43b,43a](#), A. Carbone [ID71a,71b](#), R. Cardarelli [ID76a](#), J.C.J. Cardenas [ID8](#), F. Cardillo [ID162](#),
 T. Carli [ID36](#), G. Carlino [ID72a](#), J.I. Carlotto [ID13](#), B.T. Carlson [ID129,r](#), E.M. Carlson [ID164,156a](#),
 L. Carminati [ID71a,71b](#), A. Carnelli [ID135](#), M. Carnesale [ID75a,75b](#), S. Caron [ID113](#), E. Carquin [ID137f](#),
 S. Carrá [ID71a,71b](#), G. Carratta [ID23b,23a](#), F. Carrio Argos [ID33g](#), J.W.S. Carter [ID155](#), T.M. Carter [ID52](#),
 M.P. Casado [ID13,i](#), M. Caspar [ID48](#), E.G. Castiglia [ID171](#), F.L. Castillo [ID4](#), L. Castillo Garcia [ID13](#),
 V. Castillo Gimenez [ID162](#), N.F. Castro [ID130a,130e](#), A. Catinaccio [ID36](#), J.R. Catmore [ID125](#), V. Cavaliere [ID29](#),
 N. Cavalli [ID23b,23a](#), V. Cavalanni [ID74a,74b](#), Y.C. Cekmecelioglu [ID48](#), E. Celebi [ID21a](#), F. Celli [ID126](#),
 M.S. Centonze [ID70a,70b](#), K. Cerny [ID122](#), A.S. Cerqueira [ID82a](#), A. Cerri [ID146](#), L. Cerrito [ID76a,76b](#),
 F. Cerutti [ID17a](#), B. Cervato [ID141](#), A. Cervelli [ID23b](#), G. Cesarini [ID53](#), S.A. Cetin [ID21d](#), Z. Chadi [ID35a](#),
 D. Chakraborty [ID115](#), M. Chala [ID130f](#), J. Chan [ID169](#), W.Y. Chan [ID153](#), J.D. Chapman [ID32](#),
 E. Chapon [ID135](#), B. Chargeishvili [ID149b](#), D.G. Charlton [ID20](#), T.P. Charman [ID94](#), M. Chatterjee [ID19](#),
 C. Chauhan [ID133](#), S. Chekanov [ID6](#), S.V. Chekulaev [ID156a](#), G.A. Chelkov [ID38,a](#), A. Chen [ID106](#),
 B. Chen [ID151](#), B. Chen [ID164](#), H. Chen [ID14c](#), H. Chen [ID29](#), J. Chen [ID62c](#), J. Chen [ID142](#), M. Chen [ID126](#),
 S. Chen [ID153](#), S.J. Chen [ID14c](#), X. Chen [ID62c](#), X. Chen [ID14b,ab](#), Y. Chen [ID62a](#), C.L. Cheng [ID169](#),
 H.C. Cheng [ID64a](#), S. Cheong [ID143](#), A. Cheplakov [ID38](#), E. Cheremushkina [ID48](#), E. Cherepanova [ID114](#),
 R. Cherkaoui El Moursli [ID35e](#), E. Cheu [ID7](#), K. Cheung [ID65](#), L. Chevalier [ID135](#), V. Chiarella [ID53](#),

G. Chiarelli ^{74a}, N. Chiedde ¹⁰², G. Chiodini ^{70a}, A.S. Chisholm ²⁰, A. Chitan ^{27b}, M. Chitishvili ¹⁶², M.V. Chizhov ³⁸, K. Choi ¹¹, A.R. Chomont ^{75a,75b}, Y. Chou ¹⁰³, E.Y.S. Chow ¹¹⁴, T. Chowdhury ^{33g}, K.L. Chu ¹⁶⁸, M.C. Chu ^{64a}, X. Chu ^{14a,14e}, J. Chudoba ¹³¹, J.J. Chwastowski ⁸⁶, D. Cieri ¹¹⁰, K.M. Ciesla ^{85a}, V. Cindro ⁹³, A. Ciocio ^{17a}, F. Cirotto ^{72a,72b}, Z.H. Citron ¹⁶⁸, M. Citterio ^{71a}, D.A. Ciubotaru ^{27b}, B.M. Ciungu ¹⁵⁵, A. Clark ⁵⁶, P.J. Clark ⁵², J.M. Clavijo Columbie ⁴⁸, S.E. Clawson ⁴⁸, C. Clement ^{47a,47b}, J. Clercx ⁴⁸, L. Clissa ^{23b,23a}, Y. Coadou ¹⁰², M. Cobal ^{69a,69c}, A. Coccaro ^{57b}, R.F. Coelho Barrue ^{130a}, R. Coelho Lopes De Sa ¹⁰³, S. Coelli ^{71a}, H. Cohen ¹⁵¹, A.E.C. Coimbra ^{71a,71b}, B. Cole ⁴¹, J. Collot ⁶⁰, P. Conde Muiño ^{130a,130g}, M.P. Connell ^{33c}, S.H. Connell ^{33c}, I.A. Connelly ⁵⁹, E.I. Conroy ¹²⁶, F. Conventi ^{72a,ad}, H.G. Cooke ²⁰, A.M. Cooper-Sarkar ¹²⁶, A. Cordeiro Oudot Choi ¹²⁷, F. Cormier ¹⁶³, L.D. Corpe ⁴⁰, M. Corradi ^{75a,75b}, F. Corriveau ^{104,w}, A. Cortes-Gonzalez ¹⁸, M.J. Costa ¹⁶², F. Costanza ⁴, D. Costanzo ¹³⁹, B.M. Cote ¹¹⁹, G. Cowan ⁹⁵, K. Cranmer ¹⁶⁹, D. Cremonini ^{23b,23a}, S. Crépe-Renaudin ⁶⁰, F. Crescioli ¹²⁷, M. Cristinziani ¹⁴¹, M. Cristoforetti ^{78a,78b}, V. Croft ¹¹⁴, J.E. Crosby ¹²¹, G. Crosetti ^{43b,43a}, A. Cueto ⁹⁹, T. Cuhadar Donszelmann ¹⁵⁹, H. Cui ^{14a,14e}, Z. Cui ⁷, W.R. Cunningham ⁵⁹, F. Curcio ^{43b,43a}, P. Czodrowski ³⁶, M.M. Czurylo ^{63b}, M.J. Da Cunha Sargedas De Sousa ^{62a}, J.V. Da Fonseca Pinto ^{82b}, C. Da Via ¹⁰¹, W. Dabrowski ^{85a}, T. Dado ⁴⁹, S. Dahbi ^{33g}, T. Dai ¹⁰⁶, C. Dallapiccola ¹⁰³, M. Dam ⁴², G. D'amen ²⁹, V. D'Amico ¹⁰⁹, J. Damp ¹⁰⁰, J.R. Dandoy ¹²⁸, M.F. Daneri ³⁰, M. Danninger ¹⁴², V. Dao ³⁶, G. Darbo ^{57b}, S. Darmora ⁶, S.J. Das ²⁹, S. D'Auria ^{71a,71b}, C. David ^{156b}, T. Davidek ¹³³, B. Davis-Purcell ³⁴, I. Dawson ⁹⁴, H.A. Day-hall ¹³², K. De ⁸, R. De Asmundis ^{72a}, N. De Biase ⁴⁸, S. De Castro ^{23b,23a}, N. De Groot ¹¹³, P. de Jong ¹¹⁴, H. De la Torre ¹⁰⁷, A. De Maria ^{14c}, A. De Salvo ^{75a}, U. De Sanctis ^{76a,76b}, A. De Santo ¹⁴⁶, J.B. De Vivie De Regie ⁶⁰, D.V. Dedovich ³⁸, J. Degens ¹¹⁴, A.M. Deiana ⁴⁴, F. Del Corso ^{23b,23a}, J. Del Peso ⁹⁹, F. Del Rio ^{63a}, F. Deliot ¹³⁵, C.M. Delitzsch ⁴⁹, M. Della Pietra ^{72a,72b}, D. Della Volpe ⁵⁶, A. Dell'Acqua ³⁶, L. Dell'Asta ^{71a,71b}, M. Delmastro ⁴, P.A. Delsart ⁶⁰, S. Demers ¹⁷¹, M. Demichev ³⁸, S.P. Denisov ³⁷, L. D'Eramo ⁴⁰, D. Derendarz ⁸⁶, F. Derue ¹²⁷, P. Dervan ⁹², K. Desch ²⁴, C. Deutsch ²⁴, F.A. Di Bello ^{57b,57a}, A. Di Ciaccio ^{76a,76b}, L. Di Ciaccio ⁴, A. Di Domenico ^{75a,75b}, C. Di Donato ^{72a,72b}, A. Di Girolamo ³⁶, G. Di Gregorio ⁵, A. Di Luca ^{78a,78b}, B. Di Micco ^{77a,77b}, R. Di Nardo ^{77a,77b}, C. Diaconu ¹⁰², F.A. Dias ¹¹⁴, T. Dias Do Vale ¹⁴², M.A. Diaz ^{137a,137b}, F.G. Diaz Capriles ²⁴, M. Didenko ¹⁶², E.B. Diehl ¹⁰⁶, L. Diehl ⁵⁴, S. Díez Cornell ⁴⁸, C. Diez Pardos ¹⁴¹, C. Dimitriadi ^{24,160}, A. Dimitrievska ^{17a}, J. Dingfelder ²⁴, I-M. Dinu ^{27b}, S.J. Dittmeier ^{63b}, F. Dittus ³⁶, F. Djama ¹⁰², T. Djobava ^{149b}, J.I. Djuvsland ¹⁶, C. Doglioni ^{101,98}, J. Dolejsi ¹³³, Z. Dolezal ¹³³, M. Donadelli ^{82c}, B. Dong ¹⁰⁷, J. Donini ⁴⁰, A. D'Onofrio ^{77a,77b}, M. D'Onofrio ⁹², J. Dopke ¹³⁴, A. Doria ^{72a}, N. Dos Santos Fernandes ^{130a}, M.T. Dova ⁹⁰, A.T. Doyle ⁵⁹, M.A. Draguet ¹²⁶, E. Dreyer ¹⁶⁸, I. Drivas-koulouris ¹⁰, A.S. Drobac ¹⁵⁸, M. Drozdova ⁵⁶, D. Du ^{62a}, T.A. du Pree ¹¹⁴, F. Dubinin ³⁷, M. Dubovsky ^{28a}, E. Duchovni ¹⁶⁸, G. Duckeck ¹⁰⁹, O.A. Ducu ^{27b}, D. Duda ⁵², A. Dudarev ³⁶, E.R. Duden ²⁶, M. D'uffici ¹⁰¹, L. Duflot ⁶⁶, M. Dührssen ³⁶, C. Dülßen ¹⁷⁰, A.E. Dumitriu ^{27b}, M. Dunford ^{63a}, S. Dungs ⁴⁹, K. Dunne ^{47a,47b}, A. Duperrin ¹⁰², H. Duran Yildiz ^{3a}, M. Düren ⁵⁸, A. Durglishvili ^{149b}, B.L. Dwyer ¹¹⁵, G.I. Dyckes ^{17a}, M. Dyndal ^{85a}, S. Dysch ¹⁰¹, B.S. Dziedzic ⁸⁶, Z.O. Earnshaw ¹⁴⁶, G.H. Eberwein ¹²⁶, B. Eckerova ^{28a}, S. Eggebrecht ⁵⁵, M.G. Eggleston ⁵¹, E. Egidio Purcino De Souza ¹²⁷, L.F. Ehrke ⁵⁶, G. Eigen ¹⁶, K. Einsweiler ^{17a}, T. Ekelof ¹⁶⁰, P.A. Ekman ⁹⁸, Y. El Ghazali ^{35b}, H. El Jarrari ^{35e,148}, A. El Moussaouy ^{35a}, V. Ellajosyula ¹⁶⁰, M. Ellert ¹⁶⁰, F. Ellinghaus ¹⁷⁰, A.A. Elliot ⁹⁴, N. Ellis ³⁶, J. Elmsheuser ²⁹, M. Elsing ³⁶, D. Emelianov ¹³⁴, Y. Enari ¹⁵³, I. Ene ^{17a}, S. Epari ¹³, J. Erdmann ⁴⁹, P.A. Erland ⁸⁶, M. Errenst ¹⁷⁰, M. Escalier ⁶⁶,

C. Escobar ¹⁶², E. Etzion ¹⁵¹, G. Evans ^{130a}, H. Evans ⁶⁸, L.S. Evans ⁹⁵, M.O. Evans ¹⁴⁶, A. Ezhilov ³⁷, S. Ezzarqtouni ^{35a}, F. Fabbri ⁵⁹, L. Fabbri ^{23b,23a}, G. Facini ⁹⁶, V. Fadeyev ¹³⁶, R.M. Fakhrutdinov ³⁷, S. Falciano ^{75a}, L.F. Falda Ulhoa Coelho ³⁶, P.J. Falke ²⁴, J. Faltova ¹³³, C. Fan ¹⁶¹, Y. Fan ^{14a}, Y. Fang ^{14a,14e}, M. Fanti ^{71a,71b}, M. Faraj ^{69a,69b}, Z. Farazpay ⁹⁷, A. Farbin ⁸, A. Farilla ^{77a}, T. Farooque ¹⁰⁷, S.M. Farrington ⁵², F. Fassi ^{35e}, D. Fassouliotis ⁹, M. Faucci Giannelli ^{76a,76b}, W.J. Fawcett ³², L. Fayard ⁶⁶, P. Federic ¹³³, P. Federicova ¹³¹, O.L. Fedin ^{37,a}, G. Fedotov ³⁷, M. Feickert ¹⁶⁹, L. Feligioni ¹⁰², A. Fell ¹³⁹, D.E. Fellers ¹²³, C. Feng ^{62b}, M. Feng ^{14b}, Z. Feng ¹¹⁴, M.J. Fenton ¹⁵⁹, A.B. Fenyuk ³⁷, L. Ferencz ⁴⁸, R.A.M. Ferguson ⁹¹, S.I. Fernandez Luengo ^{137f}, J.A. Fernandez Pretel ⁵⁴, M.J.V. Fernoux ¹⁰², J. Ferrando ⁴⁸, A. Ferrari ¹⁶⁰, P. Ferrari ^{114,113}, R. Ferrari ^{73a}, D. Ferrere ⁵⁶, C. Ferretti ¹⁰⁶, F. Fiedler ¹⁰⁰, A. Filipčič ⁹³, E.K. Filmer ¹, F. Filthaut ¹¹³, M.C.N. Fiolhais ^{130a,130c,c}, L. Fiorini ¹⁶², W.C. Fisher ¹⁰⁷, T. Fitschen ¹⁰¹, P.M. Fitzhugh ¹³⁵, I. Fleck ¹⁴¹, P. Fleischmann ¹⁰⁶, T. Flick ¹⁷⁰, L. Flores ¹²⁸, M. Flores ^{33d}, L.R. Flores Castillo ^{64a}, L. Flores Sanz De Acedo ³⁶, F.M. Follega ^{78a,78b}, N. Fomin ¹⁶, J.H. Foo ¹⁵⁵, B.C. Forland ⁶⁸, A. Formica ¹³⁵, A.C. Forti ¹⁰¹, E. Fortin ³⁶, A.W. Fortman ⁶¹, M.G. Foti ^{17a}, L. Fountas ⁹, D. Fournier ⁶⁶, H. Fox ⁹¹, P. Francavilla ^{74a,74b}, S. Francescato ⁶¹, S. Franchellucci ⁵⁶, M. Franchini ^{23b,23a}, S. Franchino ^{63a}, D. Francis ³⁶, L. Franco ¹¹³, L. Franconi ⁴⁸, M. Franklin ⁶¹, G. Frattari ²⁶, A.C. Freegard ⁹⁴, W.S. Freund ^{82b}, Y.Y. Frid ¹⁵¹, N. Fritzsche ⁵⁰, A. Froch ⁵⁴, D. Froidevaux ³⁶, J.A. Frost ¹²⁶, Y. Fu ^{62a}, M. Fujimoto ¹¹⁸, E. Fullana Torregrosa ^{162,*}, K.Y. Fung ^{64a}, E. Furtado De Simas Filho ^{82b}, M. Furukawa ¹⁵³, J. Fuster ¹⁶², A. Gabrielli ^{23b,23a}, A. Gabrielli ¹⁵⁵, P. Gadow ⁴⁸, G. Gagliardi ^{57b,57a}, L.G. Gagnon ^{17a}, E.J. Gallas ¹²⁶, B.J. Gallop ¹³⁴, K.K. Gan ¹¹⁹, S. Ganguly ¹⁵³, J. Gao ^{62a}, Y. Gao ⁵², F.M. Garay Walls ^{137a,137b}, B. Garcia ^{29,ae}, C. García ¹⁶², A. Garcia Alonso ¹¹⁴, A.G. Garcia Caffaro ¹⁷¹, J.E. García Navarro ¹⁶², M. Garcia-Sciveres ^{17a}, G.L. Gardner ¹²⁸, R.W. Gardner ³⁹, N. Garelli ¹⁵⁸, D. Garg ⁸⁰, R.B. Garg ¹⁴³, J.M. Gargan ⁵², C.A. Garner ¹⁵⁵, S.J. Gasiorowski ¹³⁸, P. Gaspar ^{82b}, G. Gaudio ^{73a}, V. Gautam ¹³, P. Gauzzi ^{75a,75b}, I.L. Gavrilenko ³⁷, A. Gavrilyuk ³⁷, C. Gay ¹⁶³, G. Gaycken ⁴⁸, E.N. Gazis ¹⁰, A.A. Geanta ^{27b}, C.M. Gee ¹³⁶, C. Gemme ^{57b}, M.H. Genest ⁶⁰, S. Gentile ^{75a,75b}, S. George ⁹⁵, W.F. George ²⁰, T. Geralis ⁴⁶, P. Gessinger-Befurt ³⁶, M.E. Geyik ¹⁷⁰, M. Ghneimat ¹⁴¹, K. Ghorbanian ⁹⁴, A. Ghosal ¹⁴¹, A. Ghosh ¹⁵⁹, A. Ghosh ⁷, B. Giacobbe ^{23b}, S. Giagu ^{75a,75b}, P. Giannetti ^{74a}, A. Giannini ^{62a}, S.M. Gibson ⁹⁵, M. Gignac ¹³⁶, D.T. Gil ^{85b}, A.K. Gilbert ^{85a}, B.J. Gilbert ⁴¹, D. Gillberg ³⁴, G. Gilles ¹¹⁴, N.E.K. Gillwald ⁴⁸, L. Ginabat ¹²⁷, D.M. Gingrich ^{2,ac}, M.P. Giordani ^{69a,69c}, P.F. Giraud ¹³⁵, G. Giugliarelli ^{69a,69c}, D. Giugni ^{71a}, F. Giuli ³⁶, I. Gkialas ^{9j}, L.K. Gladilin ³⁷, C. Glasman ⁹⁹, G.R. Gledhill ¹²³, M. Glisic ¹²³, I. Gnesi ^{43b,f}, Y. Go ^{29,ae}, M. Goblirsch-Kolb ³⁶, B. Gocke ⁴⁹, D. Godin ¹⁰⁸, B. Gokturk ^{21a}, S. Goldfarb ¹⁰⁵, T. Golling ⁵⁶, M.G.D. Gololo ^{33g}, D. Golubkov ³⁷, J.P. Gombas ¹⁰⁷, A. Gomes ^{130a,130b}, G. Gomes Da Silva ¹⁴¹, A.J. Gomez Delegido ¹⁶², R. Gonçalo ^{130a,130c}, G. Gonella ¹²³, L. Gonella ²⁰, A. Gongadze ³⁸, F. Gonnella ²⁰, J.L. Gonski ⁴¹, S. González de la Hoz ¹⁶², S. Gonzalez Fernandez ¹³, R. Gonzalez Lopez ⁹², C. Gonzalez Renteria ^{17a}, R. Gonzalez Suarez ¹⁶⁰, S. Gonzalez-Sevilla ⁵⁶, G.R. Gonzalvo Rodriguez ¹⁶², R.Y. González Andana ⁵², L. Goossens ³⁶, P.A. Gorbounov ³⁷, B. Gorini ³⁶, E. Gorini ^{70a,70b}, A. Gorišek ⁹³, T.C. Gosart ¹²⁸, A.T. Goshaw ⁵¹, M.I. Gostkin ³⁸, S. Goswami ¹²¹, C.A. Gottardo ³⁶, M. Gouighri ^{35b}, V. Goumarre ⁴⁸, A.G. Goussiou ¹³⁸, N. Govender ^{33c}, I. Grabowska-Bold ^{85a}, K. Graham ³⁴, E. Gramstad ¹²⁵, S. Grancagnolo ^{70a,70b}, M. Grandi ¹⁴⁶, V. Gratchev ^{37,*}, P.M. Gravila ^{27f}, F.G. Gravili ^{70a,70b}, H.M. Gray ^{17a}, M. Greco ^{70a,70b}, C. Grefe ²⁴, I.M. Gregor ⁴⁸, P. Grenier ¹⁴³, C. Grieco ¹³, A.A. Grillo ¹³⁶, K. Grimm ³¹, S. Grinstein ^{13,t}, J.-F. Grivaz ⁶⁶, E. Gross ¹⁶⁸, J. Grosse-Knetter ⁵⁵, C. Grud ¹⁰⁶, J.C. Grundy ¹²⁶, L. Guan ¹⁰⁶, W. Guan ¹⁶⁹, C. Gubbels ¹⁶³, J.G.R. Guerrero Rojas ¹⁶²,

G. Guerrieri ^{69a,69b}, F. Guescini ¹¹⁰, R. Gugel ¹⁰⁰, J.A.M. Guhit ¹⁰⁶, A. Guida ¹⁸,
T. Guillemain ⁴, E. Guilloton ^{166,134}, S. Guindon ³⁶, F. Guo ^{14a,14e}, J. Guo ^{62c}, L. Guo ⁴⁸,
Y. Guo ¹⁰⁶, R. Gupta ⁴⁸, S. Gurbuz ²⁴, S.S. Gurdasani ⁵⁴, G. Gustavino ³⁶, M. Guth ⁵⁶,
P. Gutierrez ¹²⁰, L.F. Gutierrez Zagazeta ¹²⁸, C. Gutschow ⁹⁶, C. Gwenlan ¹²⁶, C.B. Gwilliam ⁹²,
E.S. Haaland ¹²⁵, A. Haas ¹¹⁷, M. Habedank ⁴⁸, C. Haber ^{17a}, H.K. Hadavand ⁸, A. Hadeef ¹⁰⁰,
S. Hadzic ¹¹⁰, J.J. Hahn ¹⁴¹, E.H. Haines ⁹⁶, M. Haleem ¹⁶⁵, J. Haley ¹²¹, J.J. Hall ¹³⁹,
G.D. Hallewell ¹⁰², L. Halser ¹⁹, K. Hamano ¹⁶⁴, H. Hamdaoui ^{35e}, M. Hamer ²⁴,
G.N. Hamity ⁵², E.J. Hampshire ⁹⁵, J. Han ^{62b}, K. Han ^{62a}, L. Han ^{14c}, L. Han ^{62a}, S. Han ^{17a},
Y.F. Han ¹⁵⁵, K. Hanagaki ⁸³, M. Hance ¹³⁶, D.A. Hangal ^{41,aa}, H. Hanif ¹⁴², M.D. Hank ¹²⁸,
R. Hankache ¹⁰¹, J.B. Hansen ⁴², J.D. Hansen ⁴², P.H. Hansen ⁴², K. Hara ¹⁵⁷, D. Harada ⁵⁶,
T. Harenberg ¹⁷⁰, S. Harkusha ³⁷, Y.T. Harris ¹²⁶, N.M. Harrison ¹¹⁹, P.F. Harrison ¹⁶⁶,
N.M. Hartman ¹⁴³, N.M. Hartmann ¹⁰⁹, Y. Hasegawa ¹⁴⁰, A. Hasib ⁵², S. Haug ¹⁹,
R. Hauser ¹⁰⁷, C.M. Hawkes ²⁰, R.J. Hawkings ³⁶, Y. Hayashi ¹⁵³, S. Hayashida ¹¹¹,
D. Hayden ¹⁰⁷, C. Hayes ¹⁰⁶, R.L. Hayes ¹¹⁴, C.P. Hays ¹²⁶, J.M. Hays ⁹⁴, H.S. Hayward ⁹²,
F. He ^{62a}, M. He ^{14a,14e}, Y. He ¹⁵⁴, Y. He ¹²⁷, N.B. Heatley ⁹⁴, V. Hedberg ⁹⁸,
A.L. Heggelund ¹²⁵, N.D. Hehir ⁹⁴, C. Heidegger ⁵⁴, K.K. Heidegger ⁵⁴, W.D. Heidorn ⁸¹,
J. Heilman ³⁴, S. Heim ⁴⁸, T. Heim ^{17a}, J.G. Heinlein ¹²⁸, J.J. Heinrich ¹²³, L. Heinrich ¹¹⁰,
J. Hejbal ¹³¹, L. Helary ⁴⁸, A. Held ¹⁶⁹, S. Hellesund ¹⁶, C.M. Helling ¹⁶³, S. Hellman ^{47a,47b},
C. Hensens ³⁶, R.C.W. Henderson ⁹¹, L. Henkelmann ³², A.M. Henriques Correia ³⁶, H. Herde ⁹⁸,
Y. Hernández Jiménez ¹⁴⁵, L.M. Herrmann ²⁴, T. Herrmann ⁵⁰, G. Herten ⁵⁴, R. Hertenberger ¹⁰⁹,
L. Hervas ³⁶, M.E. Hespings ¹⁰⁰, N.P. Hessey ^{156a}, H. Hibi ⁸⁴, S.J. Hillier ²⁰, J.R. Hinds ¹⁰⁷,
F. Hinterkeuser ²⁴, M. Hirose ¹²⁴, S. Hirose ¹⁵⁷, D. Hirschbuehl ¹⁷⁰, T.G. Hitchings ¹⁰¹,
B. Hiti ⁹³, J. Hobbs ¹⁴⁵, R. Hobincu ^{27e}, N. Hod ¹⁶⁸, M.C. Hodgkinson ¹³⁹, B.H. Hodgkinson ³²,
A. Hoecker ³⁶, J. Hofer ⁴⁸, T. Holm ²⁴, M. Holzbock ¹¹⁰, L.B.A.H. Hommels ³², B.P. Honan ¹⁰¹,
J. Hong ^{62c}, T.M. Hong ¹²⁹, B.H. Hooberman ¹⁶¹, W.H. Hopkins ⁶, Y. Horii ¹¹¹, S. Hou ¹⁴⁸,
A.S. Howard ⁹³, J. Howarth ⁵⁹, J. Hoya ⁶, M. Hrabovsky ¹²², A. Hrynevich ⁴⁸, T. Hryn'ova ⁴,
P.J. Hsu ⁶⁵, S.-C. Hsu ¹³⁸, Q. Hu ⁴¹, Y.F. Hu ^{14a,14e}, S. Huang ^{64b}, X. Huang ^{14c}, Y. Huang ^{62a},
Y. Huang ^{14a}, Z. Huang ¹⁰¹, Z. Hubacek ¹³², M. Huebner ²⁴, F. Huegging ²⁴, T.B. Huffman ¹²⁶,
C.A. Hugli ⁴⁸, M. Huhtinen ³⁶, S.K. Huiberts ¹⁶, R. Hulsken ¹⁰⁴, N. Huseynov ^{12,a},
J. Huston ¹⁰⁷, J. Huth ⁶¹, R. Hyneman ¹⁴³, G. Iacobucci ⁵⁶, G. Iakovidis ²⁹, I. Ibragimov ¹⁴¹,
L. Iconomidou-Fayard ⁶⁶, P. Iengo ^{72a,72b}, R. Iguchi ¹⁵³, T. Iizawa ⁸³, Y. Ikegami ⁸³, N. Ilic ¹⁵⁵,
H. Imam ^{35a}, M. Ince Lezki ⁵⁶, T. Ingebretsen Carlson ^{47a,47b}, G. Introzzi ^{73a,73b}, M. Iodice ^{77a},
V. Ippolito ^{75a,75b}, R.K. Irwin ⁹², M. Ishino ¹⁵³, W. Islam ¹⁶⁹, C. Issever ^{18,48}, S. Istin ^{21a},
H. Ito ¹⁶⁷, J.M. Iturbe Ponce ^{64a}, R. Iuppa ^{78a,78b}, A. Ivina ¹⁶⁸, J.M. Izen ⁴⁵, V. Izzo ^{72a},
P. Jacka ^{131,132}, P. Jackson ¹, R.M. Jacobs ⁴⁸, B.P. Jaeger ¹⁴², C.S. Jagfeld ¹⁰⁹, P. Jain ⁵⁴,
G. Jäkel ¹⁷⁰, K. Jakobs ⁵⁴, T. Jakoubek ¹⁶⁸, J. Jamieson ⁵⁹, K.W. Janas ^{85a}, A.E. Jaspán ⁹²,
M. Javurkova ¹⁰³, F. Jeanneau ¹³⁵, L. Jeanty ¹²³, J. Jejelava ^{149a,z}, P. Jenni ^{54,g},
C.E. Jessiman ³⁴, S. Jézéquel ⁴, C. Jia ^{62b}, J. Jia ¹⁴⁵, X. Jia ⁶¹, X. Jia ^{14a,14e}, Z. Jia ^{14c},
Y. Jiang ^{62a}, S. Jiggins ⁴⁸, J. Jimenez Pena ¹³, S. Jin ^{14c}, A. Jinaru ^{27b}, O. Jinnouchi ¹⁵⁴,
P. Johansson ¹³⁹, K.A. Johns ⁷, J.W. Johnson ¹³⁶, D.M. Jones ³², E. Jones ⁴⁸, P. Jones ³²,
R.W.L. Jones ⁹¹, T.J. Jones ⁹², R. Joshi ¹¹⁹, J. Jovicevic ¹⁵, X. Ju ^{17a}, J.J. Junggeburth ³⁶,
T. Junkermann ^{63a}, A. Juste Rozas ^{13,t}, M.K. Juzek ⁸⁶, S. Kabana ^{137e}, A. Kaczmarzka ⁸⁶,
M. Kado ¹¹⁰, H. Kagan ¹¹⁹, M. Kagan ¹⁴³, A. Kahn ⁴¹, A. Kahn ¹²⁸, C. Kahra ¹⁰⁰, T. Kaji ¹⁶⁷,
E. Kajomovitz ¹⁵⁰, N. Kakati ¹⁶⁸, I. Kalaitzidou ⁵⁴, C.W. Kalderon ²⁹, A. Kamenshchikov ¹⁵⁵,
S. Kanayama ¹⁵⁴, N.J. Kang ¹³⁶, D. Kar ^{33g}, K. Karava ¹²⁶, M.J. Kareem ^{156b}, E. Karentzos ⁵⁴,
I. Karknias ¹⁵², O. Karkout ¹¹⁴, S.N. Karpov ³⁸, Z.M. Karpova ³⁸, V. Kartvelishvili ⁹¹,
A.N. Karyukhin ³⁷, E. Kasimi ¹⁵², J. Katzy ⁴⁸, S. Kaur ³⁴, K. Kawade ¹⁴⁰, T. Kawamoto ¹³⁵,

E.F. Kay [ID36](#), F.I. Kaya [ID158](#), S. Kazakos [ID13](#), V.F. Kazanin [ID37](#), Y. Ke [ID145](#), J.M. Keaveney [ID33a](#),
 R. Keeler [ID164](#), G.V. Kehris [ID61](#), J.S. Keller [ID34](#), A.S. Kelly⁹⁶, J.J. Kempster [ID146](#), K.E. Kennedy [ID41](#),
 P.D. Kennedy [ID100](#), O. Kepka [ID131](#), B.P. Kerridge [ID166](#), S. Kersten [ID170](#), B.P. Kerševan [ID93](#),
 S. Keshri [ID66](#), L. Keszeghova [ID28a](#), S. Ketabchi Haghghat [ID155](#), M. Khandoga [ID127](#), A. Khanov [ID121](#),
 A.G. Kharlamov [ID37](#), T. Kharlamova [ID37](#), E.E. Khoda [ID138](#), T.J. Khoo [ID18](#), G. Khorauli [ID165](#),
 J. Khubua [ID149b](#), Y.A.R. Khwaira [ID66](#), M. Kiehn [ID36](#), A. Kilgallon [ID123](#), D.W. Kim [ID47a,47b](#),
 Y.K. Kim [ID39](#), N. Kimura [ID96](#), A. Kirchhoff [ID55](#), C. Kirfel [ID24](#), F. Kirfel [ID24](#), J. Kirk [ID134](#),
 A.E. Kiryunin [ID110](#), C. Kitsaki [ID10](#), O. Kivernyk [ID24](#), M. Klassen [ID63a](#), C. Klein [ID34](#), L. Klein [ID165](#),
 M.H. Klein [ID106](#), M. Klein [ID92](#), S.B. Klein [ID56](#), U. Klein [ID92](#), P. Klimek [ID36](#), A. Klimentov [ID29](#),
 T. Klioutchnikova [ID36](#), P. Kluit [ID114](#), S. Kluth [ID110](#), E. Kneringer [ID79](#), T.M. Knight [ID155](#), A. Knue [ID54](#),
 R. Kobayashi [ID87](#), S.F. Koch [ID126](#), M. Kocian [ID143](#), P. Kodyš [ID133](#), D.M. Koeck [ID123](#), P.T. Koenig [ID24](#),
 T. Koffas [ID34](#), M. Kolb [ID135](#), I. Koletsou [ID4](#), T. Komarek [ID122](#), K. Köneke [ID54](#), A.X.Y. Kong [ID1](#),
 T. Kono [ID118](#), R. Konoplich [ID117,ag](#), N. Konstantinidis [ID96](#), B. Konya [ID98](#), R. Kopeliansky [ID68](#),
 S. Koperny [ID85a](#), K. Korcyl [ID86](#), K. Kordas [ID152,e](#), G. Koren [ID151](#), A. Korn [ID96](#), S. Korn [ID55](#),
 I. Korolkov [ID13](#), N. Korotkova [ID37](#), B. Kortman [ID114](#), O. Kortner [ID110](#), S. Kortner [ID110](#),
 W.H. Kostecka [ID115](#), V.V. Kostyukhin [ID141](#), A. Kotsokechagia [ID135](#), A. Kotwal [ID51](#), A. Koulouris [ID36](#),
 A. Kourkoumeli-Charalampidi [ID73a,73b](#), C. Kourkoumelis [ID9](#), E. Kourlitis [ID6](#), O. Kovanda [ID146](#),
 R. Kowalewski [ID164](#), W. Kozanecki [ID135](#), A.S. Kozhin [ID37](#), V.A. Kramarenko [ID37](#), G. Kramberger [ID93](#),
 P. Kramer [ID100](#), M.W. Krasny [ID127](#), A. Krasznahorkay [ID36](#), J.W. Kraus [ID170](#), J.A. Kremer [ID100](#),
 T. Kresse [ID50](#), J. Kretschmar [ID92](#), K. Kreul [ID18](#), P. Krieger [ID155](#), S. Krishnamurthy [ID103](#),
 M. Krivos [ID133](#), K. Krizka [ID20](#), K. Kroeninger [ID49](#), H. Kroha [ID110](#), J. Kroll [ID131](#), J. Kroll [ID128](#),
 K.S. Krowpman [ID107](#), U. Kruchonak [ID38](#), H. Krüger [ID24](#), N. Krumnack⁸¹, M.C. Kruse [ID51](#),
 J.A. Krzysiak [ID86](#), O. Kuchinskaia [ID37](#), S. Kuday [ID3a](#), S. Kuehn [ID36](#), R. Kuesters [ID54](#), T. Kuhl [ID48](#),
 V. Kukhtin [ID38](#), Y. Kulchitsky [ID37,a](#), S. Kuleshov [ID137d,137b](#), M. Kumar [ID33g](#), N. Kumari [ID102](#),
 A. Kupco [ID131](#), T. Kupfer⁴⁹, A. Kupich [ID37](#), O. Kuprash [ID54](#), H. Kurashige [ID84](#), L.L. Kurchaninov [ID156a](#),
 O. Kurdysh [ID66](#), Y.A. Kurochkin [ID37](#), A. Kurova [ID37](#), M. Kuze [ID154](#), A.K. Kvam [ID103](#), J. Kvita [ID122](#),
 T. Kwan [ID104](#), N.G. Kyriacou [ID106](#), L.A.O. Laatu [ID102](#), C. Lacasta [ID162](#), F. Lacava [ID75a,75b](#),
 H. Lacker [ID18](#), D. Lacour [ID127](#), N.N. Lad [ID96](#), E. Ladygin [ID38](#), B. Laforge [ID127](#), T. Lagouri [ID137e](#),
 S. Lai [ID55](#), I.K. Lakomic [ID85a](#), N. Lalloue [ID60](#), J.E. Lambert [ID164,1](#), S. Lammers [ID68](#), W. Lampl [ID7](#),
 C. Lampoudis [ID152,e](#), A.N. Lancaster [ID115](#), E. Lançon [ID29](#), U. Landgraf [ID54](#), M.P.J. Landon [ID94](#),
 V.S. Lang [ID54](#), R.J. Langenberg [ID103](#), O.K.B. Langrekken [ID125](#), A.J. Lankford [ID159](#), F. Lanni [ID36](#),
 K. Lantzs [ID24](#), A. Lanza [ID73a](#), A. Lapertosa [ID57b,57a](#), J.F. Laporte [ID135](#), T. Lari [ID71a](#),
 F. Lasagni Manghi [ID23b](#), M. Lassnig [ID36](#), V. Latonova [ID131](#), A. Laudrain [ID100](#), A. Laurier [ID150](#),
 S.D. Lawlor [ID95](#), Z. Lawrence [ID101](#), M. Lazzaroni [ID71a,71b](#), B. Le¹⁰¹, E.M. Le Boulicaut [ID51](#),
 B. Leban [ID93](#), A. Lebedev [ID81](#), M. LeBlanc [ID36](#), F. Ledroit-Guillon [ID60](#), A.C.A. Lee⁹⁶, S.C. Lee [ID148](#),
 S. Lee [ID47a,47b](#), T.F. Lee [ID92](#), L.L. Leeuw [ID33c](#), H.P. Lefebvre [ID95](#), M. Lefebvre [ID164](#), C. Leggett [ID17a](#),
 G. Lehmann Miotto [ID36](#), M. Leigh [ID56](#), W.A. Leight [ID103](#), W. Leinonen [ID113](#), A. Leisos [ID152,s](#),
 M.A.L. Leite [ID82c](#), C.E. Leitgeb [ID48](#), R. Leitner [ID133](#), K.J.C. Leney [ID44](#), T. Lenz [ID24](#), S. Leone [ID74a](#),
 C. Leonidopoulos [ID52](#), A. Leopold [ID144](#), C. Leroy [ID108](#), R. Les [ID107](#), C.G. Lester [ID32](#),
 M. Levchenko [ID37](#), J. Levêque [ID4](#), D. Levin [ID106](#), L.J. Levinson [ID168](#), M.P. Lewicki [ID86](#), D.J. Lewis [ID4](#),
 A. Li [ID5](#), B. Li [ID62b](#), C. Li [ID62a](#), C-Q. Li [ID62c](#), H. Li [ID62a](#), H. Li [ID62b](#), H. Li [ID14c](#), H. Li [ID62b](#), K. Li [ID138](#),
 L. Li [ID62c](#), M. Li [ID14a,14e](#), Q.Y. Li [ID62a](#), S. Li [ID14a,14e](#), S. Li [ID62d,62c,d](#), T. Li [ID5,b](#), X. Li [ID104](#), Z. Li [ID126](#),
 Z. Li [ID104](#), Z. Li [ID92](#), Z. Li [ID14a,14e](#), Z. Liang [ID14a](#), M. Liberatore [ID48](#), B. Liberti [ID76a](#), K. Lie [ID64c](#),
 J. Lieber Marin [ID82b](#), H. Lien [ID68](#), K. Lin [ID107](#), R.E. Lindley [ID7](#), J.H. Lindon [ID2](#), A. Linss [ID48](#),
 E. Lipeles [ID128](#), A. Lipniacka [ID16](#), A. Lister [ID163](#), J.D. Little [ID4](#), B. Liu [ID14a](#), B.X. Liu [ID142](#),
 D. Liu [ID62d,62c](#), J.B. Liu [ID62a](#), J.K.K. Liu [ID32](#), K. Liu [ID62d,62c](#), M. Liu [ID62a](#), M.Y. Liu [ID62a](#), P. Liu [ID14a](#),
 Q. Liu [ID62d,138,62c](#), X. Liu [ID62a](#), Y. Liu [ID14d,14e](#), Y.L. Liu [ID106](#), Y.W. Liu [ID62a](#), J. Llorente Merino [ID142](#),

S.L. Lloyd ⁹⁴, E.M. Lobodzinska ⁴⁸, P. Loch ⁷, S. Loffredo ^{76a,76b}, T. Lohse ¹⁸,
K. Lohwasser ¹³⁹, E. Loiacono ⁴⁸, M. Lokajicek ¹³¹, J.D. Lomas ²⁰, J.D. Long ¹⁶¹,
I. Longarini ¹⁵⁹, L. Longo ^{70a,70b}, R. Longo ¹⁶¹, I. Lopez Paz ⁶⁷, A. Lopez Solis ⁴⁸,
J. Lorenz ¹⁰⁹, N. Lorenzo Martinez ⁴, A.M. Lory ¹⁰⁹, O. Loseva ³⁷, X. Lou ^{47a,47b},
X. Lou ^{14a,14c}, A. Lounis ⁶⁶, J. Love ⁶, P.A. Love ⁹¹, G. Lu ^{14a,14c}, M. Lu ⁸⁰, S. Lu ¹²⁸,
Y.J. Lu ⁶⁵, H.J. Lubatti ¹³⁸, C. Luci ^{75a,75b}, F.L. Lucio Alves ^{14c}, A. Lucotte ⁶⁰, F. Luehring ⁶⁸,
I. Luise ¹⁴⁵, O. Lukianchuk ⁶⁶, O. Lundberg ¹⁴⁴, B. Lund-Jensen ¹⁴⁴, N.A. Luongo ¹²³,
M.S. Lutz ¹⁵¹, D. Lynn ²⁹, H. Lyons ⁹², R. Lysak ¹³¹, E. Lytken ⁹⁸, V. Lyubushkin ³⁸,
T. Lyubushkina ³⁸, M.M. Lyukova ¹⁴⁵, H. Ma ²⁹, L.L. Ma ^{62b}, Y. Ma ¹²¹, D.M. Mac Donell ¹⁶⁴,
G. Maccarrone ⁵³, J.C. MacDonald ¹⁰⁰, R. Madar ⁴⁰, W.F. Mader ⁵⁰, J. Maeda ⁸⁴, T. Maeno ²⁹,
M. Maerker ⁵⁰, H. Maguire ¹³⁹, V. Maiboroda ¹³⁵, A. Maio ^{130a,130b,130d}, K. Maj ^{85a},
O. Majersky ⁴⁸, S. Majewski ¹²³, N. Makovec ⁶⁶, V. Maksimovic ¹⁵, B. Malaescu ¹²⁷,
Pa. Malecki ⁸⁶, V.P. Maleev ³⁷, F. Malek ⁶⁰, M. Mali ⁹³, D. Malito ^{95,o}, U. Mallik ⁸⁰,
S. Maltezos ¹⁰, S. Malyukov ³⁸, J. Mamuzic ¹³, G. Mancini ⁵³, G. Manco ^{73a,73b}, J.P. Mandalia ⁹⁴,
I. Mandić ⁹³, L. Manhaes de Andrade Filho ^{82a}, I.M. Maniatis ¹⁶⁸, J. Manjarres Ramos ¹⁰²,
D.C. Mankad ¹⁶⁸, A. Mann ¹⁰⁹, B. Mansoulie ¹³⁵, S. Manzoni ³⁶, A. Marantis ¹⁵²,
G. Marchiori ⁵, M. Marcisovsky ¹³¹, C. Marcon ^{71a,71b}, M. Marinescu ²⁰, M. Marjanovic ¹²⁰,
E.J. Marshall ⁹¹, Z. Marshall ^{17a}, S. Marti-Garcia ¹⁶², T.A. Martin ¹⁶⁶, V.J. Martin ⁵²,
B. Martin dit Latour ¹⁶, L. Martinelli ^{75a,75b}, M. Martinez ^{13,t}, P. Martinez Agullo ¹⁶²,
V.I. Martinez Outschoorn ¹⁰³, P. Martinez Suarez ¹³, S. Martin-Haugh ¹³⁴, V.S. Martoiu ^{27b},
A.C. Martyniuk ⁹⁶, A. Marzin ³⁶, D. Mascione ^{78a,78b}, L. Masetti ¹⁰⁰, T. Mashimo ¹⁵³,
J. Masik ¹⁰¹, A.L. Maslennikov ³⁷, L. Massa ^{23b}, P. Massarotti ^{72a,72b}, P. Mastrandrea ^{74a,74b},
A. Mastroberardino ^{43b,43a}, T. Masubuchi ¹⁵³, T. Mathisen ¹⁶⁰, J. Matousek ¹³³, N. Matsuzawa ¹⁵³,
J. Maurer ^{27b}, B. Maček ⁹³, D.A. Maximov ³⁷, R. Mazini ¹⁴⁸, I. Maznas ¹⁵², M. Mazza ¹⁰⁷,
S.M. Mazza ¹³⁶, E. Mazzeo ^{71a,71b}, C. Mc Ginn ²⁹, J.P. Mc Gowan ¹⁰⁴, S.P. Mc Kee ¹⁰⁶,
E.F. McDonald ¹⁰⁵, A.E. McDougall ¹¹⁴, J.A. Mcfayden ¹⁴⁶, R.P. McGovern ¹²⁸,
G. Mchedlidze ^{149b}, R.P. Mckenzie ^{33g}, T.C. Mclachlan ⁴⁸, D.J. Mclaughlin ⁹⁶, K.D. McLean ¹⁶⁴,
S.J. McMahon ¹³⁴, P.C. McNamara ¹⁰⁵, C.M. Mcpartland ⁹², R.A. McPherson ^{164,w},
S. Mehlhase ¹⁰⁹, A. Mehta ⁹², D. Melini ¹⁵⁰, B.R. Mellado Garcia ^{33g}, A.H. Melo ⁵⁵,
F. Meloni ⁴⁸, A.M. Mendes Jacques Da Costa ¹⁰¹, H.Y. Meng ¹⁵⁵, L. Meng ⁹¹, S. Menke ¹¹⁰,
M. Mentink ³⁶, E. Meoni ^{43b,43a}, C. Merlassino ¹²⁶, L. Merola ^{72a,72b}, C. Meroni ^{71a}, G. Merz ¹⁰⁶,
O. Meshkov ³⁷, J. Metcalfe ⁶, A.S. Mete ⁶, C. Meyer ⁶⁸, J-P. Meyer ¹³⁵, R.P. Middleton ¹³⁴,
L. Mijović ⁵², G. Mikenberg ¹⁶⁸, M. Mikesstikova ¹³¹, M. Mikuž ⁹³, H. Mildner ¹⁰⁰, A. Milic ³⁶,
C.D. Milke ⁴⁴, D.W. Miller ³⁹, L.S. Miller ³⁴, A. Milov ¹⁶⁸, D.A. Milstead ^{47a,47b}, T. Min ^{14c},
A.A. Minaenko ³⁷, I.A. Minashvili ^{149b}, L. Mince ⁵⁹, A.I. Mincer ¹¹⁷, B. Mindur ^{85a},
M. Mineev ³⁸, Y. Mino ⁸⁷, L.M. Mir ¹³, M. Miralles Lopez ¹⁶², M. Mironova ^{17a}, A. Mishima ¹⁵³,
M.C. Missio ¹¹³, T. Mitani ¹⁶⁷, A. Mitra ¹⁶⁶, V.A. Mitsou ¹⁶², O. Miu ¹⁵⁵, P.S. Miyagawa ⁹⁴,
Y. Miyazaki ⁸⁹, A. Mizukami ⁸³, T. Mkrtychyan ^{63a}, M. Mlinarevic ⁹⁶, T. Mlinarevic ⁹⁶,
M. Mlynarikova ³⁶, S. Mobius ¹⁹, K. Mochizuki ¹⁰⁸, P. Moder ⁴⁸, P. Mogg ¹⁰⁹,
A.F. Mohammed ^{14a,14c}, S. Mohapatra ⁴¹, G. Mokgatitswane ^{33g}, L. Moleri ¹⁶⁸, B. Mondal ¹⁴¹,
S. Mondal ¹³², G. Monig ¹⁴⁶, K. Mönig ⁴⁸, E. Monnier ¹⁰², L. Monsonis Romero ¹⁶²,
J. Montejo Berlingen ^{13,83}, M. Montella ¹¹⁹, F. Monticelli ⁹⁰, S. Monzani ^{69a,69c}, N. Morange ⁶⁶,
A.L. Moreira De Carvalho ^{130a}, M. Moreno Llácer ¹⁶², C. Moreno Martinez ⁵⁶, P. Morettini ^{57b},
S. Morgenstern ³⁶, M. Morii ⁶¹, M. Morinaga ¹⁵³, A.K. Morley ³⁶, F. Morodei ^{75a,75b},
L. Morvaj ³⁶, P. Moschovakos ³⁶, B. Moser ³⁶, M. Mosidze ^{149b}, T. Moskalets ⁵⁴,
P. Moskvitina ¹¹³, J. Moss ^{31,m}, E.J.W. Moyses ¹⁰³, O. Mtintsilana ^{33g}, S. Muanza ¹⁰²,
J. Mueller ¹²⁹, D. Muenstermann ⁹¹, R. Müller ¹⁹, G.A. Mullier ¹⁶⁰, A.J. Mullin ³², J.J. Mullin ¹²⁸,

D.P. Mungo ¹⁵⁵, D. Munoz Perez ¹⁶², F.J. Munoz Sanchez ¹⁰¹, M. Murin ¹⁰¹, W.J. Murray ^{166,134},
 A. Murrone ^{71a,71b}, J.M. Muse ¹²⁰, M. Muškinja ^{17a}, C. Mwewa ²⁹, A.G. Myagkov ^{37,a},
 A.J. Myers ⁸, A.A. Myers ¹²⁹, G. Myers ⁶⁸, M. Myska ¹³², B.P. Nachman ^{17a}, O. Nackenhorst ⁴⁹,
 A.Nag Nag ⁵⁰, K. Nagai ¹²⁶, K. Nagano ⁸³, J.L. Nagle ^{29,ae}, E. Nagy ¹⁰², A.M. Nairz ³⁶,
 Y. Nakahama ⁸³, K. Nakamura ⁸³, K. Nakkalil ⁵, H. Nanjo ¹²⁴, R. Narayan ⁴⁴,
 E.A. Narayanan ¹¹², I. Naryshkin ³⁷, M. Naseri ³⁴, S. Nasri ^{116b}, C. Nass ²⁴, G. Navarro ^{22a},
 J. Navarro-Gonzalez ¹⁶², R. Nayak ¹⁵¹, A. Nayaz ¹⁸, P.Y. Nechaeva ³⁷, F. Nechansky ⁴⁸,
 L. Nedic ¹²⁶, T.J. Neep ²⁰, A. Negri ^{73a,73b}, M. Negrini ^{23b}, C. Nellist ¹¹⁴, C. Nelson ¹⁰⁴,
 K. Nelson ¹⁰⁶, S. Nemecek ¹³¹, M. Nessi ^{36,h}, M.S. Neubauer ¹⁶¹, F. Neuhaus ¹⁰⁰,
 J. Neundorf ⁴⁸, R. Newhouse ¹⁶³, P.R. Newman ²⁰, C.W. Ng ¹²⁹, Y.W.Y. Ng ⁴⁸, B. Ngair ^{35e},
 H.D.N. Nguyen ¹⁰⁸, R.B. Nickerson ¹²⁶, R. Nicolaidou ¹³⁵, J. Nielsen ¹³⁶, M. Niemeyer ⁵⁵,
 J. Niermann ^{55,36}, N. Nikiforou ³⁶, V. Nikolaenko ^{37,a}, I. Nikolic-Audit ¹²⁷, K. Nikolopoulos ²⁰,
 P. Nilsson ²⁹, I. Ninca ⁴⁸, H.R. Nindhito ⁵⁶, G. Ninio ¹⁵¹, A. Nisati ^{75a}, N. Nishu ²,
 R. Nisius ¹¹⁰, J-E. Nitschke ⁵⁰, E.K. Nkadimeng ^{33g}, S.J. Noacco Rosende ⁹⁰, T. Nobe ¹⁵³,
 D.L. Noel ³², T. Nommensen ¹⁴⁷, M.B. Norfolk ¹³⁹, R.R.B. Norisam ⁹⁶, B.J. Norman ³⁴,
 J. Novak ⁹³, T. Novak ⁴⁸, L. Novotny ¹³², R. Novotny ¹¹², L. Nozka ¹²², K. Ntekas ¹⁵⁹,
 N.M.J. Nunes De Moura Junior ^{82b}, E. Nurse ⁹⁶, J. Ocariz ¹²⁷, A. Ochi ⁸⁴, I. Ochoa ^{130a},
 S. Oerdek ¹⁶⁰, J.T. Offermann ³⁹, A. Ogrodnik ¹³³, A. Oh ¹⁰¹, C.C. Ohm ¹⁴⁴, H. Oide ⁸³,
 R. Oishi ¹⁵³, M.L. Ojeda ⁴⁸, Y. Okazaki ⁸⁷, M.W. O'Keefe ⁹², Y. Okumura ¹⁵³,
 L.F. Oleiro Seabra ^{130a}, S.A. Olivares Pino ^{137d}, D. Oliveira Damazio ²⁹, D. Oliveira Goncalves ^{82a},
 J.L. Oliver ¹⁵⁹, M.J.R. Olsson ¹⁵⁹, A. Olszewski ⁸⁶, Ö.O. Öncel ⁵⁴, D.C. O'Neil ¹⁴²,
 A.P. O'Neill ¹⁹, A. Onofre ^{130a,130e}, P.U.E. Onyisi ¹¹, M.J. Oreglia ³⁹, G.E. Orellana ⁹⁰,
 D. Orestano ^{77a,77b}, N. Orlando ¹³, R.S. Orr ¹⁵⁵, V. O'Shea ⁵⁹, R. Ospanov ^{62a},
 G. Otero y Garzon ³⁰, H. Otono ⁸⁹, P.S. Ott ^{63a}, G.J. Ottino ^{17a}, M. Ouchrif ^{35d}, J. Ouellette ²⁹,
 F. Ould-Saada ¹²⁵, M. Owen ⁵⁹, R.E. Owen ¹³⁴, K.Y. Oyulmaz ^{21a}, V.E. Ozcan ^{21a}, N. Ozturk ⁸,
 S. Ozturk ^{21d}, H.A. Pacey ³², A. Pacheco Pages ¹³, C. Padilla Aranda ¹³, G. Padovano ^{75a,75b},
 S. Pagan Griso ^{17a}, G. Palacino ⁶⁸, A. Palazzo ^{70a,70b}, S. Palestini ³⁶, J. Pan ¹⁷¹, T. Pan ^{64a},
 D.K. Panchal ¹¹, C.E. Pandini ¹¹⁴, J.G. Panduro Vazquez ⁹⁵, H. Pang ^{14b}, P. Pani ⁴⁸,
 G. Panizzo ^{69a,69c}, L. Paolozzi ⁵⁶, C. Papadatos ¹⁰⁸, S. Parajuli ⁴⁴, A. Paramonov ⁶,
 C. Paraskevopoulos ¹⁰, D. Paredes Hernandez ^{64b}, T.H. Park ¹⁵⁵, M.A. Parker ³², F. Parodi ^{57b,57a},
 E.W. Parrish ¹¹⁵, V.A. Parrish ⁵², J.A. Parsons ⁴¹, U. Parzefall ⁵⁴, B. Pascual Dias ¹⁰⁸,
 L. Pascual Dominguez ¹⁵¹, F. Pasquali ¹¹⁴, E. Pasqualucci ^{75a}, S. Passaggio ^{57b}, F. Pastore ⁹⁵,
 P. Pasuwan ^{47a,47b}, P. Patel ⁸⁶, U.M. Patel ⁵¹, J.R. Pater ¹⁰¹, T. Pauly ³⁶, J. Pearkes ¹⁴³,
 M. Pedersen ¹²⁵, R. Pedro ^{130a}, S.V. Peleganchuk ³⁷, O. Penc ³⁶, E.A. Pender ⁵², H. Peng ^{62a},
 K.E. Pensi ¹⁰⁹, M. Penzin ³⁷, B.S. Peralva ^{82d,82d}, A.P. Pereira Peixoto ⁶⁰,
 L. Pereira Sanchez ^{47a,47b}, D.V. Perepelitsa ^{29,ae}, E. Perez Codina ^{156a}, M. Perganti ¹⁰,
 L. Perini ^{71a,71b,*}, H. Pernegger ³⁶, A. Perrevoort ¹¹³, O. Perrin ⁴⁰, K. Peters ⁴⁸,
 R.F.Y. Peters ¹⁰¹, B.A. Petersen ³⁶, T.C. Petersen ⁴², E. Petit ¹⁰², V. Petousis ¹³²,
 C. Petridou ^{152,e}, A. Petrukhin ¹⁴¹, M. Pettee ^{17a}, N.E. Pettersson ³⁶, A. Petukhov ³⁷,
 K. Petukhova ¹³³, A. Peyaud ¹³⁵, R. Pezoa ^{137f}, L. Pezzotti ³⁶, G. Pezzullo ¹⁷¹, T.M. Pham ¹⁶⁹,
 T. Pham ¹⁰⁵, P.W. Phillips ¹³⁴, G. Piacquadio ¹⁴⁵, E. Pianori ^{17a}, F. Piazza ^{71a,71b}, R. Piegai ³⁰,
 D. Pietreanu ^{27b}, A.D. Pilkington ¹⁰¹, M. Pinamonti ^{69a,69c}, J.L. Pinfeld ²,
 B.C. Pinheiro Pereira ^{130a}, A.E. Pinto Pinoargote ¹³⁵, C. Pitman Donaldson ⁹⁶, D.A. Pizzi ³⁴,
 L. Pizzimento ^{76a,76b}, A. Pizzini ¹¹⁴, M.-A. Pleier ²⁹, V. Plesanovs ⁵⁴, V. Pleskot ¹³³, E. Plotnikova ³⁸,
 G. Poddar ⁴, R. Poettgen ⁹⁸, L. Poggioli ¹²⁷, I. Pokharel ⁵⁵, S. Polacek ¹³³, G. Polesello ^{73a},
 A. Poley ^{142,156a}, R. Polifka ¹³², A. Polini ^{23b}, C.S. Pollard ¹⁶⁶, Z.B. Pollock ¹¹⁹,
 V. Polychronakos ²⁹, E. Pompa Pacchi ^{75a,75b}, D. Ponomarenko ¹¹³, L. Pontecorvo ³⁶, S. Popa ^{27a},

G.A. Popeneacu [id](#)^{27d}, A. Poreba [id](#)³⁶, D.M. Portillo Quintero [id](#)^{156a}, S. Pospisil [id](#)¹³², M.A. Postill [id](#)¹³⁹, P. Postolache [id](#)^{27c}, K. Potamianos [id](#)¹⁶⁶, P.P. Potepa [id](#)^{85a}, I.N. Potrap [id](#)³⁸, C.J. Potter [id](#)³², H. Potti [id](#)¹, T. Poulsen [id](#)⁴⁸, J. Poveda [id](#)¹⁶², M.E. Pozo Astigarraga [id](#)³⁶, A. Prades Ibanez [id](#)¹⁶², D. Price [id](#)¹⁰¹, M. Primavera [id](#)^{70a}, M.A. Principe Martin [id](#)⁹⁹, R. Privara [id](#)¹²², T. Procter [id](#)⁵⁹, M.L. Proffitt [id](#)¹³⁸, N. Proklova [id](#)¹²⁸, K. Prokofiev [id](#)^{64c}, G. Proto [id](#)¹¹⁰, S. Protopopescu [id](#)²⁹, J. Proudfoot [id](#)⁶, M. Przybycien [id](#)^{85a}, W.W. Przygoda [id](#)^{85b}, J.E. Puddefoot [id](#)¹³⁹, D. Pudzha [id](#)³⁷, D. Pyatiizbyantseva [id](#)³⁷, J. Qian [id](#)¹⁰⁶, D. Qichen [id](#)¹⁰¹, Y. Qin [id](#)¹⁰¹, T. Qiu [id](#)⁵², A. Quadt [id](#)⁵⁵, M. Queitsch-Maitland [id](#)¹⁰¹, G. Quetant [id](#)⁵⁶, G. Rabanal Bolanos [id](#)⁶¹, D. Rafanoharana [id](#)⁵⁴, F. Ragusa [id](#)^{71a,71b}, J.L. Rainbolt [id](#)³⁹, J.A. Raine [id](#)⁵⁶, S. Rajagopalan [id](#)²⁹, E. Ramakoti [id](#)³⁷, K. Ran [id](#)^{48,14e}, N.P. Rapheeha [id](#)^{33g}, H. Rasheed [id](#)^{27b}, V. Raskina [id](#)¹²⁷, D.F. Rassloff [id](#)^{63a}, S. Rave [id](#)¹⁰⁰, B. Ravina [id](#)⁵⁵, I. Ravinovich [id](#)¹⁶⁸, M. Raymond [id](#)³⁶, A.L. Read [id](#)¹²⁵, N.P. Readioff [id](#)¹³⁹, D.M. Rebutti [id](#)^{73a,73b}, G. Redlinger [id](#)²⁹, A.S. Reed [id](#)¹¹⁰, K. Reeves [id](#)²⁶, J.A. Reidelsturz [id](#)¹⁷⁰, D. Reikher [id](#)¹⁵¹, A. Rej [id](#)¹⁴¹, C. Rembser [id](#)³⁶, A. Renardi [id](#)⁴⁸, M. Renda [id](#)^{27b}, M.B. Rendel [id](#)¹¹⁰, F. Renner [id](#)⁴⁸, A.G. Rennie [id](#)⁵⁹, S. Resconi [id](#)^{71a}, M. Ressegotti [id](#)^{57b,57a}, S. Rettie [id](#)³⁶, J.G. Reyes Rivera [id](#)¹⁰⁷, B. Reynolds [id](#)¹¹⁹, E. Reynolds [id](#)^{17a}, O.L. Rezanova [id](#)³⁷, P. Reznicek [id](#)¹³³, N. Ribaric [id](#)⁹¹, E. Ricci [id](#)^{78a,78b}, R. Richter [id](#)¹¹⁰, S. Richter [id](#)^{47a,47b}, E. Richter-Was [id](#)^{85b}, M. Ridel [id](#)¹²⁷, S. Ridouani [id](#)^{35d}, P. Rieck [id](#)¹¹⁷, P. Riedler [id](#)³⁶, M. Rijssenbeek [id](#)¹⁴⁵, A. Rimoldi [id](#)^{73a,73b}, M. Rimoldi [id](#)⁴⁸, L. Rinaldi [id](#)^{23b,23a}, T.T. Rinn [id](#)²⁹, M.P. Rinnagel [id](#)¹⁰⁹, G. Ripellino [id](#)¹⁶⁰, I. Riu [id](#)¹³, P. Rivadeneira [id](#)⁴⁸, J.C. Rivera Vergara [id](#)¹⁶⁴, F. Rizatdinova [id](#)¹²¹, E. Rizvi [id](#)⁹⁴, B.A. Roberts [id](#)¹⁶⁶, B.R. Roberts [id](#)^{17a}, S.H. Robertson [id](#)^{104,w}, M. Robin [id](#)⁴⁸, D. Robinson [id](#)³², C.M. Robles Gajardo [id](#)^{137f}, M. Robles Manzano [id](#)¹⁰⁰, A. Robson [id](#)⁵⁹, A. Rocchi [id](#)^{76a,76b}, C. Roda [id](#)^{74a,74b}, S. Rodriguez Bosca [id](#)^{63a}, Y. Rodriguez Garcia [id](#)^{22a}, A. Rodriguez Rodriguez [id](#)⁵⁴, A.M. Rodríguez Vera [id](#)^{156b}, S. Roe [id](#)³⁶, J.T. Roemer [id](#)¹⁵⁹, A.R. Roepe-Gier [id](#)¹³⁶, J. Roggel [id](#)¹⁷⁰, O. Røhne [id](#)¹²⁵, R.A. Rojas [id](#)¹⁰³, C.P.A. Roland [id](#)⁶⁸, J. Roloff [id](#)²⁹, A. Romaniouk [id](#)³⁷, E. Romano [id](#)^{73a,73b}, M. Romano [id](#)^{23b}, A.C. Romero Hernandez [id](#)¹⁶¹, N. Rompotis [id](#)⁹², L. Roos [id](#)¹²⁷, S. Rosati [id](#)^{75a}, B.J. Rosser [id](#)³⁹, E. Rossi [id](#)¹²⁶, E. Rossi [id](#)^{72a,72b}, L.P. Rossi [id](#)^{57b}, L. Rossini [id](#)⁴⁸, R. Rosten [id](#)¹¹⁹, M. Rotaru [id](#)^{27b}, B. Rottler [id](#)⁵⁴, C. Rougier [id](#)¹⁰², D. Rousseau [id](#)⁶⁶, D. Rousso [id](#)³², A. Roy [id](#)¹⁶¹, S. Roy-Garand [id](#)¹⁵⁵, A. Rozanov [id](#)¹⁰², Y. Rozen [id](#)¹⁵⁰, X. Ruan [id](#)^{33g}, A. Rubio Jimenez [id](#)¹⁶², A.J. Ruby [id](#)⁹², V.H. Ruelas Rivera [id](#)¹⁸, T.A. Ruggeri [id](#)¹, A. Ruggiero [id](#)¹²⁶, A. Ruiz-Martinez [id](#)¹⁶², A. Rummler [id](#)³⁶, Z. Rurikova [id](#)⁵⁴, N.A. Rusakovich [id](#)³⁸, H.L. Russell [id](#)¹⁶⁴, G. Russo [id](#)^{75a,75b}, J.P. Rutherford [id](#)⁷, S. Rutherford Colmenares [id](#)³², K. Rybacki [id](#)⁹¹, M. Rybar [id](#)¹³³, E.B. Rye [id](#)¹²⁵, A. Ryzhov [id](#)⁴⁴, J.A. Sabater Iglesias [id](#)⁵⁶, P. Sabatini [id](#)¹⁶², L. Sabetta [id](#)^{75a,75b}, H.F-W. Sadrozinski [id](#)¹³⁶, F. Safai Tehrani [id](#)^{75a}, B. Safarzadeh Samani [id](#)¹⁴⁶, M. Safdari [id](#)¹⁴³, S. Saha [id](#)¹⁶⁴, M. Sahinsoy [id](#)¹¹⁰, M. Saimpert [id](#)¹³⁵, M. Saito [id](#)¹⁵³, T. Saito [id](#)¹⁵³, D. Salamani [id](#)³⁶, A. Salnikov [id](#)¹⁴³, J. Salt [id](#)¹⁶², A. Salvador Salas [id](#)¹³, D. Salvatore [id](#)^{43b,43a}, F. Salvatore [id](#)¹⁴⁶, A. Salzburger [id](#)³⁶, D. Sammel [id](#)⁵⁴, D. Sampsonidis [id](#)^{152,e}, D. Sampsonidou [id](#)¹²³, J. Sánchez [id](#)¹⁶², A. Sanchez Pineda [id](#)⁴, V. Sanchez Sebastian [id](#)¹⁶², H. Sandaker [id](#)¹²⁵, C.O. Sander [id](#)⁴⁸, J.A. Sandesara [id](#)¹⁰³, M. Sandhoff [id](#)¹⁷⁰, C. Sandoval [id](#)^{22b}, D.P.C. Sankey [id](#)¹³⁴, T. Sano [id](#)⁸⁷, A. Sansoni [id](#)⁵³, L. Santi [id](#)^{75a,75b}, C. Santoni [id](#)⁴⁰, H. Santos [id](#)^{130a,130b}, S.N. Santpur [id](#)^{17a}, A. Santra [id](#)¹⁶⁸, K.A. Saoucha [id](#)¹³⁹, J.G. Saraiva [id](#)^{130a,130d}, J. Sardain [id](#)⁷, O. Sasaki [id](#)⁸³, K. Sato [id](#)¹⁵⁷, C. Sauer [id](#)^{63b}, F. Sauerburger [id](#)⁵⁴, E. Sauvan [id](#)⁴, P. Savard [id](#)^{155,ac}, R. Sawada [id](#)¹⁵³, C. Sawyer [id](#)¹³⁴, L. Sawyer [id](#)⁹⁷, I. Sayago Galvan [id](#)¹⁶², C. Sbarra [id](#)^{23b}, A. Sbrizzi [id](#)^{23b,23a}, T. Scanlon [id](#)⁹⁶, J. Schaarschmidt [id](#)¹³⁸, P. Schacht [id](#)¹¹⁰, D. Schaefer [id](#)³⁹, U. Schäfer [id](#)¹⁰⁰, A.C. Schaffer [id](#)^{66,44}, D. Schaile [id](#)¹⁰⁹, R.D. Schamberger [id](#)¹⁴⁵, C. Scharf [id](#)¹⁸, M.M. Schefer [id](#)¹⁹, V.A. Schegelsky [id](#)³⁷, D. Scheirich [id](#)¹³³, F. Schenck [id](#)¹⁸, M. Schernau [id](#)¹⁵⁹, C. Scheulen [id](#)⁵⁵, C. Schiavi [id](#)^{57b,57a}, E.J. Schioppa [id](#)^{70a,70b}, M. Schioppa [id](#)^{43b,43a}, B. Schlag [id](#)¹⁴³, K.E. Schleicher [id](#)⁵⁴, S. Schlenker [id](#)³⁶, J. Schmeing [id](#)¹⁷⁰, M.A. Schmidt [id](#)¹⁷⁰, K. Schmieden [id](#)¹⁰⁰, C. Schmitt [id](#)¹⁰⁰, S. Schmitt [id](#)⁴⁸, L. Schoeffel [id](#)¹³⁵, A. Schoening [id](#)^{63b}, P.G. Scholer [id](#)⁵⁴, E. Schopf [id](#)¹²⁶, M. Schott [id](#)¹⁰⁰, J. Schovancova [id](#)³⁶,

S. Schramm ⁵⁶, F. Schroeder ¹⁷⁰, T. Schroer ⁵⁶, H-C. Schultz-Coulon ^{63a}, M. Schumacher ⁵⁴,
 B.A. Schumm ¹³⁶, Ph. Schune ¹³⁵, A.J. Schuy ¹³⁸, H.R. Schwartz ¹³⁶, A. Schwartzman ¹⁴³,
 T.A. Schwarz ¹⁰⁶, Ph. Schwemling ¹³⁵, R. Schwienhorst ¹⁰⁷, A. Sciandra ¹³⁶, G. Sciolla ²⁶,
 F. Scuri ^{74a}, C.D. Sebastiani ⁹², K. Sedlaczek ¹¹⁵, P. Seema ¹⁸, S.C. Seidel ¹¹², A. Seiden ¹³⁶,
 B.D. Seidlitz ⁴¹, C. Seitz ⁴⁸, J.M. Seixas ^{82b}, G. Sekhniaidze ^{72a}, S.J. Sekula ⁴⁴, L. Selem ⁶⁰,
 N. Semprini-Cesari ^{23b,23a}, D. Sengupta ⁵⁶, V. Senthilkumar ¹⁶², L. Serin ⁶⁶, L. Serkin ^{69a,69b},
 M. Sessa ^{76a,76b}, H. Severini ¹²⁰, F. Sforza ^{57b,57a}, A. Sfyrla ⁵⁶, E. Shabalina ⁵⁵, R. Shaheen ¹⁴⁴,
 J.D. Shahinian ¹²⁸, D. Shaked Renous ¹⁶⁸, L.Y. Shan ^{14a}, M. Shapiro ^{17a}, A. Sharma ³⁶,
 A.S. Sharma ¹⁶³, P. Sharma ⁸⁰, S. Sharma ⁴⁸, P.B. Shatalov ³⁷, K. Shaw ¹⁴⁶, S.M. Shaw ¹⁰¹,
 A. Shcherbakova ³⁷, Q. Shen ^{62c,5}, P. Sherwood ⁹⁶, L. Shi ⁹⁶, X. Shi ^{14a}, C.O. Shimmin ¹⁷¹,
 Y. Shimogama ¹⁶⁷, J.D. Shinner ⁹⁵, I.P.J. Shipsey ¹²⁶, S. Shirabe ^{56,h}, M. Shiyakova ³⁸,
 J. Shlomi ¹⁶⁸, M.J. Shochet ³⁹, J. Shojaii ¹⁰⁵, D.R. Shope ¹²⁵, S. Shrestha ^{119,af}, E.M. Shrif ^{33g},
 M.J. Shroff ¹⁶⁴, P. Sicho ¹³¹, A.M. Sickles ¹⁶¹, E. Sideras Haddad ^{33g}, A. Sidoti ^{23b},
 F. Siegert ⁵⁰, Dj. Sijacki ¹⁵, R. Sikora ^{85a}, F. Sili ⁹⁰, J.M. Silva ²⁰, M.V. Silva Oliveira ²⁹,
 S.B. Silverstein ^{47a}, S. Simion ⁶⁶, R. Simoniello ³⁶, E.L. Simpson ⁵⁹, H. Simpson ¹⁴⁶,
 L.R. Simpson ¹⁰⁶, N.D. Simpson ⁹⁸, S. Simsek ^{21d}, S. Sindhu ⁵⁵, P. Sinervo ¹⁵⁵, S. Singh ¹⁵⁵,
 S. Sinha ⁴⁸, S. Sinha ¹⁰¹, M. Sioli ^{23b,23a}, I. Siral ³⁶, E. Sitnikova ⁴⁸, S.Yu. Sivoklov ^{37,*},
 J. Sjölin ^{47a,47b}, A. Skaf ⁵⁵, E. Skorda ⁹⁸, P. Skubic ¹²⁰, M. Slawinska ⁸⁶, V. Smakhtin ¹⁶⁸,
 B.H. Smart ¹³⁴, J. Smiesko ³⁶, S.Yu. Smirnov ³⁷, Y. Smirnov ³⁷, L.N. Smirnova ^{37,a},
 O. Smirnova ⁹⁸, A.C. Smith ⁴¹, E.A. Smith ³⁹, H.A. Smith ¹²⁶, J.L. Smith ⁹², R. Smith ¹⁴³,
 M. Smizanska ⁹¹, K. Smolek ¹³², A.A. Snesarev ³⁷, S.R. Snider ¹⁵⁵, H.L. Snoek ¹¹⁴,
 S. Snyder ²⁹, R. Sobie ^{164,w}, A. Soffer ¹⁵¹, C.A. Solans Sanchez ³⁶, E.Yu. Soldatov ³⁷,
 U. Soldevila ¹⁶², A.A. Solodkov ³⁷, S. Solomon ²⁶, A. Soloshenko ³⁸, K. Solovieva ⁵⁴,
 O.V. Solovyanov ⁴⁰, V. Solovyev ³⁷, P. Sommer ³⁶, A. Sonay ¹³, W.Y. Song ^{156b},
 J.M. Sonneveld ¹¹⁴, A. Sopczak ¹³², A.L. Sopio ⁹⁶, F. Sopkova ^{28b}, V. Sothilingam ^{63a},
 S. Sottocornola ⁶⁸, R. Soualah ^{116c}, Z. Soumami ^{35e}, D. South ⁴⁸, S. Spagnolo ^{70a,70b},
 M. Spalla ¹¹⁰, D. Sperlich ⁵⁴, G. Spigo ³⁶, M. Spina ¹⁴⁶, S. Spinali ⁹¹, D.P. Spiteri ⁵⁹,
 M. Spousta ¹³³, E.J. Staats ³⁴, A. Stabile ^{71a,71b}, R. Stamen ^{63a}, M. Stamenkovic ¹¹⁴,
 A. Stampeki ²⁰, M. Standke ²⁴, E. Stanecka ⁸⁶, M.V. Stange ⁵⁰, B. Stanislaus ^{17a},
 M.M. Stanitzki ⁴⁸, B. Stapf ⁴⁸, E.A. Starchenko ³⁷, G.H. Stark ¹³⁶, J. Stark ¹⁰², D.M. Starko ^{156b},
 P. Staroba ¹³¹, P. Starovoitov ^{63a}, S. Stärz ¹⁰⁴, R. Staszewski ⁸⁶, G. Stavropoulos ⁴⁶,
 J. Steentoft ¹⁶⁰, P. Steinberg ²⁹, B. Stelzer ^{142,156a}, H.J. Stelzer ¹²⁹, O. Stelzer-Chilton ^{156a},
 H. Stenzel ⁵⁸, T.J. Stevenson ¹⁴⁶, G.A. Stewart ³⁶, J.R. Stewart ¹²¹, M.C. Stockton ³⁶,
 G. Stoicea ^{27b}, M. Stolarski ^{130a}, S. Stonjek ¹¹⁰, A. Straessner ⁵⁰, J. Strandberg ¹⁴⁴,
 S. Strandberg ^{47a,47b}, M. Strauss ¹²⁰, T. Strebler ¹⁰², P. Strizenec ^{28b}, R. Ströhmer ¹⁶⁵,
 D.M. Strom ¹²³, L.R. Strom ⁴⁸, R. Stroynowski ⁴⁴, A. Strubig ^{47a,47b}, S.A. Stucci ²⁹,
 B. Stugu ¹⁶, J. Stupak ¹²⁰, N.A. Styles ⁴⁸, D. Su ¹⁴³, S. Su ^{62a}, W. Su ^{62d}, X. Su ^{62a,66},
 K. Sugizaki ¹⁵³, V.V. Sulin ³⁷, M.J. Sullivan ⁹², D.M.S. Sultan ^{78a,78b}, L. Sultanaliev ³⁷,
 S. Sultansoy ^{3b}, T. Sumida ⁸⁷, S. Sun ¹⁰⁶, S. Sun ¹⁶⁹, O. Sunneborn Gudnadottir ¹⁶⁰,
 M.R. Sutton ¹⁴⁶, H. Suzuki ¹⁵⁷, M. Svatos ¹³¹, M. Swiatlowski ^{156a}, T. Swirski ¹⁶⁵,
 I. Sykora ^{28a}, M. Sykora ¹³³, T. Sykora ¹³³, D. Ta ¹⁰⁰, K. Tackmann ^{48,u}, A. Taffard ¹⁵⁹,
 R. Tafirout ^{156a}, J.S. Tafoya Vargas ⁶⁶, R. Takashima ⁸⁸, E.P. Takeva ⁵², Y. Takubo ⁸³,
 M. Talby ¹⁰², A.A. Talyshev ³⁷, K.C. Tam ^{64b}, N.M. Tamir ¹⁵¹, A. Tanaka ¹⁵³, J. Tanaka ¹⁵³,
 R. Tanaka ⁶⁶, M. Tanasini ^{57b,57a}, Z. Tao ¹⁶³, S. Tapia Araya ^{137f}, S. Tapprogge ¹⁰⁰,
 A. Tarek Abouelfadl Mohamed ¹⁰⁷, S. Tarem ¹⁵⁰, K. Tariq ^{62b}, G. Tarna ^{102,27b}, G.F. Tartarelli ^{71a},
 P. Tas ¹³³, M. Tasevsky ¹³¹, E. Tassi ^{43b,43a}, A.C. Tate ¹⁶¹, G. Tateno ¹⁵³, Y. Tayalati ^{35e,v},
 G.N. Taylor ¹⁰⁵, W. Taylor ^{156b}, H. Teagle ⁹², A.S. Tee ¹⁶⁹, R. Teixeira De Lima ¹⁴³,

P. Teixeira-Dias [ID⁹⁵](#), J.J. Teoh [ID¹⁵⁵](#), K. Terashi [ID¹⁵³](#), J. Terron [ID⁹⁹](#), S. Terzo [ID¹³](#), M. Testa [ID⁵³](#),
 R.J. Teuscher [ID^{155,w}](#), A. Thaler [ID⁷⁹](#), O. Theiner [ID⁵⁶](#), N. Themistokleous [ID⁵²](#), T. Thevenaux-Pelzer [ID¹⁰²](#),
 O. Thielmann [ID¹⁷⁰](#), D.W. Thomas [ID⁹⁵](#), J.P. Thomas [ID²⁰](#), E.A. Thompson [ID^{17a}](#), P.D. Thompson [ID²⁰](#),
 E. Thomson [ID¹²⁸](#), Y. Tian [ID⁵⁵](#), V. Tikhomirov [ID^{37,a}](#), Yu.A. Tikhonov [ID³⁷](#), S. Timoshenko [ID³⁷](#),
 D. Timoshyn [ID¹³³](#), E.X.L. Ting [ID¹](#), P. Tipton [ID¹⁷¹](#), S.H. Tlou [ID^{33g}](#), A. Tnourji [ID⁴⁰](#), K. Todome [ID^{23b,23a}](#),
 S. Todorova-Nova [ID¹³³](#), S. Todt [ID⁵⁰](#), M. Togawa [ID⁸³](#), J. Tojo [ID⁸⁹](#), S. Tokár [ID^{28a}](#), K. Tokushuku [ID⁸³](#),
 O. Toldaiev [ID⁶⁸](#), R. Tombs [ID³²](#), M. Tomoto [ID^{83,111}](#), L. Tompkins [ID¹⁴³](#), K.W. Topolnicki [ID^{85b}](#),
 E. Torrence [ID¹²³](#), H. Torres [ID¹⁰²](#), E. Torró Pastor [ID¹⁶²](#), M. Toscani [ID³⁰](#), C. Tosciri [ID³⁹](#), M. Tost [ID¹¹](#),
 D.R. Tovey [ID¹³⁹](#), A. Traet [ID¹⁶](#), I.S. Trandafir [ID^{27b}](#), T. Trefzger [ID¹⁶⁵](#), A. Tricoli [ID²⁹](#), I.M. Trigger [ID^{156a}](#),
 S. Trincaz-Duvoid [ID¹²⁷](#), D.A. Trischuk [ID²⁶](#), B. Trocmé [ID⁶⁰](#), C. Troncon [ID^{71a}](#), L. Truong [ID^{33c}](#),
 M. Trzebinski [ID⁸⁶](#), A. Trzupsek [ID⁸⁶](#), F. Tsai [ID¹⁴⁵](#), M. Tsai [ID¹⁰⁶](#), A. Tsiamis [ID^{152,e}](#), P.V. Tsiareshka [ID³⁷](#),
 S. Tsigaridas [ID^{156a}](#), A. Tsirigotis [ID^{152,s}](#), V. Tsiskaridze [ID¹⁵⁵](#), E.G. Tskhadadze [ID^{149a}](#), M. Tsopoulou [ID^{152,e}](#),
 Y. Tsujikawa [ID⁸⁷](#), I.I. Tsukerman [ID³⁷](#), V. Tsulaia [ID^{17a}](#), S. Tsuno [ID⁸³](#), O. Tsur [ID¹⁵⁰](#), K. Tsur [ID¹¹⁸](#),
 D. Tsybychev [ID¹⁴⁵](#), Y. Tu [ID^{64b}](#), A. Tudorache [ID^{27b}](#), V. Tudorache [ID^{27b}](#), A.N. Tuna [ID³⁶](#), S. Turchikhin [ID³⁸](#),
 I. Turk Cakir [ID^{3a}](#), R. Turra [ID^{71a}](#), T. Turtuvshin [ID^{38,x}](#), P.M. Tuts [ID⁴¹](#), S. Tzamarias [ID^{152,e}](#), P. Tzanis [ID¹⁰](#),
 E. Tzovara [ID¹⁰⁰](#), K. Uchida [ID¹⁵³](#), F. Ukegawa [ID¹⁵⁷](#), P.A. Ulloa Poblete [ID^{137c,137b}](#), E.N. Umaka [ID²⁹](#),
 G. Unal [ID³⁶](#), M. Unal [ID¹¹](#), A. Undrus [ID²⁹](#), G. Unel [ID¹⁵⁹](#), J. Urban [ID^{28b}](#), P. Urquijo [ID¹⁰⁵](#), G. Usai [ID⁸](#),
 R. Ushioda [ID¹⁵⁴](#), M. Usman [ID¹⁰⁸](#), Z. Uysal [ID^{21b}](#), L. Vacavant [ID¹⁰²](#), V. Vacek [ID¹³²](#), B. Vachon [ID¹⁰⁴](#),
 K.O.H. Vadla [ID¹²⁵](#), T. Vafeiadis [ID³⁶](#), A. Vaitkus [ID⁹⁶](#), C. Valderanis [ID¹⁰⁹](#), E. Valdes Santurio [ID^{47a,47b}](#),
 M. Valente [ID^{156a}](#), S. Valentinetti [ID^{23b,23a}](#), A. Valero [ID¹⁶²](#), E. Valiente Moreno [ID¹⁶²](#), A. Vallier [ID¹⁰²](#),
 J.A. Valls Ferrer [ID¹⁶²](#), D.R. Van Arneman [ID¹¹⁴](#), T.R. Van Daalen [ID¹³⁸](#), A. Van Der Graaf [ID⁴⁹](#),
 P. Van Gemmeren [ID⁶](#), M. Van Rijnbach [ID^{125,36}](#), S. Van Stroud [ID⁹⁶](#), I. Van Vulpen [ID¹¹⁴](#),
 M. Vanadia [ID^{76a,76b}](#), W. Vandelli [ID³⁶](#), M. Vandenbroucke [ID¹³⁵](#), E.R. Vandewall [ID¹²¹](#), D. Vannicola [ID¹⁵¹](#),
 L. Vannoli [ID^{57b,57a}](#), R. Vari [ID^{75a}](#), E.W. Varnes [ID⁷](#), C. Varni [ID^{17a}](#), T. Varol [ID¹⁴⁸](#), D. Varouchas [ID⁶⁶](#),
 L. Varriale [ID¹⁶²](#), K.E. Varvell [ID¹⁴⁷](#), M.E. Vasile [ID^{27b}](#), L. Vaslin [ID⁴⁰](#), G.A. Vasquez [ID¹⁶⁴](#), F. Vazeille [ID⁴⁰](#),
 T. Vazquez Schroeder [ID³⁶](#), J. Veatch [ID³¹](#), V. Vecchio [ID¹⁰¹](#), M.J. Veen [ID¹⁰³](#), I. Veliscek [ID¹²⁶](#),
 L.M. Veloce [ID¹⁵⁵](#), F. Veloso [ID^{130a,130c}](#), S. Veneziano [ID^{75a}](#), A. Ventura [ID^{70a,70b}](#), A. Verbytskyi [ID¹¹⁰](#),
 M. Verducci [ID^{74a,74b}](#), C. Vergis [ID²⁴](#), M. Verissimo De Araujo [ID^{82b}](#), W. Verkerke [ID¹¹⁴](#),
 J.C. Vermeulen [ID¹¹⁴](#), C. Vernieri [ID¹⁴³](#), P.J. Verschuuren [ID⁹⁵](#), M. Vessella [ID¹⁰³](#), M.C. Vetterli [ID^{142,ac}](#),
 A. Vgenopoulos [ID^{152,e}](#), N. Viaux Maira [ID^{137f}](#), T. Vickey [ID¹³⁹](#), O.E. Vickey Boeriu [ID¹³⁹](#),
 G.H.A. Viehhauser [ID¹²⁶](#), L. Vigani [ID^{63b}](#), M. Villa [ID^{23b,23a}](#), M. Villaplana Perez [ID¹⁶²](#), E.M. Villhauer [ID⁵²](#),
 E. Vilucchi [ID⁵³](#), M.G. Vincter [ID³⁴](#), G.S. Virdee [ID²⁰](#), A. Vishwakarma [ID⁵²](#), A. Visibile [ID¹¹⁴](#), C. Vittori [ID³⁶](#),
 I. Vivarelli [ID¹⁴⁶](#), V. Vladimirov [ID¹⁶⁶](#), E. Voevodina [ID¹¹⁰](#), F. Vogel [ID¹⁰⁹](#), P. Vokac [ID¹³²](#), J. Von Ahnen [ID⁴⁸](#),
 E. Von Toerne [ID²⁴](#), B. Vormwald [ID³⁶](#), V. Vorobel [ID¹³³](#), K. Vorobev [ID³⁷](#), M. Vos [ID¹⁶²](#), K. Voss [ID¹⁴¹](#),
 J.H. Vossebeld [ID⁹²](#), M. Vozak [ID¹¹⁴](#), L. Vozdecky [ID⁹⁴](#), N. Vranjes [ID¹⁵](#), M. Vranjes Milosavljevic [ID¹⁵](#),
 M. Vreeswijk [ID¹¹⁴](#), N.K. Vu [ID^{62d,62c}](#), R. Vuillermet [ID³⁶](#), O. Vujinovic [ID¹⁰⁰](#), I. Vukotic [ID³⁹](#),
 S. Wada [ID¹⁵⁷](#), C. Wagner [ID¹⁰³](#), J.M. Wagner [ID^{17a}](#), W. Wagner [ID¹⁷⁰](#), S. Wahdan [ID¹⁷⁰](#), H. Wahlberg [ID⁹⁰](#),
 R. Wakasa [ID¹⁵⁷](#), M. Wakida [ID¹¹¹](#), J. Walder [ID¹³⁴](#), R. Walker [ID¹⁰⁹](#), W. Walkowiak [ID¹⁴¹](#), A. Wall [ID¹²⁸](#),
 T. Wamorkar [ID⁶](#), A.Z. Wang [ID¹⁶⁹](#), C. Wang [ID¹⁰⁰](#), C. Wang [ID^{62c}](#), H. Wang [ID^{17a}](#), J. Wang [ID^{64a}](#),
 R.-J. Wang [ID¹⁰⁰](#), R. Wang [ID⁶¹](#), R. Wang [ID⁶](#), S.M. Wang [ID¹⁴⁸](#), S. Wang [ID^{62b}](#), T. Wang [ID^{62a}](#),
 W.T. Wang [ID⁸⁰](#), X. Wang [ID^{14c}](#), X. Wang [ID¹⁶¹](#), X. Wang [ID^{62c}](#), Y. Wang [ID^{62d}](#), Y. Wang [ID^{14c}](#),
 Z. Wang [ID¹⁰⁶](#), Z. Wang [ID^{62d,51,62c}](#), Z. Wang [ID¹⁰⁶](#), A. Warburton [ID¹⁰⁴](#), R.J. Ward [ID²⁰](#), N. Warrack [ID⁵⁹](#),
 A.T. Watson [ID²⁰](#), H. Watson [ID⁵⁹](#), M.F. Watson [ID²⁰](#), E. Watton [ID^{59,134}](#), G. Watts [ID¹³⁸](#), B.M. Waugh [ID⁹⁶](#),
 C. Weber [ID²⁹](#), H.A. Weber [ID¹⁸](#), M.S. Weber [ID¹⁹](#), S.M. Weber [ID^{63a}](#), C. Wei [ID^{62a}](#), Y. Wei [ID¹²⁶](#),
 A.R. Weidberg [ID¹²⁶](#), E.J. Weik [ID¹¹⁷](#), J. Weingarten [ID⁴⁹](#), M. Weirich [ID¹⁰⁰](#), C. Weiser [ID⁵⁴](#), C.J. Wells [ID⁴⁸](#),
 T. Wenaus [ID²⁹](#), B. Wendland [ID⁴⁹](#), T. Wengler [ID³⁶](#), N.S. Wenke [ID¹¹⁰](#), N. Wermes [ID²⁴](#), M. Wessels [ID^{63a}](#),
 K. Whalen [ID¹²³](#), A.M. Wharton [ID⁹¹](#), A.S. White [ID⁶¹](#), A. White [ID⁸](#), M.J. White [ID¹](#), D. Whiteson [ID¹⁵⁹](#),

L. Wickremasinghe ¹²⁴, W. Wiedenmann ¹⁶⁹, C. Wiel ⁵⁰, M. Wielers ¹³⁴, C. Wiglesworth ⁴², D.J. Wilbern ¹²⁰, H.G. Wilkens ³⁶, D.M. Williams ⁴¹, H.H. Williams ¹²⁸, S. Williams ³², S. Willocq ¹⁰³, B.J. Wilson ¹⁰¹, P.J. Windischhofer ³⁹, F.I. Winkel ³⁰, F. Winklmeier ¹²³, B.T. Winter ⁵⁴, J.K. Winter ¹⁰¹, M. Wittgen ¹⁴³, M. Wobisch ⁹⁷, Z. Wolffs ¹¹⁴, R. Wölker ¹²⁶, J. Wollrath ¹⁵⁹, M.W. Wolter ⁸⁶, H. Wolters ^{130a,130c}, A.F. Wongel ⁴⁸, S.D. Worm ⁴⁸, B.K. Wosiek ⁸⁶, K.W. Woźniak ⁸⁶, S. Wozniowski ⁵⁵, K. Wraight ⁵⁹, C. Wu ²⁰, J. Wu ^{14a,14e}, M. Wu ^{64a}, M. Wu ¹¹³, S.L. Wu ¹⁶⁹, X. Wu ⁵⁶, Y. Wu ^{62a}, Z. Wu ¹³⁵, J. Wuerzinger ¹¹⁰, T.R. Wyatt ¹⁰¹, B.M. Wynne ⁵², S. Xella ⁴², L. Xia ^{14c}, M. Xia ^{14b}, J. Xiang ^{64c}, X. Xiao ¹⁰⁶, M. Xie ^{62a}, X. Xie ^{62a}, S. Xin ^{14a,14e}, J. Xiong ^{17a}, D. Xu ^{14a}, H. Xu ^{62a}, L. Xu ^{62a}, R. Xu ¹²⁸, T. Xu ¹⁰⁶, Y. Xu ^{14b}, Z. Xu ⁵², Z. Xu ^{14a}, B. Yabsley ¹⁴⁷, S. Yacoob ^{33a}, N. Yamaguchi ⁸⁹, Y. Yamaguchi ¹⁵⁴, E. Yamashita ¹⁵³, H. Yamauchi ¹⁵⁷, T. Yamazaki ^{17a}, Y. Yamazaki ⁸⁴, J. Yan ^{62c}, S. Yan ¹²⁶, Z. Yan ²⁵, H.J. Yang ^{62c,62d}, H.T. Yang ^{62a}, S. Yang ^{62a}, T. Yang ^{64c}, X. Yang ^{62a}, X. Yang ^{14a}, Y. Yang ⁴⁴, Z. Yang ^{62a}, W-M. Yao ^{17a}, Y.C. Yap ⁴⁸, H. Ye ^{14c}, H. Ye ⁵⁵, J. Ye ⁴⁴, S. Ye ²⁹, X. Ye ^{62a}, Y. Yeh ⁹⁶, I. Yeletsikh ³⁸, B.K. Yeo ^{17a}, M.R. Yexley ⁹⁶, P. Yin ⁴¹, K. Yorita ¹⁶⁷, S. Younas ^{27b}, C.J.S. Young ⁵⁴, C. Young ¹⁴³, Y. Yu ^{62a}, M. Yuan ¹⁰⁶, R. Yuan ^{62b,k}, L. Yue ⁹⁶, M. Zaazoua ^{62a}, B. Zabinski ⁸⁶, E. Zaid ⁵², T. Zakareishvili ^{149b}, N. Zakharchuk ³⁴, S. Zambito ⁵⁶, J.A. Zamora Saa ^{137d,137b}, J. Zang ¹⁵³, D. Zanzi ⁵⁴, O. Zaplatilek ¹³², C. Zeitnitz ¹⁷⁰, H. Zeng ^{14a}, J.C. Zeng ¹⁶¹, D.T. Zenger Jr ²⁶, O. Zenin ³⁷, T. Ženiš ^{28a}, S. Zenz ⁹⁴, S. Zerradi ^{35a}, D. Zerwas ⁶⁶, M. Zhai ^{14a,14e}, B. Zhang ^{14c}, D.F. Zhang ¹³⁹, J. Zhang ^{62b}, J. Zhang ⁶, K. Zhang ^{14a,14e}, L. Zhang ^{14c}, P. Zhang ^{14a,14e}, R. Zhang ¹⁶⁹, S. Zhang ¹⁰⁶, T. Zhang ¹⁵³, X. Zhang ^{62c}, X. Zhang ^{62b}, Y. Zhang ^{62c,5}, Y. Zhang ⁹⁶, Z. Zhang ^{17a}, Z. Zhang ⁶⁶, H. Zhao ¹³⁸, P. Zhao ⁵¹, T. Zhao ^{62b}, Y. Zhao ¹³⁶, Z. Zhao ^{62a}, A. Zhemchugov ³⁸, K. Zheng ¹⁶¹, X. Zheng ^{62a}, Z. Zheng ¹⁴³, D. Zhong ¹⁶¹, B. Zhou ¹⁰⁶, H. Zhou ⁷, N. Zhou ^{62c}, Y. Zhou ⁷, C.G. Zhu ^{62b}, J. Zhu ¹⁰⁶, Y. Zhu ^{62c}, Y. Zhu ^{62a}, X. Zhuang ^{14a}, K. Zhukov ³⁷, V. Zhulanov ³⁷, N.I. Zimine ³⁸, J. Zinsser ^{63b}, M. Ziolkowski ¹⁴¹, L. Živković ¹⁵, A. Zoccoli ^{23b,23a}, K. Zoch ⁵⁶, T.G. Zorbas ¹³⁹, O. Zormpa ⁴⁶, W. Zou ⁴¹, L. Zwalinski ³⁶.

¹Department of Physics, University of Adelaide, Adelaide; Australia.

²Department of Physics, University of Alberta, Edmonton AB; Canada.

³(*a*)Department of Physics, Ankara University, Ankara; (*b*)Division of Physics, TOBB University of Economics and Technology, Ankara; Türkiye.

⁴LAPP, Univ. Savoie Mont Blanc, CNRS/IN2P3, Annecy; France.

⁵APC, Université Paris Cité, CNRS/IN2P3, Paris; France.

⁶High Energy Physics Division, Argonne National Laboratory, Argonne IL; United States of America.

⁷Department of Physics, University of Arizona, Tucson AZ; United States of America.

⁸Department of Physics, University of Texas at Arlington, Arlington TX; United States of America.

⁹Physics Department, National and Kapodistrian University of Athens, Athens; Greece.

¹⁰Physics Department, National Technical University of Athens, Zografou; Greece.

¹¹Department of Physics, University of Texas at Austin, Austin TX; United States of America.

¹²Institute of Physics, Azerbaijan Academy of Sciences, Baku; Azerbaijan.

¹³Institut de Física d'Altes Energies (IFAE), Barcelona Institute of Science and Technology, Barcelona; Spain.

¹⁴(*a*)Institute of High Energy Physics, Chinese Academy of Sciences, Beijing; (*b*)Physics Department, Tsinghua University, Beijing; (*c*)Department of Physics, Nanjing University, Nanjing; (*d*)School of Science, Shenzhen Campus of Sun Yat-sen University; (*e*)University of Chinese Academy of Science (UCAS), Beijing; China.

- ¹⁵Institute of Physics, University of Belgrade, Belgrade; Serbia.
- ¹⁶Department for Physics and Technology, University of Bergen, Bergen; Norway.
- ¹⁷(^a)Physics Division, Lawrence Berkeley National Laboratory, Berkeley CA;(^b)University of California, Berkeley CA; United States of America.
- ¹⁸Institut für Physik, Humboldt Universität zu Berlin, Berlin; Germany.
- ¹⁹Albert Einstein Center for Fundamental Physics and Laboratory for High Energy Physics, University of Bern, Bern; Switzerland.
- ²⁰School of Physics and Astronomy, University of Birmingham, Birmingham; United Kingdom.
- ²¹(^a)Department of Physics, Bogazici University, Istanbul;(^b)Department of Physics Engineering, Gaziantep University, Gaziantep;(^c)Department of Physics, Istanbul University, Istanbul;(^d)Istinye University, Sariyer, Istanbul; Türkiye.
- ²²(^a)Facultad de Ciencias y Centro de Investigaciones, Universidad Antonio Nariño, Bogotá;(^b)Departamento de Física, Universidad Nacional de Colombia, Bogotá;(^c)Pontificia Universidad Javeriana, Bogota; Colombia.
- ²³(^a)Dipartimento di Fisica e Astronomia A. Righi, Università di Bologna, Bologna;(^b)INFN Sezione di Bologna; Italy.
- ²⁴Physikalisches Institut, Universität Bonn, Bonn; Germany.
- ²⁵Department of Physics, Boston University, Boston MA; United States of America.
- ²⁶Department of Physics, Brandeis University, Waltham MA; United States of America.
- ²⁷(^a)Transilvania University of Brasov, Brasov;(^b)Horia Hulubei National Institute of Physics and Nuclear Engineering, Bucharest;(^c)Department of Physics, Alexandru Ioan Cuza University of Iasi, Iasi;(^d)National Institute for Research and Development of Isotopic and Molecular Technologies, Physics Department, Cluj-Napoca;(^e)University Politehnica Bucharest, Bucharest;(^f)West University in Timisoara, Timisoara;(^g)Faculty of Physics, University of Bucharest, Bucharest; Romania.
- ²⁸(^a)Faculty of Mathematics, Physics and Informatics, Comenius University, Bratislava;(^b)Department of Subnuclear Physics, Institute of Experimental Physics of the Slovak Academy of Sciences, Kosice; Slovak Republic.
- ²⁹Physics Department, Brookhaven National Laboratory, Upton NY; United States of America.
- ³⁰Universidad de Buenos Aires, Facultad de Ciencias Exactas y Naturales, Departamento de Física, y CONICET, Instituto de Física de Buenos Aires (IFIBA), Buenos Aires; Argentina.
- ³¹California State University, CA; United States of America.
- ³²Cavendish Laboratory, University of Cambridge, Cambridge; United Kingdom.
- ³³(^a)Department of Physics, University of Cape Town, Cape Town;(^b)iThemba Labs, Western Cape;(^c)Department of Mechanical Engineering Science, University of Johannesburg, Johannesburg;(^d)National Institute of Physics, University of the Philippines Diliman (Philippines);(^e)University of South Africa, Department of Physics, Pretoria;(^f)University of Zululand, KwaDlangezwa;(^g)School of Physics, University of the Witwatersrand, Johannesburg; South Africa.
- ³⁴Department of Physics, Carleton University, Ottawa ON; Canada.
- ³⁵(^a)Faculté des Sciences Ain Chock, Réseau Universitaire de Physique des Hautes Energies - Université Hassan II, Casablanca;(^b)Faculté des Sciences, Université Ibn-Tofail, Kénitra;(^c)Faculté des Sciences Semlalia, Université Cadi Ayyad, LPHEA-Marrakech;(^d)LPMR, Faculté des Sciences, Université Mohamed Premier, Oujda;(^e)Faculté des sciences, Université Mohammed V, Rabat;(^f)Institute of Applied Physics, Mohammed VI Polytechnic University, Ben Guerir; Morocco.
- ³⁶CERN, Geneva; Switzerland.
- ³⁷Affiliated with an institute covered by a cooperation agreement with CERN.
- ³⁸Affiliated with an international laboratory covered by a cooperation agreement with CERN.
- ³⁹Enrico Fermi Institute, University of Chicago, Chicago IL; United States of America.

- ⁴⁰LPC, Université Clermont Auvergne, CNRS/IN2P3, Clermont-Ferrand; France.
- ⁴¹Nevis Laboratory, Columbia University, Irvington NY; United States of America.
- ⁴²Niels Bohr Institute, University of Copenhagen, Copenhagen; Denmark.
- ⁴³(^a)Dipartimento di Fisica, Università della Calabria, Rende; (^b)INFN Gruppo Collegato di Cosenza, Laboratori Nazionali di Frascati; Italy.
- ⁴⁴Physics Department, Southern Methodist University, Dallas TX; United States of America.
- ⁴⁵Physics Department, University of Texas at Dallas, Richardson TX; United States of America.
- ⁴⁶National Centre for Scientific Research "Demokritos", Agia Paraskevi; Greece.
- ⁴⁷(^a)Department of Physics, Stockholm University; (^b)Oskar Klein Centre, Stockholm; Sweden.
- ⁴⁸Deutsches Elektronen-Synchrotron DESY, Hamburg and Zeuthen; Germany.
- ⁴⁹Fakultät Physik , Technische Universität Dortmund, Dortmund; Germany.
- ⁵⁰Institut für Kern- und Teilchenphysik, Technische Universität Dresden, Dresden; Germany.
- ⁵¹Department of Physics, Duke University, Durham NC; United States of America.
- ⁵²SUPA - School of Physics and Astronomy, University of Edinburgh, Edinburgh; United Kingdom.
- ⁵³INFN e Laboratori Nazionali di Frascati, Frascati; Italy.
- ⁵⁴Physikalisches Institut, Albert-Ludwigs-Universität Freiburg, Freiburg; Germany.
- ⁵⁵II. Physikalisches Institut, Georg-August-Universität Göttingen, Göttingen; Germany.
- ⁵⁶Département de Physique Nucléaire et Corpusculaire, Université de Genève, Genève; Switzerland.
- ⁵⁷(^a)Dipartimento di Fisica, Università di Genova, Genova; (^b)INFN Sezione di Genova; Italy.
- ⁵⁸II. Physikalisches Institut, Justus-Liebig-Universität Giessen, Giessen; Germany.
- ⁵⁹SUPA - School of Physics and Astronomy, University of Glasgow, Glasgow; United Kingdom.
- ⁶⁰LPSC, Université Grenoble Alpes, CNRS/IN2P3, Grenoble INP, Grenoble; France.
- ⁶¹Laboratory for Particle Physics and Cosmology, Harvard University, Cambridge MA; United States of America.
- ⁶²(^a)Department of Modern Physics and State Key Laboratory of Particle Detection and Electronics, University of Science and Technology of China, Hefei; (^b)Institute of Frontier and Interdisciplinary Science and Key Laboratory of Particle Physics and Particle Irradiation (MOE), Shandong University, Qingdao; (^c)School of Physics and Astronomy, Shanghai Jiao Tong University, Key Laboratory for Particle Astrophysics and Cosmology (MOE), SKLPPC, Shanghai; (^d)Tsung-Dao Lee Institute, Shanghai; China.
- ⁶³(^a)Kirchhoff-Institut für Physik, Ruprecht-Karls-Universität Heidelberg, Heidelberg; (^b)Physikalisches Institut, Ruprecht-Karls-Universität Heidelberg, Heidelberg; Germany.
- ⁶⁴(^a)Department of Physics, Chinese University of Hong Kong, Shatin, N.T., Hong Kong; (^b)Department of Physics, University of Hong Kong, Hong Kong; (^c)Department of Physics and Institute for Advanced Study, Hong Kong University of Science and Technology, Clear Water Bay, Kowloon, Hong Kong; China.
- ⁶⁵Department of Physics, National Tsing Hua University, Hsinchu; Taiwan.
- ⁶⁶IJCLab, Université Paris-Saclay, CNRS/IN2P3, 91405, Orsay; France.
- ⁶⁷Centro Nacional de Microelectrónica (IMB-CNM-CSIC), Barcelona; Spain.
- ⁶⁸Department of Physics, Indiana University, Bloomington IN; United States of America.
- ⁶⁹(^a)INFN Gruppo Collegato di Udine, Sezione di Trieste, Udine; (^b)ICTP, Trieste; (^c)Dipartimento Politecnico di Ingegneria e Architettura, Università di Udine, Udine; Italy.
- ⁷⁰(^a)INFN Sezione di Lecce; (^b)Dipartimento di Matematica e Fisica, Università del Salento, Lecce; Italy.
- ⁷¹(^a)INFN Sezione di Milano; (^b)Dipartimento di Fisica, Università di Milano, Milano; Italy.
- ⁷²(^a)INFN Sezione di Napoli; (^b)Dipartimento di Fisica, Università di Napoli, Napoli; Italy.
- ⁷³(^a)INFN Sezione di Pavia; (^b)Dipartimento di Fisica, Università di Pavia, Pavia; Italy.
- ⁷⁴(^a)INFN Sezione di Pisa; (^b)Dipartimento di Fisica E. Fermi, Università di Pisa, Pisa; Italy.
- ⁷⁵(^a)INFN Sezione di Roma; (^b)Dipartimento di Fisica, Sapienza Università di Roma, Roma; Italy.
- ⁷⁶(^a)INFN Sezione di Roma Tor Vergata; (^b)Dipartimento di Fisica, Università di Roma Tor Vergata,

Roma; Italy.

^{77(a)}INFN Sezione di Roma Tre; ^(b)Dipartimento di Matematica e Fisica, Università Roma Tre, Roma; Italy.

^{78(a)}INFN-TIFPA; ^(b)Università degli Studi di Trento, Trento; Italy.

⁷⁹Universität Innsbruck, Department of Astro and Particle Physics, Innsbruck; Austria.

⁸⁰University of Iowa, Iowa City IA; United States of America.

⁸¹Department of Physics and Astronomy, Iowa State University, Ames IA; United States of America.

^{82(a)}Departamento de Engenharia Elétrica, Universidade Federal de Juiz de Fora (UFJF), Juiz de Fora; ^(b)Universidade Federal do Rio De Janeiro COPPE/EE/IF, Rio de Janeiro; ^(c)Instituto de Física, Universidade de São Paulo, São Paulo; ^(d)Rio de Janeiro State University, Rio de Janeiro; Brazil.

⁸³KEK, High Energy Accelerator Research Organization, Tsukuba; Japan.

⁸⁴Graduate School of Science, Kobe University, Kobe; Japan.

^{85(a)}AGH University of Science and Technology, Faculty of Physics and Applied Computer Science, Krakow; ^(b)Marian Smoluchowski Institute of Physics, Jagiellonian University, Krakow; Poland.

⁸⁶Institute of Nuclear Physics Polish Academy of Sciences, Krakow; Poland.

⁸⁷Faculty of Science, Kyoto University, Kyoto; Japan.

⁸⁸Kyoto University of Education, Kyoto; Japan.

⁸⁹Research Center for Advanced Particle Physics and Department of Physics, Kyushu University, Fukuoka ; Japan.

⁹⁰Instituto de Física La Plata, Universidad Nacional de La Plata and CONICET, La Plata; Argentina.

⁹¹Physics Department, Lancaster University, Lancaster; United Kingdom.

⁹²Oliver Lodge Laboratory, University of Liverpool, Liverpool; United Kingdom.

⁹³Department of Experimental Particle Physics, Jožef Stefan Institute and Department of Physics, University of Ljubljana, Ljubljana; Slovenia.

⁹⁴School of Physics and Astronomy, Queen Mary University of London, London; United Kingdom.

⁹⁵Department of Physics, Royal Holloway University of London, Egham; United Kingdom.

⁹⁶Department of Physics and Astronomy, University College London, London; United Kingdom.

⁹⁷Louisiana Tech University, Ruston LA; United States of America.

⁹⁸Fysiska institutionen, Lunds universitet, Lund; Sweden.

⁹⁹Departamento de Física Teórica C-15 and CIAFF, Universidad Autónoma de Madrid, Madrid; Spain.

¹⁰⁰Institut für Physik, Universität Mainz, Mainz; Germany.

¹⁰¹School of Physics and Astronomy, University of Manchester, Manchester; United Kingdom.

¹⁰²CPPM, Aix-Marseille Université, CNRS/IN2P3, Marseille; France.

¹⁰³Department of Physics, University of Massachusetts, Amherst MA; United States of America.

¹⁰⁴Department of Physics, McGill University, Montreal QC; Canada.

¹⁰⁵School of Physics, University of Melbourne, Victoria; Australia.

¹⁰⁶Department of Physics, University of Michigan, Ann Arbor MI; United States of America.

¹⁰⁷Department of Physics and Astronomy, Michigan State University, East Lansing MI; United States of America.

¹⁰⁸Group of Particle Physics, University of Montreal, Montreal QC; Canada.

¹⁰⁹Fakultät für Physik, Ludwig-Maximilians-Universität München, München; Germany.

¹¹⁰Max-Planck-Institut für Physik (Werner-Heisenberg-Institut), München; Germany.

¹¹¹Graduate School of Science and Kobayashi-Maskawa Institute, Nagoya University, Nagoya; Japan.

¹¹²Department of Physics and Astronomy, University of New Mexico, Albuquerque NM; United States of America.

¹¹³Institute for Mathematics, Astrophysics and Particle Physics, Radboud University/Nikhef, Nijmegen; Netherlands.

- ¹¹⁴Nikhef National Institute for Subatomic Physics and University of Amsterdam, Amsterdam; Netherlands.
- ¹¹⁵Department of Physics, Northern Illinois University, DeKalb IL; United States of America.
- ¹¹⁶(^a)New York University Abu Dhabi, Abu Dhabi; (^b)United Arab Emirates University, Al Ain; (^c)University of Sharjah, Sharjah; United Arab Emirates.
- ¹¹⁷Department of Physics, New York University, New York NY; United States of America.
- ¹¹⁸Ochanomizu University, Otsuka, Bunkyo-ku, Tokyo; Japan.
- ¹¹⁹Ohio State University, Columbus OH; United States of America.
- ¹²⁰Homer L. Dodge Department of Physics and Astronomy, University of Oklahoma, Norman OK; United States of America.
- ¹²¹Department of Physics, Oklahoma State University, Stillwater OK; United States of America.
- ¹²²Palacký University, Joint Laboratory of Optics, Olomouc; Czech Republic.
- ¹²³Institute for Fundamental Science, University of Oregon, Eugene, OR; United States of America.
- ¹²⁴Graduate School of Science, Osaka University, Osaka; Japan.
- ¹²⁵Department of Physics, University of Oslo, Oslo; Norway.
- ¹²⁶Department of Physics, Oxford University, Oxford; United Kingdom.
- ¹²⁷LPNHE, Sorbonne Université, Université Paris Cité, CNRS/IN2P3, Paris; France.
- ¹²⁸Department of Physics, University of Pennsylvania, Philadelphia PA; United States of America.
- ¹²⁹Department of Physics and Astronomy, University of Pittsburgh, Pittsburgh PA; United States of America.
- ¹³⁰(^a)Laboratório de Instrumentação e Física Experimental de Partículas - LIP, Lisboa; (^b)Departamento de Física, Faculdade de Ciências, Universidade de Lisboa, Lisboa; (^c)Departamento de Física, Universidade de Coimbra, Coimbra; (^d)Centro de Física Nuclear da Universidade de Lisboa, Lisboa; (^e)Departamento de Física, Universidade do Minho, Braga; (^f)Departamento de Física Teórica y del Cosmos, Universidad de Granada, Granada (Spain); (^g)Departamento de Física, Instituto Superior Técnico, Universidade de Lisboa, Lisboa; Portugal.
- ¹³¹Institute of Physics of the Czech Academy of Sciences, Prague; Czech Republic.
- ¹³²Czech Technical University in Prague, Prague; Czech Republic.
- ¹³³Charles University, Faculty of Mathematics and Physics, Prague; Czech Republic.
- ¹³⁴Particle Physics Department, Rutherford Appleton Laboratory, Didcot; United Kingdom.
- ¹³⁵IRFU, CEA, Université Paris-Saclay, Gif-sur-Yvette; France.
- ¹³⁶Santa Cruz Institute for Particle Physics, University of California Santa Cruz, Santa Cruz CA; United States of America.
- ¹³⁷(^a)Departamento de Física, Pontificia Universidad Católica de Chile, Santiago; (^b)Millennium Institute for Subatomic physics at high energy frontier (SAPHIR), Santiago; (^c)Instituto de Investigación Multidisciplinario en Ciencia y Tecnología, y Departamento de Física, Universidad de La Serena; (^d)Universidad Andres Bello, Department of Physics, Santiago; (^e)Instituto de Alta Investigación, Universidad de Tarapacá, Arica; (^f)Departamento de Física, Universidad Técnica Federico Santa María, Valparaíso; Chile.
- ¹³⁸Department of Physics, University of Washington, Seattle WA; United States of America.
- ¹³⁹Department of Physics and Astronomy, University of Sheffield, Sheffield; United Kingdom.
- ¹⁴⁰Department of Physics, Shinshu University, Nagano; Japan.
- ¹⁴¹Department Physik, Universität Siegen, Siegen; Germany.
- ¹⁴²Department of Physics, Simon Fraser University, Burnaby BC; Canada.
- ¹⁴³SLAC National Accelerator Laboratory, Stanford CA; United States of America.
- ¹⁴⁴Department of Physics, Royal Institute of Technology, Stockholm; Sweden.
- ¹⁴⁵Departments of Physics and Astronomy, Stony Brook University, Stony Brook NY; United States of

America.

¹⁴⁶Department of Physics and Astronomy, University of Sussex, Brighton; United Kingdom.

¹⁴⁷School of Physics, University of Sydney, Sydney; Australia.

¹⁴⁸Institute of Physics, Academia Sinica, Taipei; Taiwan.

¹⁴⁹(^a)E. Andronikashvili Institute of Physics, Iv. Javakhishvili Tbilisi State University, Tbilisi; (^b)High Energy Physics Institute, Tbilisi State University, Tbilisi; (^c)University of Georgia, Tbilisi; Georgia.

¹⁵⁰Department of Physics, Technion, Israel Institute of Technology, Haifa; Israel.

¹⁵¹Raymond and Beverly Sackler School of Physics and Astronomy, Tel Aviv University, Tel Aviv; Israel.

¹⁵²Department of Physics, Aristotle University of Thessaloniki, Thessaloniki; Greece.

¹⁵³International Center for Elementary Particle Physics and Department of Physics, University of Tokyo, Tokyo; Japan.

¹⁵⁴Department of Physics, Tokyo Institute of Technology, Tokyo; Japan.

¹⁵⁵Department of Physics, University of Toronto, Toronto ON; Canada.

¹⁵⁶(^a)TRIUMF, Vancouver BC; (^b)Department of Physics and Astronomy, York University, Toronto ON; Canada.

¹⁵⁷Division of Physics and Tomonaga Center for the History of the Universe, Faculty of Pure and Applied Sciences, University of Tsukuba, Tsukuba; Japan.

¹⁵⁸Department of Physics and Astronomy, Tufts University, Medford MA; United States of America.

¹⁵⁹Department of Physics and Astronomy, University of California Irvine, Irvine CA; United States of America.

¹⁶⁰Department of Physics and Astronomy, University of Uppsala, Uppsala; Sweden.

¹⁶¹Department of Physics, University of Illinois, Urbana IL; United States of America.

¹⁶²Instituto de Física Corpuscular (IFIC), Centro Mixto Universidad de Valencia - CSIC, Valencia; Spain.

¹⁶³Department of Physics, University of British Columbia, Vancouver BC; Canada.

¹⁶⁴Department of Physics and Astronomy, University of Victoria, Victoria BC; Canada.

¹⁶⁵Fakultät für Physik und Astronomie, Julius-Maximilians-Universität Würzburg, Würzburg; Germany.

¹⁶⁶Department of Physics, University of Warwick, Coventry; United Kingdom.

¹⁶⁷Waseda University, Tokyo; Japan.

¹⁶⁸Department of Particle Physics and Astrophysics, Weizmann Institute of Science, Rehovot; Israel.

¹⁶⁹Department of Physics, University of Wisconsin, Madison WI; United States of America.

¹⁷⁰Fakultät für Mathematik und Naturwissenschaften, Fachgruppe Physik, Bergische Universität Wuppertal, Wuppertal; Germany.

¹⁷¹Department of Physics, Yale University, New Haven CT; United States of America.

^a Also Affiliated with an institute covered by a cooperation agreement with CERN.

^b Also at APC, Université Paris Cité, CNRS/IN2P3, Paris; France.

^c Also at Borough of Manhattan Community College, City University of New York, New York NY; United States of America.

^d Also at Center for High Energy Physics, Peking University; China.

^e Also at Center for Interdisciplinary Research and Innovation (CIRI-AUTH), Thessaloniki ; Greece.

^f Also at Centro Studi e Ricerche Enrico Fermi; Italy.

^g Also at CERN, Geneva; Switzerland.

^h Also at Département de Physique Nucléaire et Corpusculaire, Université de Genève, Genève; Switzerland.

ⁱ Also at Departament de Física de la Universitat Autònoma de Barcelona, Barcelona; Spain.

^j Also at Department of Financial and Management Engineering, University of the Aegean, Chios; Greece.

^k Also at Department of Physics and Astronomy, Michigan State University, East Lansing MI; United States of America.

- l* Also at Department of Physics and Astronomy, University of Victoria, Victoria BC; Canada.
- m* Also at Department of Physics, California State University, Sacramento; United States of America.
- n* Also at Department of Physics, King's College London, London; United Kingdom.
- o* Also at Department of Physics, Royal Holloway University of London, Egham; United Kingdom.
- p* Also at Department of Physics, University of Fribourg, Fribourg; Switzerland.
- q* Also at Department of Physics, University of Thessaly; Greece.
- r* Also at Department of Physics, Westmont College, Santa Barbara; United States of America.
- s* Also at Hellenic Open University, Patras; Greece.
- t* Also at Institutio Catalana de Recerca i Estudis Avancats, ICREA, Barcelona; Spain.
- u* Also at Institut für Experimentalphysik, Universität Hamburg, Hamburg; Germany.
- v* Also at Institute of Applied Physics, Mohammed VI Polytechnic University, Ben Guerir; Morocco.
- w* Also at Institute of Particle Physics (IPP); Canada.
- x* Also at Institute of Physics and Technology, Ulaanbaatar; Mongolia.
- y* Also at Institute of Physics, Azerbaijan Academy of Sciences, Baku; Azerbaijan.
- z* Also at Institute of Theoretical Physics, Ilia State University, Tbilisi; Georgia.
- aa* Also at Lawrence Livermore National Laboratory, Livermore; United States of America.
- ab* Also at The Collaborative Innovation Center of Quantum Matter (CICQM), Beijing; China.
- ac* Also at TRIUMF, Vancouver BC; Canada.
- ad* Also at Università di Napoli Parthenope, Napoli; Italy.
- ae* Also at University of Colorado Boulder, Department of Physics, Colorado; United States of America.
- af* Also at Washington College, Chestertown, MD; United States of America.
- ag* Also at Manhattan College, New York NY; United States of America.
- * Deceased